University of Massachusetts Medical School

eScholarship@UMMS

2017-01-12

Novel Mechanisms Regulating Dopamine Transporter Endocytic Trafficking: Ack1-Controlled Endocytosis And Retromer-Mediated Recycling

Sijia Wu
University of Massachusetts Medical School

Let us know how access to this document benefits you.

Repository Citation

NOVEL MECHANISMS REGULATING DOPAMINE TRANSPORTER ENDOCYTIC TRAFFICKING: ACK1-CONTROLLED ENDOCYTOSIS AND RETROMER-MEDIATED RECYCLING

A Dissertation Presented

By

SIJIA WU

Submitted to the Faculty of the

Graduate School of Biomedical Sciences, Worcester

In partially fulfillment of the requirement of the degree of

DOCTOR OF PHILOSOPHY

JANUARY 12TH, 2017

PROGRAM IN NEUROSCIENCE

NOVEL MECHANISMS REGULATING DOPAMINE TRANSPORTER ENDOCYTIC TRAFFICKING: ACK1-CONTROLLED ENDOCYTOSIS AND RETROMER-MEDIATED RECYCLING

A Dissertation Presented

By

SIJIA WU

Dissertation Defense Committee GSBS Members

Mary Munson, Ph.D.

Biochemistry and Molecular Pharmacology

David G. Lambright, Ph.D.

Program in Molecular Medicine

Vivian Budnik, Ph.D.

Program in Neuroscience

Chair of the Dissertation Committee

Andrew R. Tapper, Ph.D.

Program in Neuroscience

External Dissertation Committee Member

Aurelio Galli, Ph.D.

Professor, Vanderbilt University

Thesis Advisor

Haley E. Melikian, Ph.D.

Program in Neuroscience

Student Program

Program in Neuroscience

January 12th, 2017

Acknowledgements

First and foremost, I would like to thank my thesis advisor Haley, who guided me through my graduate research, kindled my scientific curiosities, trained me to think rigorously, and most importantly, taught me how to be a good scientist. Her mentoring definitely changed me beyond the scientific research and molded me into who I am now, and showed me who I can be.

When I first joined the Melikian lab, back in 2011, I did not have a lot of bench work experience and Haley walked me through most of the experiments. Haley is always available to answer questions and give advice. Even so, I had three binders of failed cloning and western blots. She told me to work harder and so I did. But being persistent is not enough, I learn from her over years that I also need to be a keen observer, be patient and think experiments steps ahead. Haley is also very supportive of my own ideas. The breakthrough of my graduate research was the discovery of a protein called Ack1 as a DAT endocytic brake molecule. I still remember on that Friday, during our weekly one-to-one meeting, I proposed the idea to her and she was very supportive and ordered two antibodies and an inhibitor for pilot experiments right away. This was the first time that I got a taste of scientific discovery and I was so thrilled! We eventually turned this idea into my first publication in PNAS and there is one more on the way. I owe much gratitude to Haley.

I would like to thank the previous and current members of the Melikian lab. Luke, who overlapped with me for three years and was literally a walking encyclopedia. Thank you for answering my silly questions. Carolyn and Rita, I enjoyed our discussions about experiments, projects and of course, the gossips. My thanks also go to Patrick, Brian, Allyson and Joanna. Thank you all and I was so lucky to have such wonderful and trustworthy labmates.

I would also like to acknowledge members of my TRAC/DEC committees: Andrew, who has being my chair since the qualify exam; Mary, David and Vivian have been in my TRAC for four years and Dr. Galli, thank you for traveling all the way from Tennessee to attend my defense. Your encouragement and advice over the years have been instrumental in my success.

Finally, I would like to dedicate this thesis to my husband Lukai and my parents Xiaoping and Jianmin. Thank you for keeping me company, for cheering me up when I am down. Without your love and support, I would not be able to succeed.

Abstract

Dopamine transporters (DAT) facilitate high-affinity presynaptic dopamine (DA) reuptake in the central nervous system, and are required to constrain extracellular DA levels and maintain presynaptic DAergic tone. DAT is the primary target for addictive and therapeutic psychostimulants, which require DAT binding to elicit reward. DAT availability at presynaptic terminals ensures its proper function, and is dynamically regulated by endocytic trafficking. My thesis research focused on two fundamental questions: 1) What are the molecular mechanisms that control DAT endocytosis? and 2) what are the mechanism(s) that govern DAT's post-endocytic fate? Using pharmacological and genetic approaches, I discovered that a non-receptor tyrosine kinase, activated by cdc42 kinase 1 (Ack1), stabilizes DAT plasma membrane expression by negatively regulating DAT endocytosis. I found that stimulated DAT endocytosis absolutely requires Ack1 inactivation. Moreover, I was able to restore normal DAT endocytosis to a trafficking dysregulated DAT coding variant identified in an Attention Deficit Hyperactivity Disorder (ADHD) patient via constitutively activating Ack1. To address what mechanisms govern DAT's post-endocytic fate, I took advantage of a small molecule labeling approach to directly couple fluorophore to the DAT surface population, and subsequently tracked DAT's temporal-spatial post-endocytic itinerary in immortalized mesencephalic cells. Using this approach, I discovered that the retromer complex mediates DAT recycling and is required to maintain DAT surface levels via a DAT C-terminal

PDZ-binding motif. Taken together, these findings shed considerable new light on DAT trafficking mechanisms, and pave the way for future studies examining the role of regulated DAT trafficking in neuropsychiatric disorders.

Table of Contents

List of Figures

List of Abbreviations

3'-UTR	3'-untranslated region
6-OHDA	6-hydroxydopamine
AADC	Aromatic L-amino acid decarboxylase
AAV2	adeno-associated virus serotype 2
Ach	Acetylcholine
AchE	Acetylcholinesterase
Ack1	Activated by cdc42 kinase 1
ADHD	Attention deficit hyperactivity disorder
ASD	autism spectrum disorders
BAR	BIN/amphiphysin/Rvs
CaMKII	Calmodulin-dependent kinase II
CCP	Clathrin-coated pit
CCV	Clathrin-coated vesicles
CNS	Central nervous system
Co-IP	Co-immunoprecipitation
COMT	Catechol-O-methyltransferase
COP	Coat protein complex
CPP	Conditioned place preference
DA	Dopamine
DAG	Diacylglycerol
DAT	Dopamine transporter
DCP	3,4-dichlorophenethylamine
EEA1	Early endosome antigen 1
EGFR	Epidermal growth factor receptor
ER	Endoplasmic reticulum
FFN	Fluorescent false neurotransmitter
Flot-1	Flotillin-1
FRET	Fluorescent resonance energy transfer
FSCV	Fast scan cyclic voltammetry
GABA	γ-aminobutyric acid
GAT	γ-aminobutyric acid transporter
GPCR	G-protein coupled receptor
HA	Hemagglutinin
HPLC	High-performance liquid-chromatography
HRP	Horseradish peroxidase
HVA	Homovanillic acid
IPD	Infantile Parkinsonism-dystonia
KI	Knock-in
KO	Knock-out
LAP	Lipolic acid acceptor peptide

LeuT	Leucine transporter
MAO	Monoamine oxidase
MAPK	Mitogen-activated protein kinase
mPFC	Medial prefrontal cortex
MPP^+	1-methyl-4-phenylpridinium
MPTP	1-methyl-4-phenyl-1,2,3,6-tetrahydropridine
NAc	Nucleus accumbens
NEDD4-2	Neural precursor cell expressed, developmentally downregulated 4-2
NET	Norepinephrine transporter
pAz	Picolyl azide
PD	Parkinson's disease
PDGFR	Platelet-derived growth factor receptor
PET	Positron emission tomography
PI3K	phosphatidylinositol 3-kinase
PICK1	Protein interact with C kinase
PIP_2	Phosphatidylinositol 4,5-bisphosphate
PKA	Protein kinase A
PKC	Protein kinase C
PMA	Phorbol 12-myristate 13-acetate
PRIME	Protein incorporation mediated by enzyme
SCAM	Substituted cysteine accessibility method
SERT	Serotonin transporter
siRNA	Small interference RNA
SLC6	Solute carrier 6
SNP	Single nucleotide polymorphism
SN_{pc}	Substantia nigra pars compacta
STZ	Streptozotocin
TCA	Tricyclic antidepressant
TfR	Transferrin receptor
TGN	Trans-Golgi network
TH	Tyrosine hydroxylase
TMD	Transmembrane domain
VMAT	Vesicular monoamine transporter
VNTR	Variable number tandem repeat
Vps35	Vacuolar protein sorting-associated protein 35
VTA	Ventral tegmental area
WT	Wild-type

List of copyright Materials Produced by the Author

Chapter II of this dissertation has appeared in a separate publication:

Wu S, Bellve KD, Fogarty KE, Melikian HE (2015) Ack1 is a dopamine transporter endocytic brake that rescues a trafficking-dysregulated ADHD coding variant. *Proc Natl Acad Sci U S A* 112:15480-15485.

CHAPTER I

INTRODUCTION

I.A Dopamine System in the CNS and Related diseases

Over sixty years ago, Arvid Carlsson discovered dopamine (DA) as a neurotransmitter. Since then, research on DA neurotransmission and signaling mechanisms have greatly impacted the development of neuropharmacology and psychiatry. Some of the medicines that are most widely prescribed in modern neurology and psychiatry, including L-DOPA, Ritalin and antipsychotic drugs, act on the brain DA system. In this section of the introduction, I will give an overview of the DA system in the central nervous system (CNS) then focus on the two major dopaminergic projections, the nigrostriatal pathway and the mesocorticolimbic pathway, and their implications in neuropsychiatric disorders.

OVERVIEW OF THE DOPAMINE SYSTEM IN THE CNS

Anatomical studies have greatly helped us to understand the contribution of dopaminergic pathways to behavior. Before the era of immunohistochemistry, sensitive visualization of neurotransmitter in a neuron was achieved by the Falck –Hillarp method developed in the early 1960s. By exposure of freeze-dried tissue to formaldehyde vapor, Falck showed that DA and norepinephrine could be transformed into fluorophores that emitted yellow-green fluorescence (Falck and Torp, 1962). Later modification of this technique with improved sensitivity and

precision enabled visualization of DA axon terminals in great details (Lindvall and Bjorklund, 1974).

Anterograde and retrograde tracing are also one of the most widely used methods to map neuronal circuitry. Based on intra-axonal transport, tract-tracing methods utilized the uptake and transport of horseradish peroxidase (HRP) to trace neuronal projections (LaVail and LaVail, 1972). More recently, a series of trans-synaptic tracers have been developed that allow identification of synaptically connected cells (Zou et al., 2001; Braz et al., 2002). Among them, Wickersham and colleagues constructed a viral tracer that crossed only one synaptic step to neurons directly connected to the starting population (Wickersham et al., 2007). Based on rabies virus, this technology enables a more detailed understanding of neuronal connectivity.

Using those techniques, DA neurons were identified and mapped in the brain. The major dopaminergic projection, the nigrostriatal pathway, consists of dopaminergic neurons in the substantia nigra pars compacta (SN_{pc}) of the midbrain that project to the dorsal striatum (caudate nucleus and putamen). The nigrostriatal pathway is responsible for voluntary movement. In addition, dopaminergic neurons in the ventral tegmental area (VTA) projection to the ventral striatum (nucleus accumbens, NAc) and prefrontal cortex (PFC) form the mesocorticolimbic pathway, which is associated with reward-related behavior (Moore and Bloom, 1978). The tuberoinfundibular pathway, which transmits DA

from hypothalamus to the pituitary gland (Bjorklund et al., 1970; Jonsson et al., 1972), controls secretion of certain hormones like prolactin (Takahara et al., 1974). Other than the three major dopaminergic projections, DA neurons also exist in retina and the olfactory bulb for vision and odor processing (Hokfelt et al., 1975; Bauer et al., 1980). These different dopaminergic pathways are illustrated in a simplified diagram in Figure I-1.
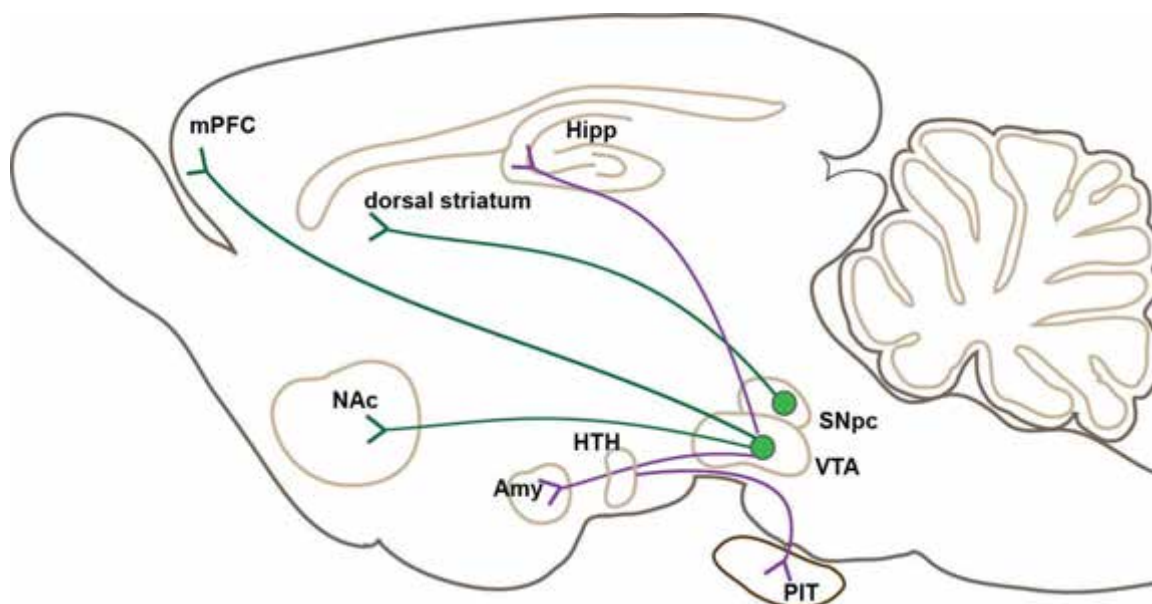
Figure I-1. DAergic pathways in the rodents brain. Cell bodies of DA neurons localize primarily in the midbrain substantial nigra and ventral tegmental area and they project to brain regions including dorsal striatum, median prefrontal cortex (mPFC), nucleus accumbens (NAc), hippocampus (Hipp) as well as amygdala (Amy). There are also DA neurons in hypothalamus (HTH) that project to pituitary gland (PIT). Two main DAergic pathways: nigrostriatal pathway and mesocorticolimbic pathway are illustrated in green.

THE NIGROSTRIATAL PATHWAY AND PARKINSON'S DISEASE (PD)

The nigrostriatal projection from the SN_{pc} to the dorsal striatum was discovered by Hornykiewcz and colleagues, who correlated the drastic reduction of DA content in the dorsal striatum of PD patients with the degeneration of SN_{pc} (Hornykiewicz, 1966). With the help of the Falck –Hillarp method, this projection was rapidly confirmed (Anden et al., 1966). The terminals of the nigrostriatal projection locate to the dorsal striatum which consists of the caudate and putamen. As the axons enter the dorsal striatum, they collateralize into branches that contain numerous small varicosities, 0.5-0.7 µm in diameter (Anden et al., 1966).

The use of the chemical neural toxin, 6-hydroxydopamine (6-OHDA), greatly helped to understand the physiological function of nigrostriatal DA neurons on their target cells in the striatum (Bloom, 1975; Ungerstedt, 1976). 6-OHDA is a hydroxylated analog of DA and selectively destroys DA and norepinephrine neurons by inducing oxidative stress and mitochondria defects in those neurons (Blum et al., 2001). When injected into the DA bundle or SN in rat, firing rates of striatal neurons increased ipsilateral to the lesion, suggesting the inhibitory nature of the nigrostriatal DA system (Arbuthnott, 1974). We now know that the nigrostriatal projection releases DA that activates dopamine receptors on the medium spiny neurons in the dorsal striatum. 6-OHDA lesions of the nigrostriatal pathway is also widely used as a behavior model that demonstrates the

importance of the nigrostriatal pathway in movement initiation and balance maintenance (Alexander et al., 1990).

Severe damage to SN_{pc} was not generally accepted as one of the hallmarks of PD pathology until neuropathological studies of Hassler, Greenfield and Bosanquet (Greenfield and Bosanquet, 1953). It is now known that neuron loss in SN_{pc} starts about six years before the first motor symptom is clinically detectable, at which point around 75% of the SN_{pc} DA neurons have died (Lees, 2007). Loss of DA in the dorsal striatum alters the downstream neurotransmission and leads to symptoms like tremor, bradykinesia and muscle rigidity (Dauer and Przedborski, 2003).

In summary, the DA nigrostriatal pathway regulates motor behavior, and aberrant DAergic neurotransmission in this pathway leads to the pathological conditions that contribute to PD.

THE MESOCORTICOLIMBIC PATHWAY AND DRUG OF ABUSE

The nucleus accumbens, also called ventral striatum, arises developmentally with the dorsal striatum, has neurons similar to the dorsal striatum, and receives a DA innervation from VTA DA neurons (Heimer et al., 1997). In 1954, Olds and Milner carried out pioneering experiments revealing that rats repeatedly press levers to stimulate certain brain regions including NAc and septum (Olds and Milner, 1954). Later studies using direct brain stimulation mapped brain regions containing reward-relevant neurons. Those studies mainly focused on the

diencephalic medial forebrain bundle where we now know as part of the mesolimbic pathway (Wise and Rompre, 1989).

Our knowledge of the neurochemical subtypes of reward-relevant neurons primarily derived from pharmacological studies, especially studies using drugs of abuse. Abusive drugs, like psychostimulants, opiates and nicotine, act through distinct molecular mechanisms to modulate DA levels within certain brain regions (Heikkila et al., 1975a; Heikkila et al., 1975b; Marks et al., 1986). Mesocorticolimbic DA pathways, which project mainly from VTA to the NA_c and PFC, were soon identified as the reward-seeking pathways for psychostimulants cocaine and amphetamine. Lesions in the NA_c blocked cocaine- and amphetamine- induced reward behavior (Lyness et al., 1979; Roberts et al., 1980). Rats could learn to self-administer amphetamine into the NA_c (Hoebel et al., 1983) as well as lever-press for cocaine into mPFC (Goeders and Smith, 1983). These results demonstrate that DAerigc neurotransmission in the mesocorticolimbic pathway is a key regulator for reward, and recently studies have shown that repeated exposure to drugs of abuse alters brain reward pathways and often leads to drug addiction (Hyman et al., 2006).

In summary, the two major DA pathways, the nigrostriatal pathway and the mesocorticolimbic pathway, are essential for key brain functions such as locomotion, reward and cognition. Dysregulation of DAergic neurotransmission in

these pathways contribute to neurological disorders such as PD, schizophrenia and drug addiction.

I.B Presynaptic Dopaminergic Neurotransmission

Dopaminergic neurotransmission is characterized by dopamine release from the presynaptic terminal, binding of DA to multiple pre- and post-synaptic receptors and reuptake of DA by the presynaptic dopamine transporter (DAT). DA and other monoamine neurotransmitters activate G-protein coupled receptors (GPCR), but not ligand-gated ion channels, to achieve their modulatory effects at the order of subseconds to minutes. This slow-acting nature of DA requires a more complicated sequence of biochemical steps including secondary messengers, protein kinases and phosphatases (Greengard, 2001). DA neurons carry two distinct firing patterns, tonic firing, in which DA neurons fire in a single spiking mode, and burst firing, consisting of consecutive spikes with decreasing amplitude and increasing duration (Grace and Bunney, 1984b, a). In this section, I will mainly focus on presynaptic DA neurotransmission with an emphasis on reuptake of neurotransmitters as a primary mechanism to terminate dopaminergic neurotransmission.

DA SYNTHESIS AND METABOLISM

The biosynthesis of DA has been established for over fifty years (Molinoff and Axelrod, 1971). The DA precursor, L-tyrosine, is converted to L-DOPA by the enzyme tyrosine hydroxylase (TH). Then, aromatic L-amino acid decarboxylase

(AADC) transforms L-DOPA to DA. The metabolism of DA involves primarily two enzymes: monoamine oxidase (MAO) and catechol-O-methyltransferase (COMT). In the 1950s, it was already known that MAO deaminated all catecholamines including DA, norepinephrine and epinephrine. However, even after the administration of MAO inhibitor, increase in the blood pressure induced by norepinephrine to cats was still rapidly reverted, which prompted researchers at that time to search for another unknown enzyme that metabolized and inactivated norepinephrine (Axelrod, 2003). Axelrod and colleagues soon purified COMT and demonstrated that it O-methylated catechols *in vitro* and *in vivo* (Axelrod and Tomchick, 1958; Axelrod and Laroche, 1959). The main metabolite for DA is homovanillic acid (HVA), which could be easily detected in urine.

DISCOVERY OF DA UPTAKE

The discoveries of enzymes like MAO, COMT and acetylcholinesterase (AchE) convinced researchers that termination of neurotransmission was mediated by enzymatic inactivation of neurotransmitters. This is true for acetylcholine (Ach) since Ach is rapidly degraded into choline and acetyl CoA by AchE. However, similar to MAO inhibition, inhibition of COMT activity also failed to block the blood pressure-elevating action of norepinephrine, suggesting other mechanisms are responsible for terminating norepinephrine action. It was not until the late 1950s, when tritium labelled catecholamines became available, that the neurotransmitter uptake mechanism was discovered. Axelrod's group first found that radioactive

norepinephrine was accumulated by sympathetic nerve terminals after intravenous injection in mice and cats (Hertting and Axelrod, 1961). Removing those sympathetic nerves strikingly reduced ^{3}[H]-norepinephrine and epinephrine in those chronically denervated structures (Hertting et al., 1961). Based on these observations, they proposed that the reuptake of norepinephrine by the same nerve that released it was a novel mechanism that terminated neurotransmission. Soon, DA and serotonin were also found to be inactivated by uptake into their respective presynaptic terminals (Snyder and Coyle, 1969; Iversen, 1971).

MEASURING DA UPTAKE *IN VIVO*

Studying DA uptake using *in vitro* systems, like brain homogenates and synaptosome preparations (Snyder and Coyle, 1969; Bonanno and Raiteri, 1987), gave important information in terms of substrate and drug affinity on the transport system, but it cannot tell how DA release and reuptake are regulated physiologically. To address this question, multiple approaches have been developed over years to measure DA release and reuptake *in vivo*. These approaches provide the temporal-spatial resolution of DA release in brain regions of interest, and measure the amount of DA that is released during neuronal stimulation.

Starting in the early 1980s, fast scan cyclic voltammetry (FSCV), in which a carbon fiber electrode implanted in the brain detects surrounding DA by oxidization, has been used to measure electrically evoked DA release and

reuptake (Marsden et al., 1988). With the subsecond temporal resolution and micrometer-dimension spatial resolution, FSCV allows acute kinetic characterization of DA release and reuptake (Nicholson, 1995). Estimates for the K_m of DA uptake ranges from 0.2 to 2 μM, depending on the brain region (McElvain and Schenk, 1992; Wu et al., 2001). V_{max}, which indicates maximum rate of release, can also be calculated from DA voltammetric recordings. DA uptake in the ventral striatum was reported to be less efficient than in the dorsal striatum (Stamford et al., 1988; Cass et al., 1992), whereas in the amygdala and mPFC, DA uptake appeared to be very low (Garris and Wightman, 1994; Jones et al., 1995). It was suggested that in regions with low dopamine transporter (DAT) expression and activity, the norepinephrine transporter (NET) may take over DAT's role to facilitate DA uptake (Yamamoto and Novotney, 1998; Moron et al., 2002). Enzymatic inactivation of DA by COMT is also involved in these brain regions (Wayment et al., 2001; Matsumoto et al., 2003). Moreover, FSCV can be achieved in a freely moving awake animal that allows studies correlating the time-course of behavior and DA signals (Robinson et al., 2003).

Another common method to monitor extracellular DA levels *in vivo* is microdialysis, in which a semi-permeable membrane containing probe is surgically implanted into the brain region of interest and perfused with fluid (Bourne, 2003). Dialysate is collected over time and analyzed using high-performance liquid-chromatography (HPLC) to quantify DA concentration changes as a function of time. This method has slow temporal resolution

(minutes to hours) and a larger dialysis probe leads to more tissue damage. However, it can also be achieved in a freely moving awake animal that allows studies correlating the time-course of behavior and events in neurochemistry.

Neither of the invasive methods mentioned above can be used in human brain. However, the development of positron emission tomography (PET) imaging and a series of radiotracers that labels dopamine receptors, DAT or precursors of DA enables direct measurement of components of the DA system in the living human brain (Volkow et al., 1996).

Taken together, the strength of presynaptic DA neurotransmission is controlled by molecular mechanisms regulating DA synthesis, release as well as reuptake. Presynaptic DA reuptake is the primary mechanism to temporally and spatially restrain DA neurotransmission. Techniques such as FSCV and microdialysis help us to elucidate mechanisms controlling DA release and reuptake *in vivo*.

I.C Dopamine Transporter: Pharmacology, Structure and Function

The discovery of a neurotransmitter reuptake mechanism by Axelrod started an area of research investigating the pharmacological properties of the reuptake sites in the brain. However, genes that encode proteins that are required for high-affinity neurotransmitter reuptake were not identified until the early 1990s, with the help of molecular biology. Using expression cloning techniques, Amara and colleagues first isolated a single cDNA clone that encoded the human norepinephrine transporter (NET) (Pacholczyk et al., 1991). The amino acid

sequence of NET shared significant amino-acid identity with the previously published rat γ-aminobutyric acid transporter (GAT) (Guastella et al., 1990). These observations led to the identification of a new gene family for neurotransmitter transporters, the *SLC6* (solute carrier 6) gene family. Using conserved sequences in NET and GAT, genes that encode DAT and the serotonin transporter (SERT) were soon discovered through homology screening in mammalian cDNA libraries, starting the era of structure, function and genetic studies of the neurotransmitter transporters (Blakely et al., 1991; Kilty et al., 1991; Shimada et al., 1991; Usdin et al., 1991). The human *DAT* gene (*SLC6A3*) maps to chromosome 5p15.3. It spans over 64 kilo base pairs, consisting of 15 exons separated by 14 introns (Kawarai et al., 1997). Hydrophobicity analysis revealed that DAT protein, as well as other neurotransmitter transporters in the same gene family, contained twelve putative transmembrane domains (TMDs), one large glycosylated loop between TMD3 and TMD4, and cytoplasmic amino and carboxyl termini. In this section, I will discuss the pharmacological properties of DAT, especially how psychostimulants cocaine and amphetamine interact with DAT and alter transporter function. Then I will focus on the structure/function analysis of DAT with an emphasis on DA transport mechanism.

PHARMACOLOGY

DAT is a well-established molecular target for many pharmacological agents that affect brain function including psychostimulants, antidepressants and neurotoxins

(Amara and Sonders, 1998). The pharmacology of DAT is mainly examined in brain synaptosome preparations or heterologous expression systems expressing DAT cDNAs. Generally, the results from the two systems agree with each other.

Ritz and colleagues first related the effect of cocaine with DAT inhibition (Ritz et al., 1987). Cocaine is a non-selective, competitive inhibitor for all three monoamine transporters including DAT, SERT and NET. Tricyclic antidepressant, methylphenidate (Ritalin), nomifensine and bupropion are selective inhibitors for DAT and NET while GBR12909 and WIN35,426 have been developed as selective DAT inhibitors (Kristensen et al., 2011). Some of these compounds are currently used in the treatment of neuropsychiatric disorders such as depression and attention deficit hyperactivity disorder (ADHD).

Amphetamines, on the other hand, are substrates for DAT. These drugs are weak bases that can reverse the direction of neurotransmitter transport through monoamine transporters and release vesicular monoamines into the cytoplasm (Sulzer et al., 1995; Jones et al., 1998a). Amphetamines' effect on blocking uptake of catecholamine into different brain regions was known long before the identification of the transporter proteins (Ferris et al., 1972). At that time, it was experimentally difficult to discriminate between release and uptake inhibition by simply measuring [^{3}H]-DA uptake since a drug that causes release and blocks uptake could release part of the previously taken up [^{3}H]-DA, making it appears as though there is uptake inhibition. Superfusion technique was first developed to

address this problem. It is based on the presumption that if the rate of perfusion is rapid enough, DAT uptake could be ignored and any change from the baseline is considered as additional release (Raiteri et al., 1974). Using this technique, it was demonstrated that amphetamine caused DA release and this release could be blocked by uptake inhibitors like cocaine (Parker and Cubeddu, 1986). *In vivo* microdialysis experiments confirmed these results and further showed that amphetamine-induced release is independent of neuron firing (Nomikos et al., 1990).

After the cloning of DAT, $[^3H]$-1-methyl-4-phenylpridinium ion (MPP^+), which could be taken up by DAT, was discovered and used to measure amphetamine-induced release or efflux. Neurotoxin MPP^+ is a major metabolite of neurotoxin 1-methyl-4-phenyl-1,2,3,6-tetrahydropridine (MPTP) that can cause permanent symptoms of PD in human and mammals. Amphetamine and its derivatives inhibited uptake of substrate $[^3H]$-MPP^+ and stimulated transporter-mediated efflux of the preloaded $[^3H]$-MPP^+ in cell lines that stably express DAT (Wall et al., 1995). The effect of cocaine and amphetamines on DAT is illustrated in Figure I-2.
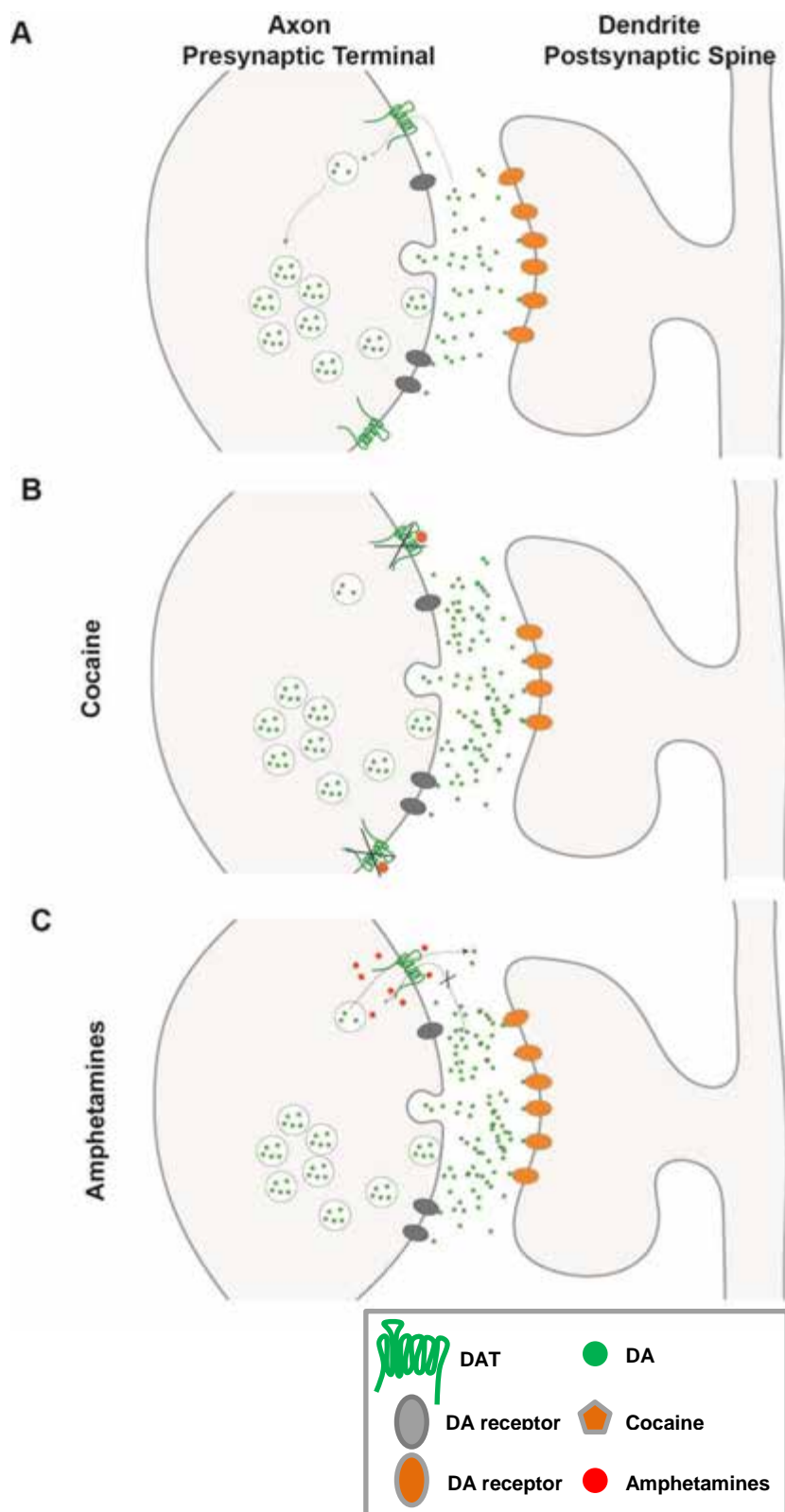
Figure I-2. DAT is a direct molecular target for psychostimulants cocaine and amphetamines. A. Normally, released DA is removed from synapses through DAT-mediated high affinity reuptake. **B.** Cocaine is a competitive inhibitor for DAT. It directly binds to DAT and inhibits DAT reuptake function that results in elevated synaptic DA levels and prolonged effect on target neurons. **C**. Amphetamines are DAT substrates that are transported into the presynapse by DAT and cause DAT-mediated DA efflux. The dual effects of uptake inhibition and DA efflux result in enhanced synaptic DA levels and prolonged stimulation on pre- and post-synaptic receptors.

STRUCTURE/FUNCTION OF NEURONAL DAT

The first insight into a DA transport mechanism came from the observation that extracellular sodium was required for substrate translocation (Wheeler et al., 1993). It is well-established that DAT requires sequential binding of two sodium ions and cotransport of one chloride ion to translocate DA across the plasma membrane. The driving force for DAT-mediated reuptake is the sodium concentration gradient across the plasma membrane generated by Na^+/K^+ ATPase. Extensive biochemical and mutagenesis studies in heterologous expression systems have been performed aiming to elucidate the secondary structure of DAT. The substituted cysteine accessibility method (SCAM) was used to determine residue accessibility and define the role of individual residues for binding of substrates or inhibitors. The Cysteine 342 at the third intracellular loop of DAT were more reactive to the thiol-modifying agents during uptake, suggesting this residue may be located on part of DAT associated with cytoplasmic gating (Chen et al., 2000). Using site-directed mutagenesis, Loland et al. showed that mutation of intracellular tyrosine to alanine (Y335A) completely abolished DA uptake, further supporting the third intracellular loop's role in the substrate translocation (Loland et al., 2002). In search for the DA binding site, studies were conducted by mutating aromatic and acidic amino acids in transmembrane domains (TMDs). Replacement of aspartate and serine residues in TMD1 and TMD7, respectively drastically reduced DA uptake (Kitayama et al., 1992) and mutating phenylalanine155 in TMD3 to alanine also abolished DA

affinity, suggesting these residues are required for substrate recognition (Lin et al., 1999).

A major breakthrough to determine the tertiary structure of DAT came from the high resolution crystal structure of bacterial Leucine transporter (LeuT) with sequence homology and functional similarities to the *SLC6* transporters (Yamashita et al., 2005). It was reported from the LeuT crystal structure that TMD1, TMD3, TMD6 and TMD8 formed the central substrate binding pocket to accommodate the substrate (Leucine) and two sodium ions. Three states of transport mechanisms were proposed: outward-facing, occluded and inward-facing. Substrate and sodium binding happened in an occluded state devoid of water.

However, the LeuT model has limitations in terms of answering questions like some parts of the structures of *SLC6* transporters that share minimum similarity to LeuT, as well as substrate selectivity and transport inhibition by addictive compounds. In 2013, a 3.0 Å x-ray crystal structure of the *Drosophila melanogaster* dopamine transporter (dDAT) in complex with TCA nortriptyline was reported (Penmatsa et al., 2013). It captured dDAT in an inhibitor-bound, outward facing conformation and showed TCA nortriptyline targeted the substrate binding site and stabilized the open conformation. Two sodium and one chloride ions were located adjacent to the nortriptyline binding pocket, indicating direct coupling of ions and inhibitor binding. Intriguingly, this crystal structure also

revealed a cholesterol binding site and a C-terminal latch that interacted with the cytoplasmic face of the transporter, presumably for modulation of transport function. More recently, the same group published another dDAT crystal structure in complex with its substrate DA, as well as psychostimulants cocaine and amphetamine (Wang et al., 2015). The DAT central binding pocket was further divided into three subsites and the subsites were responsible for defining ligand specificity. Substrates including DA, DA analogue 3,4-dichlorophenethylamine (DCP) and amphetamine were bound to DAT prior to full closure of the extracellular gate, rather than the occluded state shown in LeuT. In contrast, inhibitors like cocaine were bound to the outward-facing DAT, acting like a wedge to block DAT in an outward-open conformation. Altogether, the structural information of DAT provides a molecular basis for designing more selective monoamine transporter inhibitors.

Other than the classic transport mechanism, DAT also exhibits channel-like activity. In human DAT-expressing Xenopus laevis oocytes, two-electrode voltage-clamp recording revealed a constitutive leak current that was different from transport-associated current in terms of ion and voltage dependence (Sonders et al., 1997). The physiological consequences of both transport-associated current and constitutive leak current was shown to modulate DA neuron excitability, as DAT substrates DA and amphetamine increased the firing rate of cultured rat DA neurons (Ingram et al., 2002; Carvelli et al., 2004).

In summary, DAT belongs to the *SLC6* gene family of sodium and chloride-dependent symporters. It is a direct molecular target for psychostimulants cocaine and amphetamines. Cocaine acts as a competitive inhibitor that binds DAT at its outward facing state, whereas amphetamines are DAT substrates that could be transported through DAT and subsequently lead to DA efflux. ADHD therapeutic agents Ritalin (methylphenidate) and Adderall (amphetamine/dextroamphetamine) also directly act on DAT, making DAT an important molecular target for treating certain types of neuropsychiatric disorders.

I.D Dopamine Transporter: Role In Neuropsychiatry Disorders

The physiologic role of DAT in an intact animal was first studied in DAT knock-out (KO) mice generated by *in vivo* homologous recombination technique (Giros et al., 1996). These mice exhibited spontaneous hyperlocomotion. Biochemical changes in striatal DA neurotransmission assessed by FSCV showed drastically increased extracellular DA clearance time in KO animals, which could explain the marked increase in the spontaneous locomotor activity. Intriguingly, KO mice also displayed significant reduction in evoked DA release, suggesting that the tissue content of DA or the releasable pool of DA were decreased. Direct measurement of DA content by HPLC revealed that DA levels were reduced by 95% in the dorsal striatum of KO mice compared with wild-type (wt) mice(Jones et al., 1998b). These results demonstrated that DAT is a key regulator of maintaining presynaptic DA homeostasis and when inactivated, profound

neuronal plasticity occurs. In this section, I will discuss DAT's role in drug addiction as well as recent human genetic studies that link DAT to multiple neuropsychiatric disorders.

DOPAMINE TRANSPORTER IN DRUG ADDICTION

As discussed previously, psychostimulants cocaine and amphetamine inhibit DAT function through different mechanisms. The net effect is a marked increase of synaptic DA levels that leads to prolonged stimulation of dopaminoceptive neurons. This event is considered as the basis for the rewarding effect of cocaine and amphetamine.

Early attempts to understand DAT's role in drug addiction came mainly from studies in DAT-KO mice. In homozygous mice, psychostimulants cocaine and amphetamine failed to further increase locomotor activity, suggesting DAT plays a vital role of locomotor effects of psychostimulants (Giros et al., 1996). Paradoxically, the rewarding property of cocaine remained. DAT KO mice still self-administrated cocaine (Rocha et al., 1998) and cocaine conditioned a place preference in these animals (Sora et al., 1998). Even though analysis of released DA by microdialysis in DAT KO mice clearly showed cocaine and amphetamine failed to increase DA levels in dorsal striatum, they still elevated DA levels in NAc (Carboni et al., 2001), probably through indirect regulation on the DA neurons in VTA (Budygin et al., 2002). Mapping of the sites of cocaine binding and neuronal activation suggested serotonergic brain regions might be involved in this

response (Rocha et al., 1998). Further studies reported that DAT and SERT double KO mice eliminated cocaine-induced CPP, indicating both dopaminergic and serotonergic mechanisms are required for the rewarding effect of cocaine (Sora et al., 2001).

Using DAT-KO mice as a model to study DAT's role in addiction raised some concerns. Most of all, complete deletion of DAT caused tremendous adaptive changes in DA neurotransmission in terms of DA synthesis, storage and receptor expression and function (Jones et al., 1999). These adaptive changes may significantly alter the normal reward pathway. Thus, Chen at al. proposed another way to test the DA hypothesis of cocaine reward by generating a knock-in (KI) mouse line expressing a mutant DAT (L104V/F105C/A109V) that could still transport DA but had substantially reduced affinity for cocaine (Chen et al., 2006). Therefore, doses of cocaine that normally inhibit wild-type DAT would not have an effect on this mutant DAT. The cocaine-insensitive DAT KI mice completely abolished cocaine-induced CPP while maintaining amphetamine's effect. Cocaine also failed to stimulate locomotor activity in these mice. Biochemically, in the NAc, there was no significant increase in extracellular DA levels following cocaine but not amphetamine treatment in the KI mice, consistent with the behavior results. These data demonstrated that blockade of DAT is required for cocaine reward in mice with a functional DAT, and further confirmed the idea that cocaine-induced increase in extracellular DA in the NAc is critical in mediating cocaine reward.

Amphetamine's action on DA neurotransmission is more complicated than cocaine. Amphetamine acts both on vesicular storage of DA and directly on DAT. Using the DAT KO mice, Jones et al determined that the vesicle-depleting action was the rate limiting factor in amphetamine's biochemical effect (Jones et al., 1998a). Since vesicular monoamine transporter (VMAT) functions to concentrate cytoplasmic DA into synaptic vesicles (Eiden et al., 2004), studies have focused on VMAT's role in amphetamine's locomotor and rewarding properties. Heterozygous VMAT2 KO mice, which expressed ~50% of VMAT2 compared to wt littermates, displayed enhanced amphetamine-induced locomotion but diminished reward behavior as measured by CPP (Takahashi et al., 1997). More recently, a selective VMAT2 inhibitor, (+)-CYY477, blocked both locomotor and self-administration behaviors stimulated by amphetamines without affecting those induced by cocaine (Freyberg et al., 2016). These results indicate that VMAT2, but not DAT, plays a critical role in the acute actions of amphetamines but not those of cocaine.

DOPAMINE TRANSPORTER IN NEUROPSYCHIATRIC DISORDERS

The fact that DAT is an important target site for some therapeutic agents makes it a candidate gene for neuropsychiatric disorders. *In vivo* brain imaging techniques, such as PET, using selective DAT ligands, have been wildly used to measure monoamine transporter levels in neuropsychiatric disorders (Laakso and Hietala, 2000). These studies reported reduced DAT densities in patients

with ADHD, PD and major depression (Kim et al., 1997; Dougherty et al., 1999; Laasonen-Balk et al., 1999). Based on this evidence, studies have been focused on the identification of polymorphic variants in the coding and non-coding regions of DAT. The first discovery that linked a DAT polymorphism to ADHD was the association between ADHD and the 10-repeat allele variable number tandem repeat (VNTR) in the 3'-untranslated region (3'-UTR) of human DAT (Cook et al., 1995; Curran et al., 2001). Studies examining the functional variants in hDAT coding sequence might help clarify relationships between DAT activity and the risk for neuropsychiatric disorders. Using temperature gradient capillary electrophoresis, Mazei-Robison and colleagues screened 112 subjects that were diagnosed with ADHD and identified one nonsynonymous single nucleotide polymorphism (SNP) A559V in two male siblings (Mazei-Robison et al., 2005). Biochemical and function analysis in heterologous expression system showed that this A559V DAT coding variant had normal DA uptake and surface expression but exhibited anomalous DA efflux (Mazei-Robison et al., 2008). Remarkably, the two most common ADHD medications, amphetamine and methylphenidate, both blocked A559V DAT-mediated DA efflux, whereas these drugs had opposite actions at wt-DAT. To pursue the significance of this finding *in vivo*, the same group generated an A559V DAT KI mouse line and observed elevated extracellular DA levels, lack of amphetamine-stimulated DA efflux and disruptions in basal and psychostimulant-evoked locomotor behavior in these animals compared with wild-type littermates (Mergy et al., 2014). Additional DAT

coding variants have been identified that are associated with ADHD, autism spectrum disorder (ASD) and adult Parkinsonism (Sakrikar et al., 2012; Hamilton et al., 2013; Hansen et al., 2014).

Other than polymorphism studies, human molecular genetic studies have recently discovered an autosomal recessive disorder that is directly caused by missense DAT mutations. To understand molecular basis of infantile parkinsonism-dystonia (IPD), Kurian and colleagues identified two *DAT* homozygous missense mutations (L368Q and P395L) in two relating families using autozygosity mapping techniques (Kurian et al., 2009). As a severe neurological syndrome that usually involves complex movement disorder with dystonia, axial hypotonia and limb hypertonicity, IPD is rare but is often misdiagnosed since the clinical symptoms can mimic certain types of cerebral palsy (Assmann et al., 2004). Functional analysis of mutant DAT proteins showed that both mutants were devoid of uptake activity and failed to express at the plasma membrane. This disorder was named dopamine transporter deficiency syndrome and the same group later identified eleven more children with this disorder (Kurian et al., 2011). These findings further demonstrate the importance of DAT in DA homeostasis in humans.

Together, the findings described above demonstrate that inhibition of DAT function in NAc is a prerequisite for the rewarding property of cocaine but not amphetamine. Loss-of-function DAT mutations cause dopamine transporter

deficiency syndrome in humans and multiple DAT coding variants are associated with neuropsychiatric disorders such as ADHD, ASD and adult parkinsonism.

I.E Dopamine Transporter: Regulation

Shortly after the cloning of the gene encoding DAT, much effort has been directed towards understanding the molecular and cellular mechanisms for regulating DAT activity and membrane availability at the presynaptic membrane. These studies have resulted in identification of kinases, receptors, lipids and scaffolding proteins that modulate DAT biosynthesis, targeting to the plasma membrane and endocytic trafficking. Key domains and residues have also been found in the DAT amino acid sequence that allows regulation of transporter function through direct protein-protein interactions. In this section, I will discuss DAT regulatory mechanisms at three different stages: synthesis and targeting to the plasma membrane, endocytosis, as well as post-endocytic sorting. Finally, I will review known DAT interacting proteins and how they regulate DAT activity.

SYNTHESIS AND TARGETING DAT TO THE PLASMA MEMBRANE

Biosynthesis and assembly of DAT, as well as other plasma membrane proteins, occurs at the endoplasmic reticulum (ER) and Golgi apparatus inside the cell. Compelling evidence suggests that DAT exists as oligomeric complexes inside the cell and oligomerization is required for successful export of transporters from the ER. The apparent molecular weight of DAT increased from approximately 85kDa to approximately 195kDa determined with nonreducing SDS-PAGE after

cross-linking with either copper phenanthroline or bis-(2-methanethiosulfonatoethyl) amine hydrochloride, indicating the transporters formed a homodimer (Hastrup et al., 2001). Cysteine 306 (Cys306) at the extracellular end of TMD6 was then identified to function at the dimerization interface. This result was confirmed later using co-immunoprecipitation (Co-IP) of DAT with different tags as well as Fluorescent Resonance Energy Transfer (FRET) on live cells (Sorkina et al., 2003; Torres et al., 2003b). FRET data suggested that DAT oligomerized both at the plasma membrane and ER and that co-expression of an ER-retained DAT blocked ER exit of wt-DAT, suggesting a role for oligomerization in efficient ER export (Sorkina et al., 2003). DAT sequence that is responsible for efficient ER export was examined using systematic deletions and alanine substitutions in the DAT C-terminus and subsequently looking at cellular localization with live cell fluorescent microscopy and cell surface biotinylation (Miranda et al., 2004). The C-terminal glycine 585, lysine 590 and glutamine 600 were identified and, when mutated into alanine, these three DAT mutants failed to traffic to the dendrites or axon processes in cultured primary rat midbrain neurons.

Anterograde transport of cargos from ER to Golgi is mediated by specific coat protein complexes (COP). Sec24 is one of the components and is involved in cargo recognition and recruitment at the ER (Lord et al., 2013). It was shown that DAT and NET, but not SERT, used Sec24D for ER export (Sucic et al., 2011). Knocking down Sec24D, but not Sec24C in Hela cells decreased DA uptake.

Moreover, the DAT C-terminal lysine leucine (KL) sequence was proposed to interact with the COPII machinery.

At the Golgi, transporters undergo post-translational modifications. N-linked glycosylation sites in the second extracellular loop were found in all monoamine transporters. Different glycosylation patterns of DAT were identified in different species, different brain regions and during development (Lew et al., 1991; Patel et al., 1993; Patel et al., 1994). Functional importance of N-linked glycosylation was examined using transporter mutants that abolished these sites. These mutants displayed reduced expression at the plasma membrane but retained ligand binding and substrate transport properties, suggesting N-linked glycosylation is essential for transporter membrane targeting (Tate and Blakely, 1994; Melikian et al., 1996; Li et al., 2004)

Following the synthesis and export from ER and the Golgi apparatus, DAT is targeted to the plasma membrane. Electron microscopy studies using immunogold labeling showed that DAT was localized at the plasma membrane of both perisynaptic region of presynaptic membrane as well as somatodendritic compartments (Hersch et al., 1997; Nirenberg et al., 1997b). Yet, the molecular mechanisms that are responsible for targeting DAT to these different subcellular locations are not clear.

Using DAT C-terminus as bait in a yeast two-hybrid screening, PICK1, a PDZ domain protein interacting with C-kinase 1, was identified as a DAT interacting

protein (Torres et al., 2001). The PDZ binding site in DAT was mapped to the last three residues at the C-terminus (LKV). Coexpression of DAT and PICK1 in HEK293 cells promoted DAT surface levels. Deletion of the PDZ-binding site of DAT abolished the PICK1 association and failed to target DAT to the axons. These results suggested that the PDZ-mediated DAT-PICK1 interaction might be involved in the presynaptic targeting of DAT. However, subsequent investigation of DAT C-terminus function revealed that disruption of the PDZ-binding domain either through addition of an alanine to the hDAT C terminus (+Ala), or alanine substitutions of LKV (AAA_618-620) affected neither plasma membrane targeting nor targeting into sprouting neurites of differentiated N2A cells (Bjerggaard et al., 2004). Instead, alanine substitutions of RHW (615-617) caused transporter ER retention while preserving its ability to bind PICK1. Thus, although residues in the hDAT C-terminus are indispensable for proper targeting, PDZ domain interactions are not required. In order to understand the functional significance of the PDZ-binding domain in DAT *in vivo*, Rickhag et al. generated two different DAT KI mice with disrupted PDZ-binding motif (DAT-AAA and DAT+Ala) (Rickhag et al., 2013). Surprisingly, both mice lines exhibited drastic loss of DAT expression in striatum that led to hyperlocomotion and attenuated response to amphetamine. These phenotypes were not dependent on PICK1 since PICK KO mice displayed normal DAT immunoreactivity both in the DA neuron cell body and terminals. These findings suggest that PDZ-domain interactions are critical for synaptic distribution of dopamine transporter *in vivo*, but DAT-PICK1

interaction may not be required. How the DAT PDZ-domain modulates its plasma membrane targeting is still not clear. I will address this question in Chapter III.

Taken together, these studies demonstrate that DAT oligomerization is required for transporter ER export and the DAT C-terminal sequence contain residues important for ER export and subsequent plasma membrane targeting.

DAT ENDOCYTOSIS

Plasma membrane DAT undergoes constitutive and regulated endocytic trafficking between plasma membrane and endosomal compartments. Elucidation of DAT primary sequence revealed potential phosphorylation sites for protein kinases such as protein kinase A and C (PKA and PKC) and calmodulin-dependent kinase II (CaMKII), indicating that phosphorylation may regulate DAT function (Gorentla et al., 2009). In COS cells transiently expressing DAT, Kitayama et al. first observed that activation of PKC using phorbol 12-myristate 13-acetate (PMA) decreased ligand binding and uptake velocity (Kitayama et al., 1994). This downregulation of DAT activity was also reported in other heterologous cell lines as well as synaptosome preparations (Copeland et al., 1996; Vaughan et al., 1997; Zhu et al., 1997). Kinetic studies of [^{3}H]-DA uptake showed that the PMA-induced reduction of DAT activity was due to a decrease in maximum uptake velocity (V_{max}) with no change in substrate affinity (K_m), suggesting PKC regulated DAT activity by decreasing DAT surface levels (Copeland et al., 1996). In addition, electron microscopy studies revealed a

significant intracellular/endosomal DAT pool in DA neurons, further supporting that DAT may undergo regulated endocytosis (Nirenberg et al., 1997b). Direct examination of DAT endocytosis using either biochemical tools or immunofluorescence demonstrated that PKC activation reduced steady-state DAT surface levels (Daniels and Amara, 1999; Melikian and Buckley, 1999). The mechanisms facilitating this sequestration were first demonstrated by Loder and Melikian. They showed that DAT robustly internalized at basal state and PKC activation accelerated DAT endocytosis and that these two processes were mediated by distinct mechanisms (Loder and Melikian, 2003).

Given that PKC activation increased DAT phosphorylation (Huff et al., 1997; Vaughan et al., 1997), it was hypothesized that the functional effect of PKC activation on DAT was directly coupled to phosphorylation. Using peptide mapping and epitope-specific immunoprecipitation, Foster et al. identified a group of six serines clustered at the distal end of the cytoplasmic N terminus that were responsible for most of the basal and PKC-stimulated DAT phosphorylation (Foster et al., 2002). However, truncation of the first 22 amino acids at the N-terminus containing these serines abolished detectable phosphorylation without affecting the PMA-induced reduction in transport capacity and endocytosis. In this background truncation construct, systematic mutation of all the phosphorylation consensus serines and threonines (Thr) in hDAT, alone and in various combinations, also did not alter the PMA effect in either HEK293 or N2A cells (Granas et al., 2003). These results indicate that PKC-stimulated DAT

endocytosis is not directly mediated by phosphorylation. The underlying mechanism and role of phosphorylation is not entirely clear. Thr53 was reported to be strongly phosphorylated by PMA in rodent striatal tissue and heterologous expression system and mutation of this residue reduced DAT V_{max} and abolished amphetamine-induced substrate efflux, suggesting Thr53 is required for transport mechanism (Foster et al., 2012). Ser6 was also reported to modulate transporter kinetics (Moritz et al., 2015).

Most of the studies mentioned above used phorbol esters such as PMA to activate PKC, which mimics diacylglycerols (DAG). There are two classes of PKC that require DAG to be activated, the conventional PKC isoforms that requires both DAG and Ca^{2+}, as well as the novel PKC isoforms that do not require Ca^{2+} for activation (Dempsey et al., 2000). What is the isoform specificity for PKC regulation of DAT? Different PKC isoform-specific inhibitors were used to identify specific PKC isoforms that could block PMA's effect on DAT-associated transport current (Doolen and Zahniser, 2002). Selective inhibitors of conventional PKC, novel PKC isoform PKCδ and Ca^{2+} chelator EGTA significantly reversed PMA's effects while novel PKC isoform, PKCε had no effect. Thus the primary PKC isoforms that regulate DAT activity and function are the conventional PKC isoforms. Further work exploring PKC isoform specificity revealed a more complicated mechanism of these kinases. Conventional PKC isoform PKCβ KO mice had reduced striatal surface DAT, [3H]-DA uptake and amphetamine-induced DA efflux yet exhibited higher novelty-induced locomotor activity,

supporting the role of PKCβ in DAT regulation (Chen et al., 2009). Moreover, PKCβ specific inhibitor LY279196 blocked the D2 agonist quinpirole-induced increase in DAT surface levels and activity, indicating that PKCβ functioned to elevate DAT surface levels, opposite to phorbol ester stimulation (Chen et al., 2013).

In addition to basal and PKC-stimulated endocytosis (Loder and Melikian, 2003; Sorkina et al., 2005), substrates and inhibitors also dynamically regulate DAT surface levels. Substrates such as DA and amphetamine promoted DAT endocytosis (Saunders et al., 2000; Chi and Reith, 2003; Johnson et al., 2005; Furman et al., 2009b), whereas cocaine exposure was reported to increase DAT surface levels (Daws et al., 2002; Little et al., 2002). Since endocytic trafficking acutely regulates plasma membrane protein availability, providing means of enhancing or diminishing DA neurotransmission, much effort has been directed towards understanding the molecular mechanisms of basal and regulated DAT endocytic trafficking. Specifically, studies have focused on two fundamental questions: 1) what are the endocytic signals that target DAT for basal and regulated endocytosis? And 2) what are the endocytic machineries that mediate basal and regulated DAT endocytosis?

By overexpressing a dominant negative dynamin-1 mutant (K44A), Daniels and Amara showed that PKC-stimulated DAT endocytosis was abolished and thus concluded that PKC-stimulated DAT endocytosis is clathrin-mediated (Daniels

and Amara, 1999). However, some forms of clathrin independent endocytosis pathways also require dynamin (Sauvonnet et al., 2005; Fattakhova et al., 2006). In clathrin-mediated endocytosis (CME), cargo protein is recruited by clathrin adaptor proteins into clathrin-coated pits (CCP). The membrane then invaginates and pinches off the plasma membrane via GTPase dynamin, giving rise to clathrin-coated vesicles (CCV). The clathrin coat eventually disassociates from the vesicle and matures into early endosomes (Saheki and De Camilli, 2012). For cargo proteins that internalize through the clathrin-dependent pathway, they usually contain two classes of endocytic signals, the dileucine and tyrosine-containing motifs, that allow clathrin adaptor proteins to recognize and recruit to CCP (Bonifacino and Traub, 2003). In searching for the DAT endocytic signals, Holton et al. tested candidate dileucine-type endocytic motifs in DAT (Holton et al., 2005). Surprisingly, after alanine-scanning mutagenesis of all the potential dileucine-type endocytic motifs, DAT still underwent basal and PKC-stimulated endocytosis tested through cell surface biotinylation, suggesting the DAT endocytic signal may not confine to the classically defined motifs. Instead, they conducted a gain-of-function screen by fusing the DAT N- and C- termini to the endocytic-defective membrane proteins and looked for robust internalization. Their results revealed that the DAT C-terminal FREKLAYAIA sequence is a novel endocytic signal for both basal and PKC-stimulated DAT endocytosis. To further define residues that governed basal and PKC-stimulated DAT endocytosis, the same group performed systematic alanine scanning mutagenesis within the

FREKLAYAIA motif and showed that alanine substituting DAT residues FREK (587-590) abolished PKC-stimulated DAT endocytosis, and markedly accelerated basal DAT internalization, comparable to that of wt-DAT during PKC activation (Boudanova et al., 2008b). Based on these results, the PKC-sensitive DAT endocytic brake model was proposed where PKC activation releases the DAT endocytic brake and the brake requires DAT FREK (587-590) residues. Consistent with the endocytic braking mechanism, DAT N-terminus was shown to negatively regulated DAT endocytosis and when deleted, DAT internalized more rapidly (Sorkina et al., 2009). These studies strongly suggested that both the intracellular DAT N- and C- termini are required for the DAT endocytic brake. Nevertheless, cellular factors that control this endocytic brake is unknown. I will address this question in Chapter II.

The fact that DAT does not contain classic endocytic signals for clathrin-mediated endocytosis raises questions about whether DAT internalizes through clathrin-dependent or independent pathways as well as whether DAT uses different endocytic machineries for basal vs. regulated endocytosis. Other than the dominant negative dynamin I mutant (K44A) (Daniels and Amara, 1999; Eriksen et al., 2009), knocking down endogenous clathrin heavy chain and dynamin II in cells lines with small interference RNA (siRNA) abolished basal and PKC-stimulated DAT endocytosis (Sorkina et al., 2005). Nonetheless, clathrin depletion over days could potentially affect other membrane trafficking processes

that also require clathrin. Thus, control experiments are necessary to test whether clathrin-independent endocytic mechanisms are intact.

On the other hand, studies that examined DAT plasma membrane distribution and microdomain association revealed that DAT at least partially resided within the membrane lipid raft microdomains in neuronal derived cell line and synaptosomes (Adkins et al., 2007; Foster et al., 2008; Navaroli et al., 2011). Given that clathrin-independent endocytosis usually occurs at the lipid raft microdomains (Doherty and McMahon, 2009), Cremona et al. sought to understand the functional importance of DAT microdomain association and identified a lipid raft associated protein, flotillin-1 (Flot-1) as a mediator for PKC-stimulated DAT endocytosis (Cremona et al., 2011). Either knocking down Flot-1 with siRNAs or alanine substitution of a Flot1 palmitoylation site (C34A) abolished PKC-stimulated DAT endocytosis. Nonetheless, this result was challenged by a follow-up study done by Sorkina et al. They also used siRNAs to knockdown endogenous Flot1 and saw no inhibition of PKC-stimulated DAT endocytosis measured by a fluorescent antibody feeding assay (Sorkina et al., 2013).

The controversial results from the early studies may arise from the fact that dominant-negative protein overexpression and siRNA knockdown experiments require multiple days of treatments that could potentially affect normal cell function and protein trafficking in general. Development of specific inhibitors to

acutely block clathrin-mediated endocytosis provided a better way to answer these questions (Hill et al., 2009; Dutta et al., 2012). In fact, using *ex vivo* mouse striatal slice biotinylation, Gabriel et al. showed that acute dynamin inhibition with specific inhibitor, dynole, blocked PKC-stimulated DAT endocytosis but basal DAT endocytosis was unaffected (Gabriel et al., 2013). Although this study demonstrated a differential dependence upon dynamin for basal vs. PKC-stimulated DAT endocytosis, it still did not address whether clathrin was required, since there are dynamin-dependent mechanisms that are independent of clathrin (Sauvonnet et al., 2005; Fattakhova et al., 2006). I will address this question in studies in Chapter II.

Additional kinase pathways have been reported to modulate DAT endocytosis. Acute inhibition of phosphatidylinositol (PI) 3-kinase (PI3K), a component of the insulin pathway, triggered DAT endocytosis in synaptosomes and HEK cells (Carvelli et al., 2002). Further investigation of the downstream signaling of the insulin pathway revealed that Akt/PKB, a protein kinase effector immediately downstream of PI3K, also negatively regulated DAT endocytosis (Garcia et al., 2005). Moreover, expression of a constitutively active Akt mutant reduced the ability of AMPH to decrease hDAT cell-surface expression, suggesting that Akt not only regulated basal DAT endocytosis but also modulate amphetamine-stimulated DAT endocytosis. These results were confirmed *in vivo* using hypoinsulinemia rats that were depleted of insulin through the diabetogenic agent streptozotocin (STZ) (Williams et al., 2007). STZ treated rats exhibited reduced

striatal Akt function, decreased DAT surface levels and impaired amphetamine-induced DA efflux and self-administration, suggesting that the insulin signaling pathway dynamically regulates DAT function and DA neurotransmission. There is also evidence that mitogen-activated protein kinase (MAPK) and tyrosine kinases negatively regulated DAT function and surface levels, reported in both heterologous expression systems and synaptosomes (Doolen and Zahniser, 2001; Moron et al., 2003; Hoover et al., 2007).

DAT POST-ENDOCYTIC SORTING

After endocytosis, cargo proteins can be sorted for degradation or export to other cellular membrane compartments like the trans-Golgi network (TGN) (retrograde) or the plasma membrane (recycling). Different endocytic trafficking pathways are illustrated in Figure I-3. Many studies have investigated DAT's post-endocytic itinerary, each with its own strengths and weaknesses. Studies have aimed to answer two fundamental questions: 1) how does DAT interact with the sorting machineries? And 2) what are the DAT post-endocytic itineraries under basal and regulated conditions?
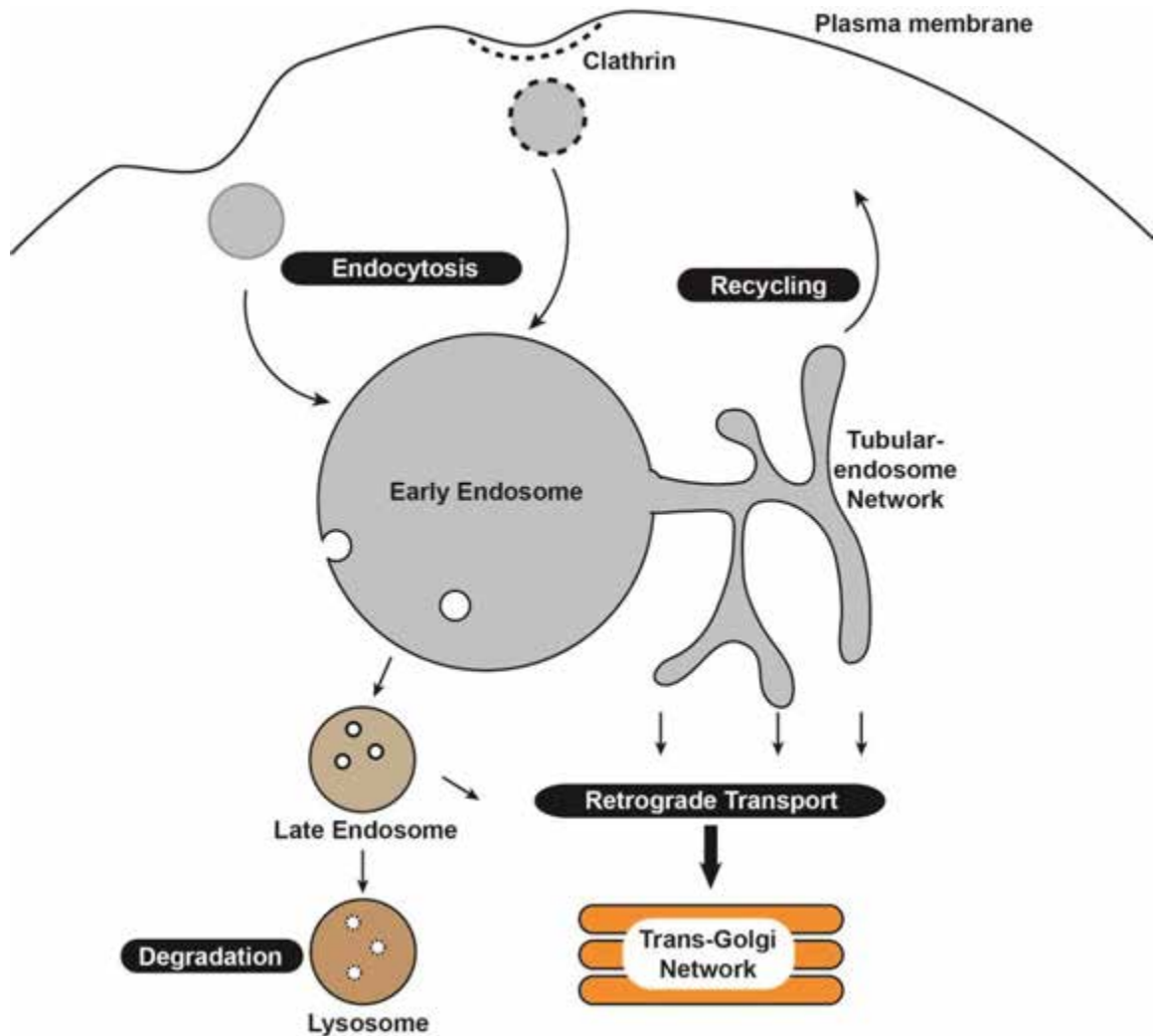
Figure I-3. Overview of endocytic trafficking pathways. Internalized cargo proteins are either sorted for degradation through the late endosome/lysosome pathway or exported to other organelles for reuse. Recycling pathways reinsert cargo protein back to the plasma membrane while retrograde pathways transport cargos to the trans-Golgi network.

Melikian et al. first showed that after subcellular fractionation, the internalized DAT was enriched in transferrin receptor (TfR)-positive endosomal recycling compartments in PC12 cells (Melikian and Buckley, 1999). Using a biotinylation assay, Loder and Melikian reported that DAT constitutively recycles and PKC activation decreased DAT recycling rate, suggesting that DAT recycles back to the plasma membrane under basal and PKC-stimulated conditions (Loder and Melikian, 2003). Consistent with this result, Lee et al. reported that DAT interacted with the DA D2 receptor and this interaction promoted DAT reinsertion into the plasma membrane (Lee et al., 2007). This process was modulated by PKCβ activity (Chen et al., 2013). More recently, Richardson et al. showed that membrane potential changes alone rapidly drive DAT internalization from and reinsertion to the plasma membrane (Richardson et al., 2016). These function studies strongly suggest that DAT recycles back to the plasma membrane after endocytosis.

Conversely, Miranda et al. showed that DAT was constitutively ubiquitinated and PKC activation drastically increased DAT ubiquitination that led to rapid transporter degradation (Miranda et al., 2005). Ubiquitination is a form of post-translational modification that is associated with the cell's major degradation pathways including lysosomes, proteasomes and autophago-lysosomes (Clague et al., 2012). Later, the same group identified an E3 ubiquitin ligase, Nedd4-2 (neural precursor cell expressed, developmentally downregulated 4-2), in a RNA interference screen, that was required for PKC-mediated DAT ubiquitination and

endocytosis (Sorkina et al., 2006). These results indicate that DAT is sorted for degradation through ubiquitin-dependent pathways.

Another set of studies aimed to understand DAT post-endocytic sorting via dynamic imaging experiments to track labeled DAT. Using a green fluorescent protein-tagged DAT (GFP-DAT), Daniels et al. reported that in an epithelia cell line, the internalized transporters were targeted to the lysosomal pathway and were completely degraded within 2 hrs of PKC activation (Daniels and Amara, 1999).

More recently, Eriksen et al. developed a fluorescent cocaine analog, JHC1-64, that enabled selective labeling of plasma membrane DAT. Using this compound, they reported that constitutively internalized DAT was primarily colocalized with late endosome marker rab7, less with short-loop recycling endosome marker rab4 and little with long-loop recycling endosome marker rab11 in AN27 cells as well as in primary cultured midbrain neurons (Eriksen et al., 2010b). Nonetheless, given the fact that cocaine itself increases DAT surface levels (Daws et al., 2002; Little et al., 2002), inhibitor analog could potentially mistarget DAT post-endocytosis. A complimentary approach was used where one transmembrane protein, Tac, was fused to the DAT N-terminus (Tac-DAT), followed by an antibody-feeding assay to track the Tac-DAT post-endocytic route (Eriksen et al., 2010b). Functional characterization revealed that the Tac-DAT fusion protein had drastically reduced uptake activity and increased apparent affinity for cocaine,

questioning the viability of this approach. Nonetheless, the same colocalization pattern was observed with Tac-DAT compared with the JHC1-64 compound. Based on these results, they concluded that constitutively internalized DAT was sorted to late endosomes/lysosomes and in part to a Rab4-mediated short loop recycling pathway.

Studying DAT post-endocytic itinerary in heterologous expression systems may not reflect what really happens in native DA neurons. To address this question, Rao et al. generated a KI mouse line expressing a hemagglutinin (HA)-tagged DAT (HA-EL2-DAT) (Rao et al., 2012). The HA epitope was inserted into the second extracellular loop (EL2) of DAT to allow selective labeling of plasma membrane DAT and subsequently tracking the transporter regional and subcellular distribution using an antibody feeding assay (Sorkina et al., 2006). Immunofluorescence and electron microscopy data revealed that in midbrain somatodendritic regions, a small fraction of HA-EL2-DAT was present in early and recycling endosomes and little in late endosomes and lysosomes (Block et al., 2015). In the dorsal striatum, little intracellular DAT was observed. However, it is unknown whether internalized DAT bound to a bulky antibody would accurately reflect native DAT endocytic targeting, particularly in light of recent studies demonstrating that proteins which undergo endocytic recycling target to degradation if they internalize bound to antibody (St Pierre et al., 2011).

Given the caveats in all of these studies, and limitations of the approaches they used, there is still an open question as to how DAT traffics in the absence of bound inhibitor analog or bulky antibodies. These questions will be addressed in the studies described in Chapter III.

REGULATION OF DAT THROUGH PROTEIN-PROTEIN INTERACTIONS

The discovery of regulated DAT trafficking indicated the involvement of transport-interacting proteins. In addition, DAT expression at the presynaptic sites of DA neurons presumably involves interactions with other intracellular proteins in DA neurons.

To test potential direct protein–protein interactions between α-synuclein and DAT, Lee et al. incorporated different domains of hDAT into the DNA binding domain of a yeast two hybrid system and examined their abilities to interact with the DNA-activating domains expressing full-length α-synuclein (Lee et al., 2001). Their results showed that DAT C-terminus directly bound to α-synuclein. The functional consequences of this interaction are unclear. In mouse fibroblast LtK(-) (leukocyte tyrosine kinase) cells, α-synuclein was reported to negatively modulate DAT activity (Wersinger and Sidhu, 2003), whereas a study in human neuronal cells revealed a 50% reduction of DAT activity upon siRNA knockdown of α-synuclein, suggesting endogenous α-synuclein promotes DAT activity (Fountaine and Wade-Martins, 2007). Nonetheless, α-synuclein KO mice did not

show any changes in DAT function (Dauer et al., 2002), questioning the importance of DAT-α-synuclein interaction *in vivo*.

Since then, yeast two hybrid screenings were widely used in search of DAT interacting proteins. Using hDAT C-terminus as a bait against human brain cDNA library, CaMKII was identified and shown to direct interacted with the DAT C-terminus last 11 amino acids and colocalize with DAT in cultured DA neurons (Fog et al., 2006). The DAT/CaMKII interaction promoted amphetamine-induced DA efflux. In addition, CaMKII phosphorylated serines in DAT distal N termini *in vitro*, and mutation of these serines abolished the stimulatory effects of CaMKII on amphetamine-induced DA efflux. These data suggest that CaMKII binding to the DAT C-terminus facilitates phosphorylation of the DAT N terminus and mediates amphetamine-induced DA efflux. Interestingly, mice that lack αCaMKII or express a permanently self-inhibited αCaMKII exhibited significantly reduced amphetamine-induced MPP$^+$ efflux (Steinkellner et al., 2012). Consistent with these findings, coexpression of a CaMKII inhibitory peptide and hDAT in DA neurons of dDAT KO larvae blunted amphetamine-induced hyperlocomotion, demonstrating the importance of DAT/CaMKII interaction in amphetamine-induced reward behavior (Pizzo et al., 2014).

Syntaxin1A was also one of the proteins that was identified through a yeast two hybrid screening and was shown to interact with the DAT N-terminus (Lee et al., 2004). Amphetamine was reported to increase the syntaxin1A/DAT association in

a cell line and in striatal synaptosomes, probably through a CaMKII-dependent mechanism (Binda et al., 2008).

Using the hDAT C-terminal novel endocytic signal sequence FREKALAYAIA as a bait to probe a human substantial nigra cDNA library, Ras-like GTPase, Rin (for Ras-like in neurons; Rit2), was identified as a protein that interacted with DAT C-terminal endocytic signal (Navaroli et al., 2011). Disruption of Rin function with GTPase mutants and shRNA-mediated Rin knockdown revealed that Rin was critical for PKC-mediated DAT internalization and functional downregulation.

Since DAT and the DA D2 receptor both localize at the presynaptic membrane of DA neurons, Lee et al. sought to test whether there was a interaction between the two. Co-IP and domain analysis revealed a interaction between the DAT N-terminus and the third intracellular loop of D2 receptor (Lee et al., 2007). This physical coupling facilitated the reinsertion of intracellular DAT to the plasma membrane and led to enhanced DA reuptake. Injecting inhibitory peptides into mice that disrupt the DAT-D2 receptor interaction resulted in decreased synaptosome DA uptake and enhanced locomotor activity, suggesting this interaction affects DA neurotransmission *in vivo*. Supporting this idea, D2 receptor KO mice displayed decreased DAT function (Dickinson et al., 1999).

Other DAT interacting proteins include protein phosphatase 2A (PP2A) (Bauman et al., 2000), LIM domain-containing adaptor protein Hic-5 (Carneiro et al., 2002), E3 ubiquitin ligase Parkin (Moszczynska et al., 2007) and synaptic vesicle protein

synaptogyrin-3 (Egana et al., 2009). The functional importance of the interactions of these proteins with DAT, especially *in vivo*, remains to be carefully characterized.

Although much progress has been made to understand how DAT surface availability and function are regulated, important questions regarding the molecular mechanisms of DAT endocytosis and post-endocytic itinerary under basal and regulated conditions remain to be elucidated. This thesis aims to address some of these questions and controversies in the field and provide insight into future studies on DAT endocytic trafficking.

PREFACE TO CHAPTER II

This chapter has been published separately in:

Wu S, Bellve KD, Fogarty KE, Melikian HE (2015) Ack1 is a dopamine transporter endocytic brake that rescues a trafficking-dysregulated ADHD coding variant. *Proc Natl Acad Sci U S A* 112:15480-15485.

Author contributions:

Wu S, Bellve KD, Fogarty KE and Melikian HE designed research.

Wu S performed research.

Bellve KD and Fogarty KE contributed new reagents/analytic tools.

Wu S and Melikian HE analyzed data.

Wu S and Melikian HE wrote the paper.

Bellve KD provided technical support for TIRF microscopy experiments.

CHAPTER II

Ack1 Is A Dopamine Transporter Endocytic Brake That Rescues A Trafficking-Dysregulated ADHD Coding Variant

II.A Summary

DAT stringently controls brain dopamine levels. Several addictive psychostimulants, antidepressants and ADHD therapeutics inhibit DAT function and multiple DAT mutants have been reported in ADHD, ASD, and Infantile Parkinsonism. Given that aberrant DAT function underlies many pathological conditions, it is critical to understand intrinsic regulatory mechanisms that modulate DAT function. DAT availability at the cell surface is dynamically modulated, but the mechanisms controlling this process are not well understood. In the current study, we identified the penultimate mechanism that controls DAT stability at the cell surface. Moreover, by genetically manipulating this mechanism we successfully rescued an ADHD-associated DAT mutant with intrinsic membrane instability. Thus, targeting DAT regulatory mechanisms may be a viable approach for treating dysregulated DAT.

II.B Introduction

Dopamine (DA) is a modulatory neurotransmitter critical for locomotion and reward (Hyman et al., 2006) and DAergic dysregulation is linked to multiple neuropsychiatric disorders, including Parkinson's Disease, schizophrenia, attention deficit-hyperactivity disorder (ADHD) and autism spectrum disorder (ASD) (Snyder, 2002; Iversen and Iversen, 2007). Presynaptic recapture, facilitated by the high-affinity DA transporter (DAT) spatially and temporally restricts extracellular DA availability (Amara and Kuhar, 1993; Kristensen et al., 2011; Broer and Gether, 2012). Addictive psychostimulants that target DAT and its monoamine transporter homologs for 5HT (SERT) and NE (NET) are either competitive ligands, such as cocaine, or competitive substrates, such as amphetamine (Torres et al., 2003b). Although these drugs interact with DAT, SERT and NET with equimolar affinity, their binding to DAT is requisite for reward (Chen et al., 2006; Thomsen et al., 2009). Transporter inhibitors with differential DAT, SERT and NET specificity are widely used to treat neuropsychiatric disorders (Gether et al., 2006; Iversen, 2006). However, their therapeutic efficacy differs significantly among patients, consistent with the model that monoamines may differentially contribute to the pathogenesis of these disorders (Tamminga et al., 2002; Iversen, 2006). Thus, regulatory mechanisms specific to DAT, SERT or NET may provide a novel route to develop transporter-specific therapeutics.

DAT plasma membrane expression is requisite for efficacious extracellular DA removal and to replenish presynaptic DA stores (Jones et al., 1998b). Indeed, DAT allelic and coding variants have been identified in a variety of neuropsychiatric disorders, including ADHD, ASD, Infantile Parkinsonism and bipolar disorder (Mazei-Robison et al., 2008; Pinsonneault et al., 2011; Sakrikar et al., 2012; Hamilton et al., 2013; Bowton et al., 2014; Hansen et al., 2014; Mergy et al., 2014), underscoring that even subtle DAT functional changes exert impactful consequences on dopaminergic neurotransmission. DAT is acutely regulated by membrane trafficking, and either protein kinase C (PKC) activation or AMPH exposure rapidly depletes DAT surface expression (Torres et al., 2003b; Melikian, 2004; Kristensen et al., 2011; Rudnick et al., 2014). Intriguingly, a DAT coding variant, R615C, identified in an ADHD proband, exhibits profound membrane instability, due to highly accelerated basal endocytosis (Sakrikar et al., 2012), suggesting that dysregulated DAT membrane trafficking may contribute to the etiology of DA-related disorders.

Studies from our lab (Boudanova et al., 2008b) and others (Sorkina et al., 2009) indicate that a unique negative regulatory mechanism, or "endocytic brake", stabilizes DAT surface expression. PKC activation releases the endocytic brake, accelerates DAT internalization, and thereby reduces DAT surface levels and function. The cellular mechanisms facilitating this negative regulatory mechanism are completely undefined. Moreover, it is unknown whether the endocytic brake exists in DAergic terminals and whether it is specific to DAT.

Activated by **c**dc42 **k**inase 1 (Ack1) is a non-receptor tyrosine kinase that is a major cdc42 effector activated via EGF, PDGF and m3 muscarinic receptor stimulation (Linseman et al., 2001; Galisteo et al., 2006). Ack1 binds directly to clathrin heavy chain (Teo et al., 2001; Yang et al., 2001) and is enriched in presynaptic terminals (Urena et al., 2005). Importantly, Ack1 is inactivated by PKC (Linseman et al., 2001) and a recent study demonstrated that Ack1 overexpression suppresses endocytosis (Shen et al., 2011). Given these attributes, we asked whether Ack1 activity is the penultimate step engaging the DAT endocytic brake.

II.C Material And Methods

Materials: Full length human Ack1 (hAck1) wild-type, K158A cDNAs in pEF-1α/pENTRA vector were kindly provided by Dr. Ingvar Ferby (Ludwig Institute for Cancer Research, Uppsala UP, Sweden) and were subcloned into pcDNA3.1(+) at BamH1/EcoR1 sites. hAck1 S445P pcDNA3.1(+) cDNA was generated from wildtype hAck1 by Quikchange mutagenesis (Agilent Technologies). Human DAT (hDAT) cDNA cloned into pcDNA3.1(+) was previously described (Gabriel et al., 2013), and hSERT and hDAT(R615C) cDNAs were the generous gift of Dr. Randy Blakely (Vanderbilt University). Rat anti-DAT (MAB369) and rabbit anti-phospho-Ack1 (pY284) were from EMD Millipore. Mouse anti-Ack1 (clone A11) and mouse anti-actin were from Santa Cruz Biotechnology. Horseradish peroxidase (HRP)-conjugated secondary antibodies were from EMD Millipore

(anti-rat), Santa Cruz (anti-rabbit) and Pierce (anti-mouse). [^{3}H]DA (dihydroxyphenylethylamine 3,4-[ring-2,5,6-^{3}H]) and L-[^{3}H]alanine were from Perkin Elmer Life and Analytical Sciences. Sulfo-NHS-SS-biotin, Tris(2-carboxyethyl)phosphine hydrochloride (TECP), and streptavidin agarose were from Thermo Fisher Scientific. AIM-100, phorbol 12-myristate 13-acetate (PMA), casin and GBR12909 (1-[2-[Bis-(4-fluorophenyl)methoxy]ethyl]-4-(3-phenylpropyl)piperazine dihydrochloride) were from Tocris Bioscience. Pirl1 (8-cyclopentyl-2,3,3a,4,5,6-hexahydro-1H-pyrazino[3,2,1-jk]carbazole methanesulfonate) was from ChemBridge Corporation and pitstop2 was from Abcam. All other chemicals and reagents were from Sigma-Aldrich or Thermo Fisher Scientific and were of highest grade possible.

Cell Culture and Transfections: SK-N-MC cells were from American Type Culture Collection (ATCC) and were maintained in MEM (Sigma-Aldrich M2279) supplemented with 10% fetal bovine serum (Invitrogen), 2mM L-glutamine, 10^2 U/ml penicillin/streptomycin, 37°C, 5% CO_2. Clonal #12 and pooled stable SK-N-MC cell lines expressing either hDAT or hSERT, respectively, were generated by transfecting 1×10^6 cells/well in 6-well culture plate with 3µg plasmid DNA using Lipofectamine 2000, at lipid:DNA ratio of 2:1 (w/w). Stably transfected cells were selected with 0.5 mg/ml G418 (Invitrogen) and resistant cells were either pooled or selected by single colonies and maintained under selective pressure in 0.2 mg/ml G418. For DAT/Ack1 transient co-transfection studies, 4×10^5 cells were

transfected with a total of 1.5µg plasmid DNA at a DAT:Ack1 (or vector) ratio of 1:4 and were assayed 48 hours post-transfection.

$[^3H]DA$ and $[^3H]$alanine Uptake Assays in Cell lines: DAT-SK-N-MC cells were seeded in 96-well tissue culture plates at a density of 7.5×10^4 cells/well one day before performing assays. Cells were washed twice with Krebs-Ringer-HEPES (KRH) buffer (120mM NaCl, 4.7mM KCl, 2.2mM $CaCl_2$, 1.2mM $MgSO_4$, 1.2mM KH_2PO_4, 10mM HEPES, pH 7.4) and incubated in KRH supplemented with 0.18% glucose (KRH/g), 37°C for the indicated times with indicated drugs. DA transport was initiated by adding either 1µM $[^3H]DA$ or 0.5mM $[^3H]$alanine in KRH/g supplemented with 10µM each pargyline and sodium L-ascorbate and proceeded for 10 min, 37°C. Transport was terminated by rapidly washing cells with ice-cold KRH buffer, cells were solubilized in scintillation fluid, and accumulated radioactivity was measured by liquid scintillation counting in a Wallac MicroBeta scintillation plate counter (Perkin Elmer). 100nM desipramine was included in all samples to block uptake contributed by endogenously expressed NET. Non-specific DA uptake was defined with 10µM GBR12909 and Na^+-dependent alanine transport was defined by substituting NaCl with 120 mM choline chloride.

Lentiviral production and transduction: Short hairpin RNA (shRNA) targeting hAck1 from Open Biosystems were purchased from University of Massachusetts Medical School RNAi Core. All shRNAs were cloned into the pGIPZ vector which co-expresses turbo GFP (tGFP). shRNA sequences were as follows:

Non-silencing (Luciferase 693):

TGCTGTTGACAGTGAGCGCTCTAAGAACGTTGTATTTATATAGTGAAGCCAC

AGATGTATATAAATACAACGTTCTTAGATTGCCTACTGCCTCGGA

Ack sh#10:

TGCTGTTGACAGTGAGCGATACCTGCTTCTTCCAGAGAAATAGTGAAGCCA

CAGATGTATTTCTCTGGAAGAAGCAGGTACTGCCTACTGCCTCGGA

Ack sh#12:

TGCTGTTGACAGTGAGCGAAAGGTGTTCAGTGGAAAGCGATAGTGAAGCCA

CAGATGTATCGCTTTCCACTGAACACCTTATGCCTACTGCCTCGGA

For lentivirus production: Replication incompetent lentiviral particles were produced according to the Addgene 2nd generation pLKO.1 protocol (https://www.addgene.org/tools/protocols/plko/). Briefly, 4.4×10^6 HEK293T cells/dish were seeded in 150mm dishes one day prior to transfection and were co-transfected with 6.25µg shRNA (or control) plasmid, 4.7µg psPAX2 packaging plasmid, 1.56µg pMD2.G envelope plasmid, combined in Opti-MEM reduced serum media (Invitrogen) with 37.5µl Fugene 6 (Promega). Transfection mixtures were added dropwise to cells, incubated at 37°C, 5% CO_2, and were removed and replaced with fresh growth medium 12-16 hours post-transfection. Viral supernatants were collected 48 and 72 hours post-transfection, aliquoted and stored at -80°C. Titers were determined by transduction into HEK293T cells and counting GFP-positive cells 48 hours post-transduction. Experiments were performed using a minimum of three independent viral preparations.

For Lentiviral Transduction: 5×10^6 DAT-SK-N-MC cells/dish were seeded into 100mm dishes one day prior to viral transduction and were infected with 50ml of the indicated crude lentivirus supplemented with 8µg/ml polybrene. Virus was removed 24 hours post-infection and transduced cells were enriched by selecting with 1µg/ml puromycin for 48 hours. Cells were replated into 6 well dishes 48 hours post-infection and were assayed 72 hours post-infection.

Cell Surface Biotinylation: DAT surface levels in SK-N-MC cells were determined by steady state biotinylation as previously described (Navaroli et al., 2011; Gabriel et al., 2013). Briefly, cells were treated with the indicated drugs for the indicated times in PBS^{2+}/g/BSA (phosphate-buffered saline, pH 7.4, supplemented with 1mM $MgCl_2$ and 0.1mM $CaCl_2$, 0.18% glucose, 0.1% IgG-/protease-free BSA), and were rapidly cooled by repeated washing in ice-cold PBS^{2+}. Cells were labeled twice, 15 min, 4°C with 1.0 mg/ml sulfo-NHS-SS-biotin in PBS^{2+} and excess biotinylation reagent was quenched twice, 15 min, 4°C with PBS^{2+}/100mM glycine. Excess glycine was removed by washing three times in ice-cold PBS^{2+} and cells were lysed in RIPA buffer (10mM Tris, pH 7.4, 150mM NaCl, 1mM EDTA, 0.1%SDS, 1%Triton-X-100, 1% sodium deoxycholate) containing protease inhibitors. Lysates were cleared by centrifugation and protein concentrations were determined by BCA protein assay kit (Pierce). Lysate aliquots were stored in denaturing SDS-PAGE sample buffer at -20°C until analysis. Biotinylated proteins from equivalent amount of cellular protein were recovered by batch streptavidin affinity chromatography (overnight, 4°C) and

bound proteins were eluted in denaturing SDS-PAGE sample buffer, 30 min, room temperature with rotation. Samples were analyzed by SDS-PAGE and indicated proteins were detected by immunoblotting. Immunoreactive bands were detected with SuperSignal West Dura (Pierce) and were captured using the VersaDoc Imaging station (Biorad). Non-saturating bands were quantified using Quantity One software (Biorad).

Mouse Striatal Slice Assays: All animals were handled in accordance with University of Massachusetts Medical School IACUC protocol A-1506 (H.E.M.). P21-P38 male C57BL/6 mice were sacrificed by cervical dislocation and decapitation and mouse brains were rapidly removed and immediately chilled in ice cold sucrose- and kynurenic acid (1mM)- supplemented artificial CSF (SACSF) (2.5mM KCl, 1.2mM NaH_2PO_4, 1.2mM $MgCl_2$, 2.4mM $CaCl_2$, 26mM $NaHCO_3$, 11mM glucose, 250mM sucrose) saturated with 95% O_2/5% CO_2. Brains were mounted on Leica VT1200S Vibratome and 300µm coronal sections were prepared. Striatal sections corresponding to the range between Bregma 1.54–0.34 (using corpus callosum as a landmark) were harvested, hemisected along the midline, and recovered 40min, 31°C in 95%O_2/5%CO_2-saturated ACSF (125mM NaCl, 2.5mM KCl, 1.2mM NaH_2PO_4, 1.2mM $MgCl_2$, 2.4mM $CaCl_2$, 26mM $NaHCO_3$, 11mM glucose) containing 1mM kynurenic acid. Hemi-slices were treated with the indicated drugs for the indicated times and temperatures in oxygenated ASCF, using the contralateral hemi-slice as the control.

For pAck1 and total Ack1 assessment: Slices were lysed in RIPA buffer containing protease inhibitors and Phosphatase Inhibitor Cocktail V (EMD Millipore) by triturating through a 200μl pipet tip and rotating 30min, 4°C. Protein concentrations were determined using the BCA protein assay and equivalent amounts of lysate were resolved by SDS-PAGE and underwent immunoblot with the indicated antibodies. pAck1 levels were normalized to total Ack1 levels, developed in parallel.

For striatal slice biotinylation: Surface proteins were covalently labeled with 1.0mg/ml sulfo-NHS-SS biotin in ice-cold ACSF, 45min, 4°C. Residual reactive biotin was quenched by incubating twice with ice-cold ACSF supplemented with glycine, 20min, 4°C. Slices were then washed with ice-cold ACSF and lysed in RIPA buffer containing protease inhibitors by triturating through a 200μl pipet tip and rotating 30min, 4°C. Protein concentrations were determined using the BCA protein assay and biotinylated proteins were isolated as described for cell lines, above, using a striatal lysate:streptavidin agarose bead ratio of 20μg lysate:30μl streptavidin agarose in order to quantitatively recover all biotinylated DAT in the linear range of recovery.

Striatal Slice [^{3}H]DA uptake: DA uptake was determined in 300μm striatal hemi-slices from P21-P24 male C57BL/6 mice, prepared as described above. Following recovery, hemi-slices were pretreated ±20μM AIM-100, 1 hr, 37°C in oxygenated ASCF, using the contralateral hemi-slice as the vehicle control. DA

transport was initiated by adding 1µM [^{3}H]DA in ACSF supplemented with 10µM each pargyline and sodium L-ascorbate and proceeded for 10min, 37°C. 100nM desipramine was included in all pretreatments to block uptake contribution from the norepinephrine transporter. Uptake was terminated by rapidly washing slices with ice-cold ACSF, followed by three 5 min incubations in ice-cold ACSF with gentle shaking. Slices were lysed in RIPA buffer containing protease inhibitors, 30 min, 4°C, and insoluble material was removed by centrifugation at 18,000 x g, 10 min, 4°C. Protein concentrations were determined using the BCA protein assay (Pierce) and accumulated [^{3}H]DA was quantified, in triplicate, from each hemi-slice lysate (150 µg total tissue lysate per replicate) by liquid scintillation counting. Given that DAT expression is highly variable along the rostral-caudal axis, relative DAT levels for each hemi-slice were determined in parallel by immunoblotting, using actin as a loading control. Hemi-slice uptake values were subsequently normalized to their respective relative DAT expression levels so that bona fide differences in uptake across slices could be accurately determined. Non-specific [^{3}H]DA accumulation was defined in the presence of 10µM GBR12909, averaged from two independent hemi-slices per mouse.

Internalization Assays: Cells were plated onto 6-well tissue culture plates at a density of 1x10^6 cell/well one day prior to assays. Cells were biotinylated twice, 15min, 4°C with 2.5 mg/ml sulfo-NHS-SS-biotin. After glycine quenching, zero time points and strip controls remained at 4°C, and internalized samples were warmed to 37°C by multiple rapid washes in prewarmed PBS^{2+}, 0.18% glucose,

0.1% IgG/protease-free BSA with the indicated drugs. Internalization proceeded in the same solutions for 10 min, 37°C, was stopped by washing repeatedly with ice-cold NT buffer(150mM NaCl, 20mM Tris, pH 8.6, 1mM EDTA, 0.2% IgG-/protease-free BSA), and residual surface biotin on experimental and strip control samples was cleaved by reducing twice for 25min, 4°C in 100mM TCEP in NT buffer. Cells were washed thrice in PBS^{2+}, lysed in RIPA buffer with protease inhibitors and biotinylated proteins were isolated and analyzed by immunoblot as described for steady state biotinylation, above. Stripping efficiencies were calculated for each sample and were >95% of total surface protein labeled at t=0. Internalization rates were calculated as the percentage DAT internalized over 10min as compared to total surface DAT labeled at t = 0.

TIRF microscopy studies: SK-N-MC cells stably expressing either TagRFP-T-DAT and eGFP-clathrin, or eGFP-clathrin alone, were plate on glass coverslips one day prior to imaging and media was replaced with KRH/0.18% glucose/0.1% BSA, 37°C for live imaging. To label transferrin receptors in eGFP-clathrin SK-N-MC cells, 1µg/ml human transferrin-Alexa594 (Life Technologies) was added in the imaging solution. TIRF images in red and green channels were captured using TESM microscope (Biomedical Imaging Group, University of Massachusetts Medical School) (Navaroli et al., 2012). Briefly, images of through-the-lens TIRF were generated using 491nm (for eGFP-clathrin) and 561nm (for TagRFP-T-DAT or transferrin-Alexa594) laser illumination together with an Olympus TIRF 60 X objective (N.A. = 1.49) at an angel set to visualize

around 200nM from the glass coverslip. Focus stabilization was controlled by an in-house made software called pgFocus (Biomedical Imaging Group, http://big.umassmed.edu/wiki/index.php/PgFocus). PgFocus is an open source and open hardware focus stabilization device that autonomously adjusts a piezo-positioned objective in response to the positional change of a reflected 808nm laser beam. PgFocus is able to modify and pass on piezo-positon control signals from other devices, which allows pgFocus to identify the expected focus position and adjust accordingly. PgFocus operates at 30Hz with ±3nm accuracy and integrates with MicroManager. Time-lapse image data were acquired at 1Hz using MicroManager open source microscopy software (https://www.micro-manager.org/). Images were then exported as tiff files and analyzed in ImageJ.

II.D Results

Ack1 negatively regulates DAT, but not SERT endocytosis.

Ack1 and its active, autophosphorylated form, pY284-Ack1 (pAck1) (Yokoyama and Miller, 2003; Galisteo et al., 2006), were readily detected in both the dopaminergic cell line SK-N-MC and mouse striatum (Figs. II-1A, II-1B). PKC activation significantly decreased pAck1 in both SK-N-MC cells (46.5±3.0% control levels, Fig. II-1A) and mouse striatum (78.3±5.2% control levels, Fig. II-1B). Likewise, the highly specific Ack1 inhibitor AIM-100 (Mahajan et al., 2010) dose-dependently decreased pAck1 in SK-N-MC cells (Fig. II-1C), and dramatically decreased mouse striatal pAck1 to 13.2±2.2% control levels (Fig. II-

1D). Thus, Ack1 is expressed in dopaminergic cell lines and striatum, and either PKC activation or AIM-100 inactivate Ack1 in both these model systems.

We predicted that if Ack1 imposes the DAT endocytic brake, then Ack1 inactivation would release the brake and decrease both DAT function and surface expression. Indeed, AIM-100 significantly decreased [^{3}H]DA uptake in SK-N-MC cells (IC_{50} = 50.2 ±9.9 µM) and striatal slices (Fig. II-2A, 2B), and significantly reduced DAT surface levels to 72.5±6.4% control levels in mouse striatum (Fig. II-2C). DAT surface loss in response to AIM-100 was due to a significant increase in the DAT internalization rate, to 192.9±28.6% control levels (Fig. II-2D), demonstrating that Ack1 negatively regulates DAT endocytosis. AIM-100 effects were specific to DAT, and had no effect on the SERT endocytic rate measured in SERT-SK-N-MC cells (Fig. II-2D, p=0.89). Interestingly, high AIM-100 concentrations (>20µM) inhibited DAT function to a much larger degree than what could be attributed to membrane trafficking. This was not due to transmembrane Na^+ gradient disruption, as AIM-100 had no effect on Na^+-dependent alanine uptake (Fig. II-3A). To our surprise, AIM-100 also dose-dependently inhibited SERT function (Fig. II-3B), despite exerting no effect on SERT trafficking (Fig. II-2D). We noted that AIM-100 bears DAT and SERT pharmacophore properties similar to piperazine derivatives, such as GBR12909 (Fig. II-3C). We therefore hypothesized that, in addition to its known function as a high affinity Ack1 inhibitor, AIM-100 may also be a low affinity, competitive DAT and SERT inhibitor. Whole cell binding studies revealed that AIM-100

competitively inhibited DAT and SERT binding to [³H]WIN 35428 and [³H]imipramine, respectively, (Fig. II-3D), supporting the premise that AIM-100 is a DAT and SERT inhibitor. However, GBR12909 had no effect on pAck1 levels (Fig. II-3E), indicating that DAT ligand binding does not globally inactivate Ack1. Moreover, a ten-fold lower AIM-100 concentration that efficaciously decreased p284-Ack1 levels (2µM, Fig. II-1C), also significantly increased DAT internalization rates (Fig. II-3F). Thus, distinct endocytic mechanisms regulate DAT and SERT, and Ack1 activity is required to impose the DAT endocytic brake. Moreover, AIM-100 is, coincidentally, a low affinity, competitive DAT and SERT inhibitor.

Constitutive and regulated DAT endocytosis are differentially dependent on clathrin

Ack1 is recruited to clathrin-coated-pits via clathrin heavy chain interactions (Teo et al., 2001; Yang et al., 2001). Thus, we hypothesized that clathrin is required to release the Ack1-imposed brake. To test this, we acutely inhibited clathrin with pitstop2 and measured DAT internalization ±AIM-100 and ±PMA. Pitstop2 pretreatment significantly attenuated both AIM-100- and PKC-stimulated DAT internalization, but had no effect on basal DAT endocytosis (Figs. II-4A, 4B) suggesting that stimulated DAT endocytosis is clathrin-dependent whereas constitutive DAT endocytosis is clathrin-independent. We further used TIRFM to examine clathrin and surface DAT under basal conditions, compared to

transferrin receptor (TfR), a protein known to undergo robust clathrin-mediated endocytosis. Alexa594-Tf co-localized markedly with eGFP-clathrin across the plasma membrane, and distinct Tf/clathrin puncta moved away from the TIRF field during imaging; consistent with clathrin-mediated endocytosis (Fig. II-4C). In contrast, TagRFP-T-DAT was diffusely distributed across the plasma membrane and was enriched in cellular microspikes, with little apparent clathrin co-localization (Fig. II-4C). Taken together with the pitstop2 data, these data support that constitutive DAT endocytosis is clathrin-independent, whereas stimulated DAT endocytosis requires clathrin.

Cdc42 negatively regulates DAT, but not SERT, endocytosis.

Ack1 is a major cdc42 effector, suggesting that cdc42 may contribute to the DAT endocytic brake, upstream of Ack1. To test this possibility we measured DAT surface levels in DAT SK-N-MC cells and striatal dopaminergic terminals following acute treatment with two structurally distinct cdc42 inhibitors, casin and pirl1. Both casin and pirl1 significantly reduced DAT surface levels in SK-N-MC cells (Fig. II-5A, 5B) and casin significantly decreased surface DAT in mouse striatum (Fig. II-5C). DAT surface loss was due to profound DAT endocytic acceleration ($238.0\pm15.5\%$ control levels, Fig. II-5D). In contrast, pirl1 did not significantly affect SERT internalization (Fig. II-5E). We further tested whether PKC and cdc42 impact DAT surface stability in independent or convergent manners. Pretreatment ±casin (Fig. II-5A) or ±pirl1 (Fig. II-5B) significantly

attenuated PKC-stimulated DAT endocytosis. Moreover, pirl1 and PMA co-application had no additive effect on DAT internalization (Fig. II-5D). Taken together, these results demonstrate that cdc42 activity is required to impose the DAT endocytic brake, likely via the same pathway as PKC and potentially upstream of Ack1. Moreover, these results further support that distinct endocytic mechanisms govern DAT and SERT surface stability.

Ack1 inactivation is required to release the DAT endocytic brake, downstream of PKC or cdc42.

We next used two efficacious hAck1-targeted shRNAs, #10 and #12 (Fig. II-6A), to test whether Ack1 is required to 1) engage the DAT endocytic brake, and 2) stimulate DAT endocytosis by PKC activation or cdc42 inhibition. The most efficacious hAck1 shRNA, #10, significantly increased basal DAT endocytosis to $138.7\pm12.3\%$ control levels (Fig. II-6C), consistent with Ack1's requisite role as the DAT endocytic brake. Moreover, Ack1 depletion with either shRNA #10 or #12 significantly attenuated stimulated DAT endocytosis, either via PKC stimulation (Fig. II-6D) or cdc42 inhibition (Fig. II-6E). In sum, these results support that Ack1 is required to engage the DAT endocytic brake.

Although perturbing Ack1 enhanced DAT endocytosis, we next asked whether there is a direct causal link between Ack1 inactivation and either cdc42 inhibition or PKC activation in order to release the DAT endocytic brake. To test this, we co-expressed DAT with either wildtype, constitutively active (S445P) or kinase

dead (K158A) Ack1 isoforms (Lin et al., 2012) (See Fig II-7A,7B,7C, for Ack1 mutant overexpression profiles). We predicted that if Ack1 inactivation were required to release the DAT endocytic brake, then S445P-Ack1 would block accelerated DAT internalization in response to either PKC activation or cdc42 inhibition. Wildtype Ack1 overexpression had no effect on basal or accelerated DAT endocytosis in response to PKC activation or cdc42 inhibition (Fig. II-7E, 7F, 7G). In contrast, S445P-Ack1 significantly attenuated both PKC-stimulated (Fig. II-7F) and pirl1-stimulated (Fig. II-7G) DAT internalization. K158A-Ack1 had no significant effect either basal ($p=0.30$) or pirl1-stimulated ($p=0.30$) DAT internalization (Fig. II-7E, II-7G), but significantly inhibited PKC-stimulated DAT endocytosis ($100.1\pm5.2\%$ control level, Fig. II-7F). Although the K158A mutant lacks kinase activity (Mahajan et al., 2005), it was unknown, *a priori,* whether this mutant would exert a dominant negative effect. Ack1 activation is required for targeting to clathrin-coated pits (Shen et al., 2011). Thus, it is not surprising the kinase dead mutant failed to exert a dominant effect on DAT internalization. Taken together, these results provide a causal link between upstream PKC, or cdc42, stimuli and Ack1 inactivation as requisite steps in releasing the DAT endocytic brake.

Ack1 activity restores normal trafficking to a DAT coding variant expressed in an ADHD proband

A recent study reported that a DAT coding variant, R615C, identified in an ADHD proband, lacks endocytic braking, resulting in enhanced basal endocytosis and inability to undergo PKC- and AMPH-stimulated endocytosis (Sakrikar et al., 2012). We asked whether constitutive Ack1 activation could restore the endocytic brake and thereby rescue the DAT(R615C) gain-of-function endocytic phenotype. DAT(R615C) expressed in SK-N-MC cells internalized significantly faster than wildtype DAT (Fig. II-10E, 10F) and was defective in PKC-stimulated endocytosis (Fig. II-7B), consistent with the previous report (Sakrikar et al., 2012). Remarkably, S445P-Ack1 significantly decreased DAT(R615C) basal endocytosis to wildtype DAT levels (Fig. II-8B), but did not restore PKC-stimulated endocytosis (Fig. II-8C).

II.E Discussion

Reuptake inhibitors are used to treat a variety of neuropsychiatric disorders, including depression, obsessive-compulsive disorder and ADHD (Iversen, 2000, 2006). These agents are differential selective for SERT, NET and DAT, and their clinical efficacy varies considerably across the population (Tamminga et al., 2002; Iversen, 2006). Transporter-specific cellular regulation has the potential to lead to novel and selective therapeutic approaches that manipulate transporters intrinsically, rather than extrinsically. In the current study, we identified an endocytic regulatory mechanism that is selective for DAT, but not SERT. We previously reported that PKC-stimulated DAT internalization is also selectively

dependent upon binding to the neuronal GTPase, Rin, whereas neither SERT nor the GABA transporter binds Rin (Navaroli et al., 2011). Taken together with our current findings, this is consistent with a model wherein distinct mechanisms differentially regulate DAT and SERT surface stability.

Conflicting reports regarding whether constitutive and regulated DAT internalization are clathrin-dependent. Gene silencing studies suggest that both constitutive and PKC-stimulated DAT internalization in non-neuronal cell lines are clathrin-dependent (Sorkina et al., 2005); although whether chronic clathrin depletion artifactually skews these studies is uncertain. A recent study examining DAT trafficking in a knock-in mouse encoding a DAT extracellular epitope tag observed only modest DAT endocytosis and little/no clathrin co-localization under basal conditions (Block et al., 2015). However, it is unclear whether antibody-bound DAT traffics similar to native DAT, as we investigate here. Multiple studies also demonstrate that DAT partitions into cholesterol-rich membrane microdomains (Adkins et al., 2007; Foster et al., 2008; Cremona et al., 2011; Navaroli et al., 2011; Jones et al., 2012; Gabriel et al., 2013; Kovtun et al., 2015), and that the membrane raft protein flotillin-1 is required for PKC- and AMPH-mediated DAT internalization (Cremona et al., 2011), consistent with a clathrin-independent endocytic mechanism. However, a separate study reported that flotillin-1 contributes to DAT membrane mobility rather than PKC-stimulated DAT internalization (Sorkina et al., 2013). Our findings suggest that basal DAT internalization is clathrin-independent, whereas stimulated DAT internalization is

clathrin-dependent. Consistent with these data, we previously reported that basal and PKC-stimulated DAT internalization are mediated by independent mechanisms (Loder and Melikian, 2003; Holton et al., 2005), and that constitutive and PKC-stimulated DAT internalization are dynamin-independent and –dependent, respectively (Gabriel et al., 2013).

Cdc42 directly activates Ack1 and cdc42 inhibition released the DAT endocytic brake in a manner that required Ack1 inactivation (Fig. II-7G). Several forms of clathrin-independent endocytosis require cdc42 (Massol et al., 1998; Sabharanjak et al., 2002; Gauthier et al., 2005). In contrast, we found that cdc42 negatively regulates DAT endocytosis via Ack1 activation (Fig. II-5), and that stimulated DAT endocytosis in response to Ack1 inactivation is clathrin-dependent (Fig. II-4). Thus, it appears that cdc42 impacts DAT internalization in a unique fashion, in contrast to its more commonly known function in promoting endocytosis.

Given our current findings, and in light of previous reports, we propose the following model of basal and PKC-regulated DAT endocytosis (Fig. II-9). Under basal conditions, an Ack1-mediated endocytic brake stabilizes DAT at the plasma membrane, and cdc42 promotes the braking mechanism via Ack1 activation. Basal internalization that occurs while the endocytic brake is engaged is clathrin-and dynamin-independent. PKC activation decreases Ack1 activity, which releases the endocytic brake and accelerates DAT internalization via a

clathrin- and dynamin-dependent mechanism, resulting in intracellular DAT sequestration.

What are the molecular players orchestrating the Ack1-imposed DAT endocytic brake and PKC-mediated Ack1 inactivation? PIP_2 depletion inactivates Ack1 (Shen et al., 2011) and both DAT (Hamilton et al., 2014) and SERT (Buchmayer et al., 2013) bind to PIP_2. However, DAT mutants lacking PIP_2 binding exhibited plasma membrane instability in HEK cells, whereas disrupting SERT/PIP_2 interactions did not affect SERT membrane trafficking. This raises the possibility that PIP_2 effects on Ack1 activity may specifically influence DAT surface stability. PKC activation also increases DAT ubiquitination via a Nedd4-2-mediated mechanism that is required for enhanced DAT endocytosis (Vina-Vilaseca and Sorkin, 2010). Nedd4-2 also interacts with Ack1 and is recruited to clathrin-rich vesicles (Chan et al., 2009), and Nedd4-2/Ack1 interactions drive Ack1 degradation in an Ack1 activity-dependent fashion. Thus, it is possible that Nedd4-2 serves as a dual function player in the DAT endocytic brake by controlling Ack1 protein turnover as well as DAT ubiquitination.

Multiple DAT coding variants and missense mutants have been reported in ADHD, ASD and Infantile Parkinsonism patients, implicating DAT dysfunction as a common risk factor for several DA-related disorders (Mazei-Robison et al., 2008; Sakrikar et al., 2012; Hamilton et al., 2013; Hansen et al., 2014). Many DAT coding variants exhibit basal anomalous dopamine efflux and loss of AMPH-

induced DA efflux. The ADHD-associated DAT(R615C) variant, however, lacks plasma membrane stability due to rapid basal endocytosis, and is unable to sequester in response to PKC activation or AMPH exposure. We were able to capitalize on the Ack1-mediated DAT endocytic brake to restore wildtype surface stability to DAT(R615C) (Fig. II-8B). Not unexpectedly, S445P- Ack1 also prevented DAT(R615C) from responding to PKC stimulation (Fig. II-8C), similar to its effect on wildtype DAT (Fig. II-7F). Nevertheless, our ability to rescue DAT(R615C) endocytic dysfunction raises the tantalizing possibility that genetically targeting DAT trafficking may hold promise for DAT coding variants with inherent membrane trafficking dysregulation.
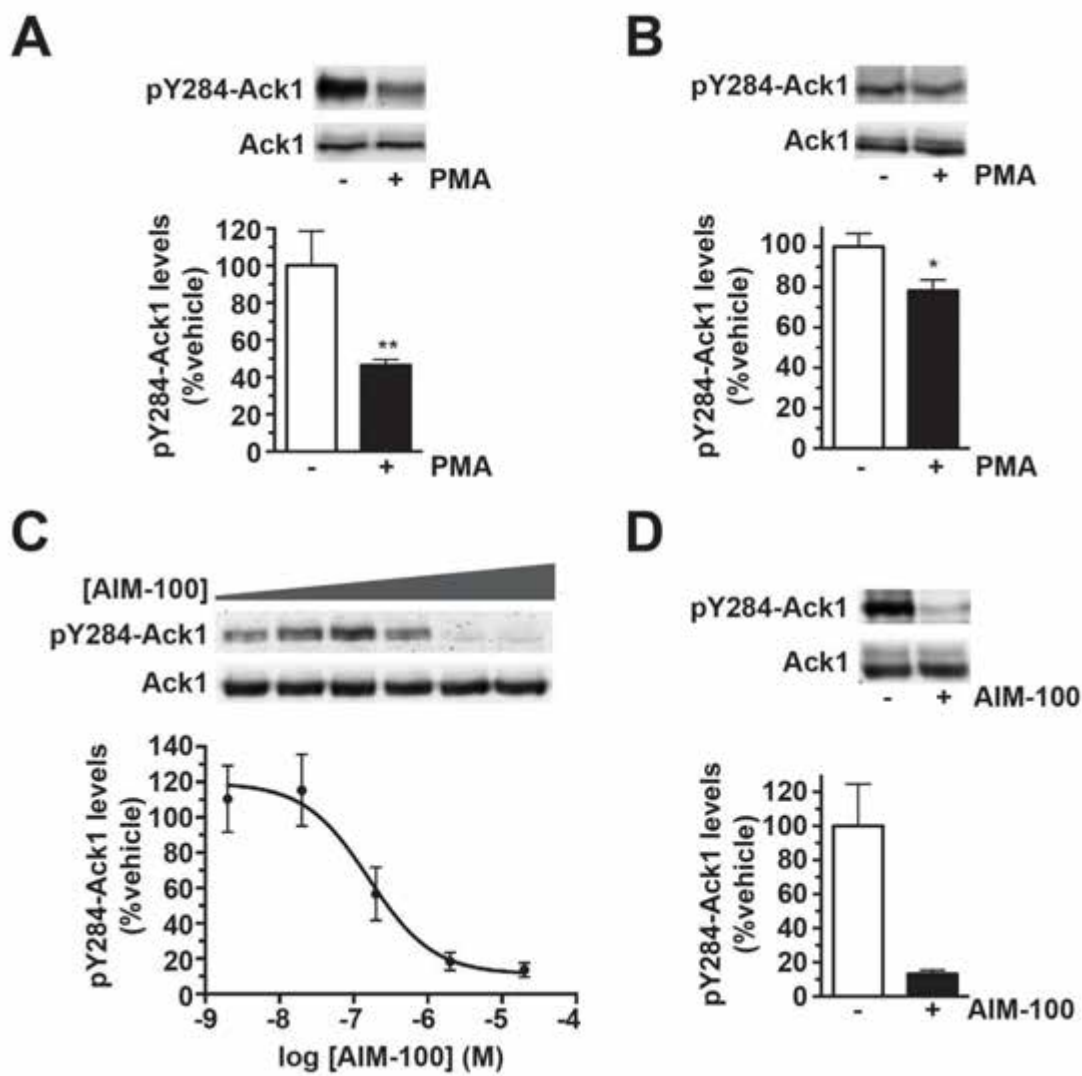
Figure II-1. Ack1 is expressed in dopaminergic SK-N-MC cells and mouse striatum, and is inactivated by PKC and the Ack1-specific inhibitor AIM-100. *pY284-Ack1 quantification.* Samples were treated as described and pY284-Ack1 protein levels were measured by immunoblotting **A., B.** DAT SK-N-MC cells (A) and mouse striatal slices (B) were treated ±1µM PMA, 30min, 37°C. *Top:* Representative pY284-Ack1 and total Ack1 blots. *Bottom:* Average pY284-Ack1 levels expressed as %vehicle-treated ±S.E.M. **p<0.01, *p<0.02, Student's t test, n=7 (A), n=9 (B). **C.** *AIM-100 dose response curves.* DAT SK-N-MC cells were treated with the indicated AIM-100 concentrations, 30min, 37°C. *Top:* Representative pY284-Ack1 and total Ack1 blots. *Bottom:* Average pY284-Ack1 levels, normalized to total Ack1. Data are expressed as %vehicle-treated ±S.E.M. n=3-4. AIM-100 decreased pY284-Ack1 levels with an IC_{50} = 220.5±42.5nM **D.** Mouse striatal slices were treated with ±20µM AIM-100, 30min, 37°C. *Top:* Representative pY284-Ack1 and Ack1 blots. *Bottom:* Average pYAck1 levels expressed as %vehicle-treated ±S.E.M. *p<0.02, Student's t test, n=3.
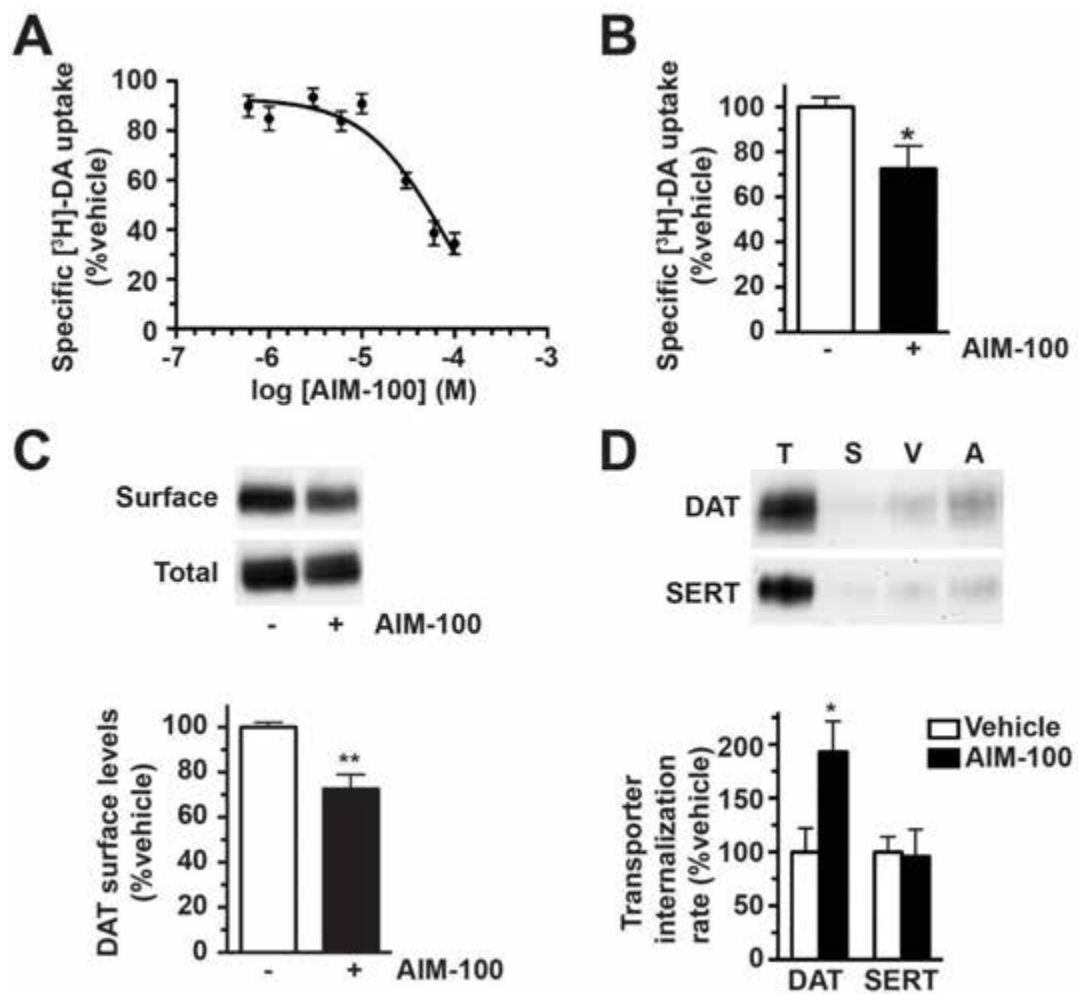
Figure II-2. Ack1 activity stabilizes DAT at the plasma membrane. A. *[^{3}H]DA uptake*: DAT SK-N-MC cells were treated with the indicated AIM-100 concentrations, 30min, 37°C and [^{3}H]DA uptake was measured as described in *Methods*. Data are expressed as %specific DA uptake ±S.E.M. (n=12). **B.** *Ex vivo slice uptake.* Striatal slices were treated ±20µM AIM-100, 60min, 37°C and [^{3}H]DA uptake was assessed as described in *Methods*. *p<0.05, Student's t test, n=6 hemislices obtained from 2 independent mice. **C.** *Ex vivo slice biotinylation.* Striatal slices were treated ±20µM AIM-100, 30min, 37°C and surface proteins were isolated by biotinylation. *Top:* Representative immunoblots. *Bottom:* Average DAT surface levels expressed as %vehicle-treated levels ±S.E.M. **p<0.01, Student's t test, n=3. **D.** *Internalization assays*: DAT and SERT internalization rates were measured in SK-N-MC cells ±20µM AIM-100 as described in *Methods*. *Top:* Representative immunoblots showing the total DAT and SERT surface pools at t=0 (T), strip control (S), and internalized protein during either vehicle (V) or AIM-100 (A) treatments. *Bottom:* Average internalization rates expressed as %vehicle-treated ±S.E.M. *p<0.02, Student's t test, n=5 (DAT), n=3 (SERT).
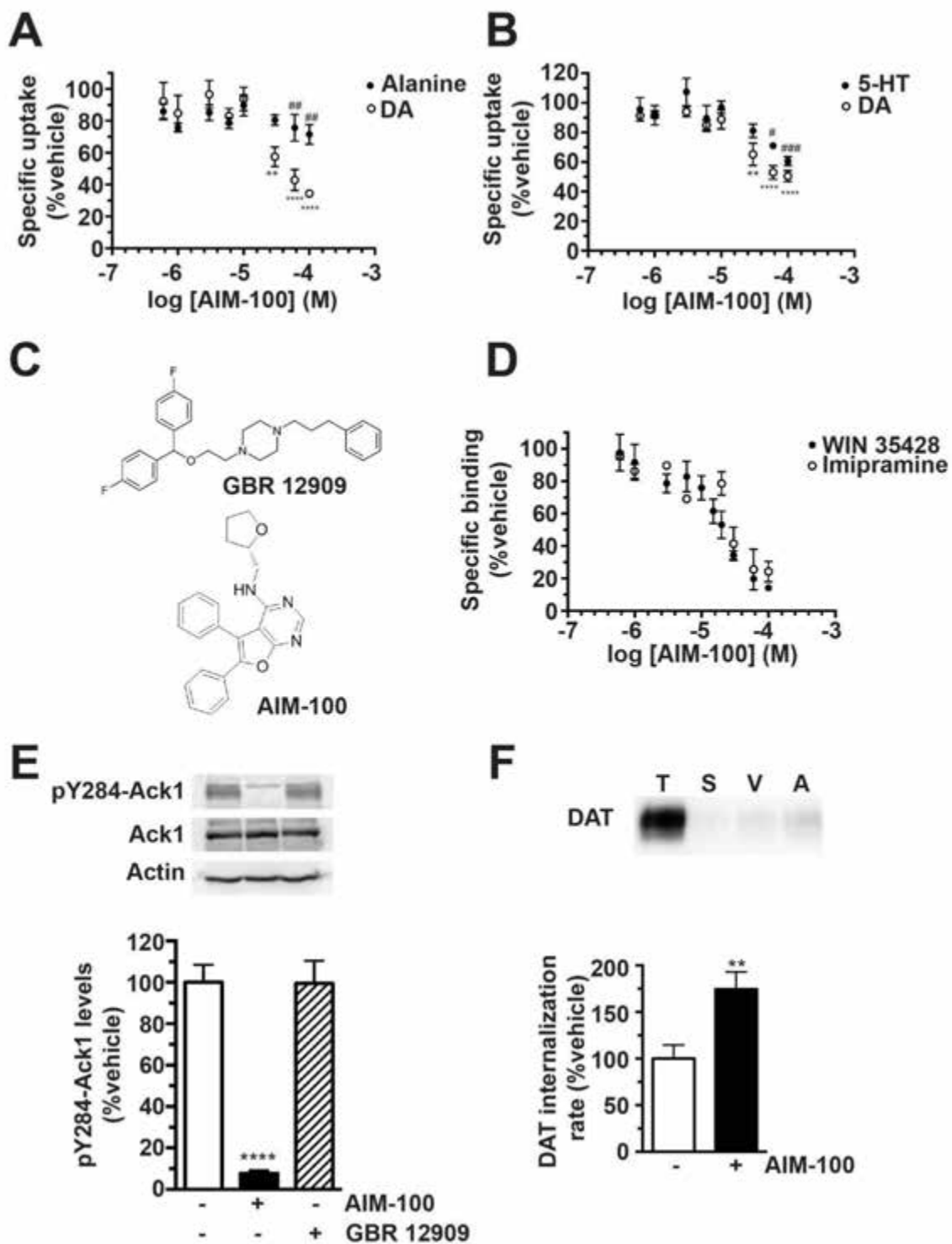
Figure II-3. AIM-100 is a low affinity, competitive monoamine transporter inhibitor. A. Effect of AIM-100 on Na^+-dependent alanine uptake and DA uptake in DAT-SK-N-MC cells. Cells were treated with the indicated concentrations of AIM-100, 30 min, 37°C and [^{3}H]alanine or [^{3}H]DA uptake were measured in parallel. Data are expressed as %non-treated controls ±S.E.M. *indicates a significance from control within each transporter type, #indicates a significant difference in uptake between DA and alanine uptake at the same AIM-100 dose, two-way ANOVA with Dunnett's multiple comparisons and Bonferroni's multiple comparison, n=4 . **B.** Effect of AIM-100 on [^{3}H]DA and [^{3}H]5-HT uptake in DAT-SK-N-MC and SERT-SK-N-MC cells, respectively. Specific uptake is expressed as %non-treated controls ±S.E.M. *indicates significantly different DA uptake compared with lowest dose, #indicates significantly different 5-HT uptake compared with lowest dose, two-way ANOVA with Dunnett's multiple comparisons, n=4. **C.** Chemical structures of AIM-100 and GBR12909. **D.** *Whole Cell Binding Assays.* DAT-SK-N-MC and SERT-SK-N-MC cells incubated with 1nM [^{3}H]WIN 35428 and 1nM [^{3}H]imipramine, respectively, 2 hrs, 4°C, in the presence of the indicated AIM-100 concentrations. Data are expressed as %bound compared to non-treated controls ±S.E.M. AIM-100 dose-dependently inhibited ligand binding with K_i values of 27.3±4.9 µM and 33.1±14.2 µM, respectively. **E.** *pY284-Ack1 quantification.* DAT-SK-N-MC cells were treated with either 20µM AIM-100 or 10µM GBR 12909, 30 min, 37°C and pY284-Ack1 levels were measured by immunoblotting as described in *Methods. Top:* Representative pAck1, total Ack1 and actin immunoblots; *Bottom:* Average pAck1 levels following the indicated drug treatments, expressed as %vehicle pAck1 levels ±S.E.M. ****Significantly different than vehicle control, one-way ANOVA with Dunnett's multiple comparison test, p<0.001, n=4-7. **F.** *Internalization Assay.* DAT internalization rates were measured as described in *Methods*, ±2µM AIM-100. *Top:* Representative DAT immunoblot showing total DAT surface pool at t=0 (T), strip control (S), and internalized DAT during either vehicle (V) or AIM-100 (A) treatments. *Bottom:* Average DAT internalization rate expressed as %vehicle-treated DAT internalization rate ±S.E.M. **Significantly different than vehicle control, Student's t test, p<0.01, n=4.
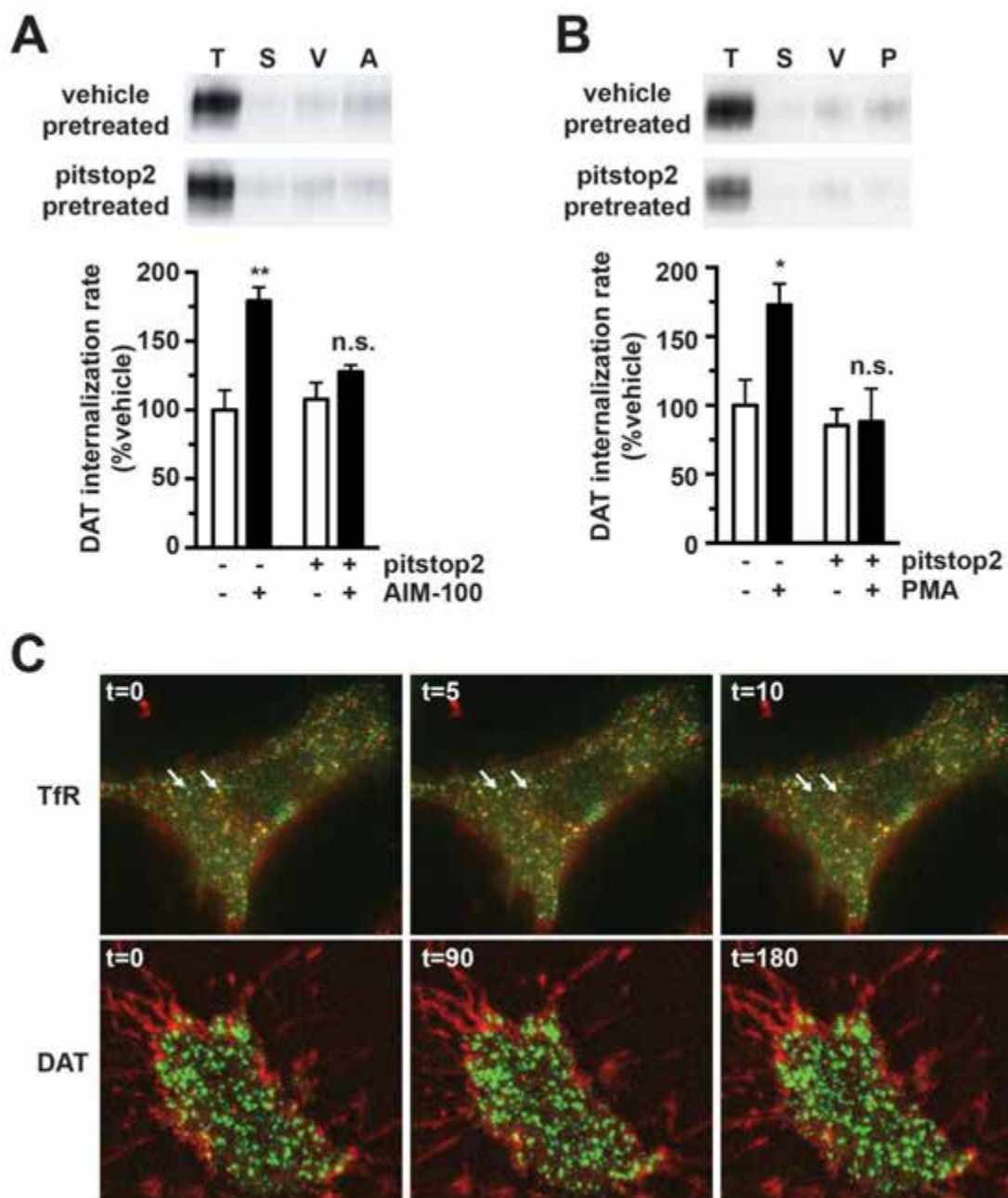
Figure II-4. Stimulated DAT endocytosis is clathrin-dependent, whereas constitutive DAT endocytosis is clathrin-independent. A., B. *DAT internalization assay.* DAT SK-N-MC cells were pretreated ±25μM pitstop2, 10min, 37°C, rapidly chilled, and DAT internalization rates were measured as described in *Methods* ±20μM AIM-100 (A) or ±1μM PMA (B). *Top:* Representative immunoblots showing total surface DAT at t=0 (T), strip control (S), and internalized DAT during vehicle (V), AIM-100 (A) or PMA (P) treatments. *Bottom:* Average DAT internalization rates expressed as %vehicle-treated ±S.E.M. Asterisks indicate a significant difference from vehicle, *p<0.03, ***p<0.005, one-way ANOVA with Bonferroni's multiple comparison test, n=7 (A), n=4-6 (B). **C.** *TIRF microscopy:* Time-lapse TIRF images were captured as described in *Methods. Top:* SK-N-MC cells stably expressing eGFP-clathrin labeled with Tf-Alexa594. White arrows indicate Tf/clathrin co-localized puncta that move away from the TIRF field during image capture. *Bottom:* SK-N-MC cells stably co-transfected with TagRFP-T-DAT and eGFP-clathrin.
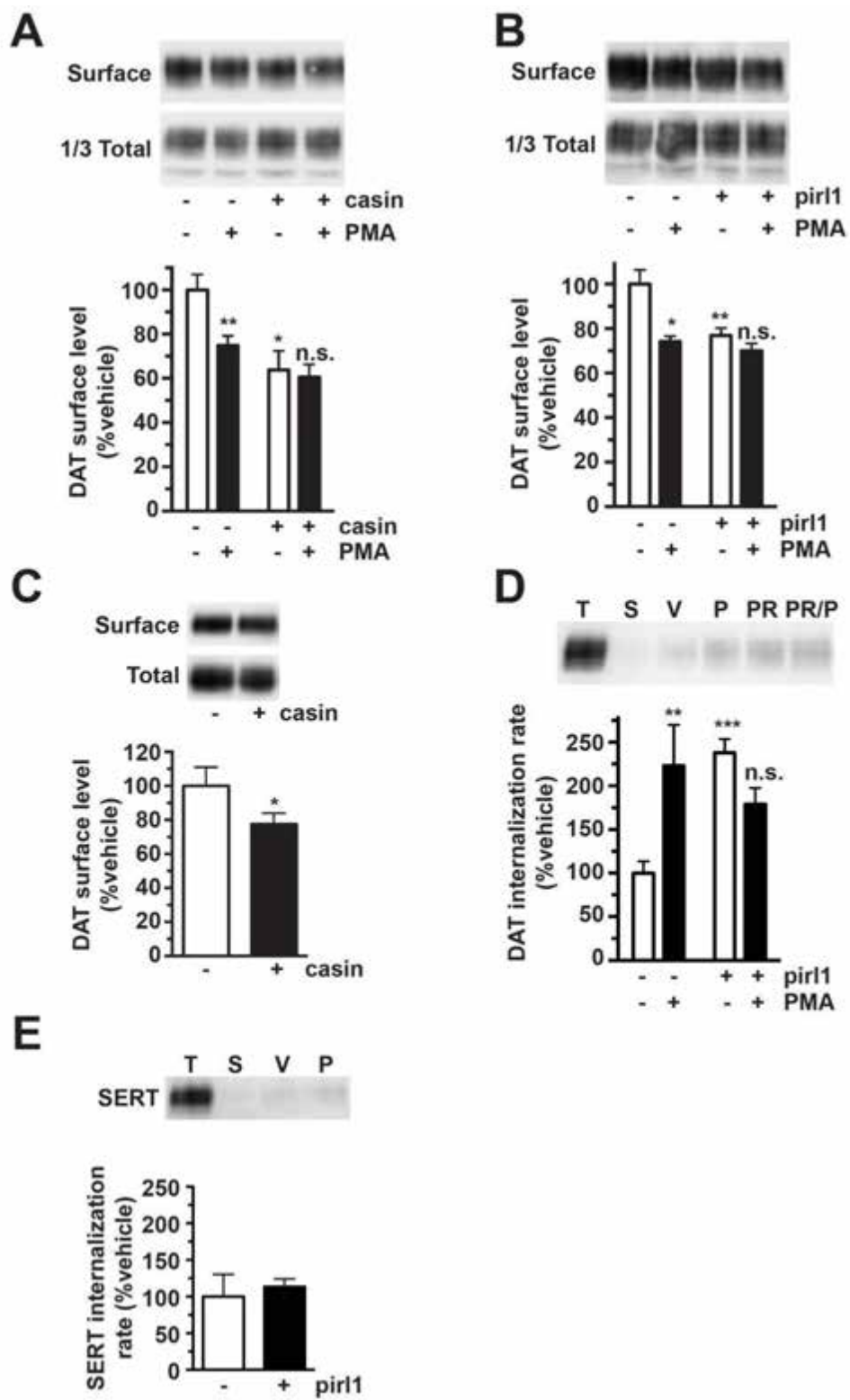
Figure II-5. Cdc42 stabilizes DAT surface expression. A., B. *Cell surface biotinylation:* DAT SK-N-MC cells were pretreated ±10μM casin (A) or ±20μM pirl1 (B), 30min, 37°C, followed by treatment ±1μM PMA, 30min, 37°C. Relative DAT surface levels were measured by biotinylation as described in *Methods.* Representative immunoblots are shown in the top of each panel. Average DAT surface levels expressed as %vehicle levels ±S.E.M. Asterisks indicate a significant difference from vehicle control, *$p < 0.05$, **$p < 0.01$, one-way ANOVA with Bonferroni's multiple comparison test, n=5-6 (A), n=3 (B). **C.** *Ex vivo* striatal slice biotinylation: Mouse striatal slices were treated ±10μM casin, 30min, 37°C and relative DAT surface levels were measured by biotinylation as described in *Methods. Top:* Representative immunoblot. *Bottom:* Average DAT surface levels expressed as %vehicle-treated ±S.E.M. *$p < 0.05$, Student's t test, n=10. **D.** *Internalization assay*: DAT internalization rates were measured ±1μM PMA, ±20μM pirl1 or with PMA/pirl1 co-application, 10min, 37°C. *Top:* Representative immunoblots showing total surface DAT at t=0 (T), strip control (S), and internalized DAT during vehicle (V), PMA (P) or pirl1 (PR) treatments. *Bottom:* Average DAT internalization rates expressed as %vehicle rate ±S.E.M. Asterisks indicate a significant difference from vehicle control, **$p < 0.01$, ***$p < 0.005$, one-way ANOVA with Bonferroni's multiple comparison test, n=9-13. **E.** Cdc42 inhibition does not affect SERT internalization. *Internalization assay:* SERT internalization rates were measured as described ±20 μM pirl1. *Top:* Representative SERT immunoblot showing total SERT surface pool at t = 0 (T), strip control (S), and internalized SERT during either vehicle (V) or pirl1 (P) treatment. *Bottom:* Average SERT internalization rates expressed as percent vehicle-treated rate ± SEM p = 0.68, Student's t test, n = 5.
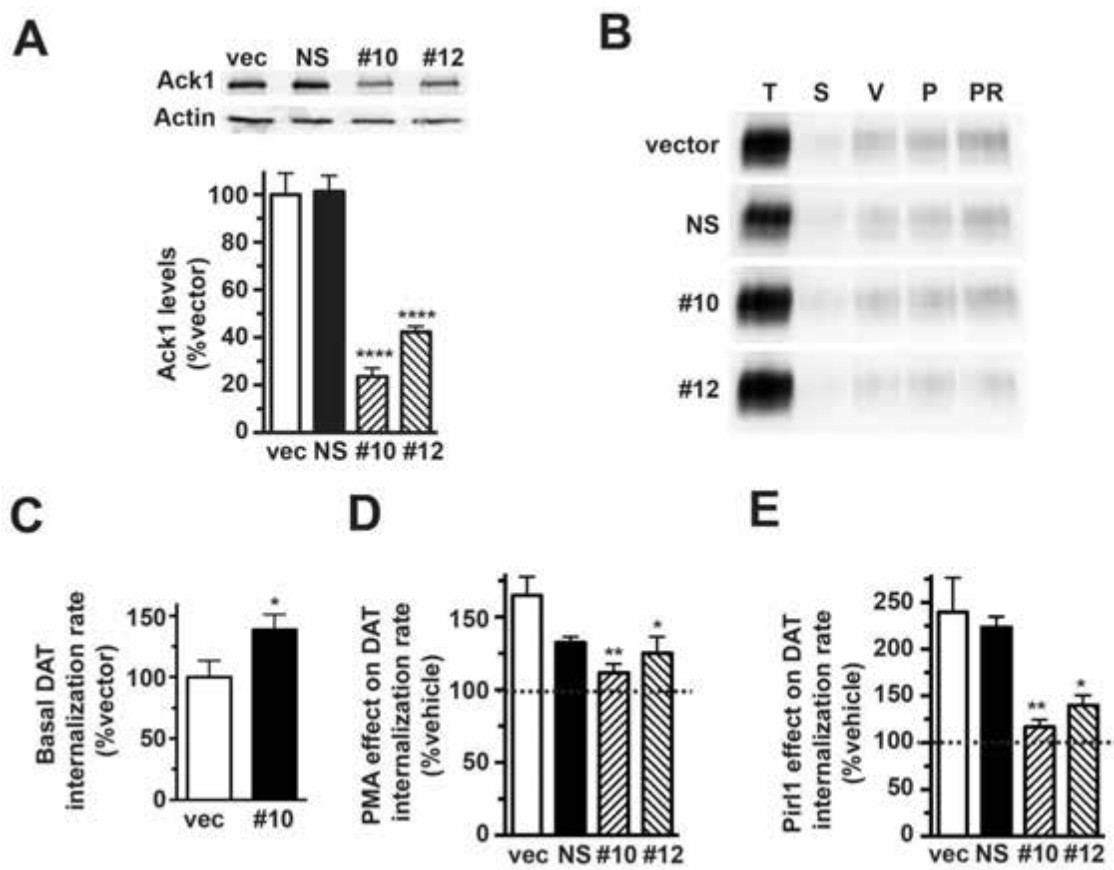
Figure II-6. ShRNA-mediated Ack1 depletion increases basal DAT internalization and abolishes stimulated DAT endocytosis in response to PKC activation or cdc42 inhibition. A. *Lentiviral-mediated hAck1 knockdown in SK-N-MC cells*: DAT SK-N-MC cells were transduced with the indicated lentiviral particles and hAck1 protein expression was measured 72 h posttransduction. *Top:* Representative immunoblots showing endogenous Ack1 levels in lysates from cells transduced with lentiviral particles expressing either pGIPZ vector (vec), nonsilencing shRNA (NS), hAck1 10 (10), or hAck1 12 (12). *Bottom:* Average hAck1 protein levels expressed as percent vector-transduced hAck1 levels ± SEM (normalized to actin loading control). ****P < 0.001 compared with vector-transduced cells, one way ANOVA with Dunnett's multiple comparison test, n = 4–7. **B-D**. *DAT internalization assays*: DAT SK-N-MC cells were transduced with lentiviral particles expressing either pGIPZ vector (vec), non-silencing (NS), hAck1#10 (#10) or hAck1#12 (#12) shRNAs and DAT internalization rates were measured ±1µM PMA (D) or ±20µM pirl1 (E) as described. **B.** Representative immunoblots for each transduction condition showing total surface DAT at t=0 (T), strip control (S), and internalized DAT during vehicle (V), PMA (P) or pirl1 (PR) treatments. **C.** Basal DAT internalization rates expressed as %vector-transduced rates ±S.E.M. *p<0.04, Student's t test, n=6. **D.** PKC-stimulated DAT internalization rates expressed as %vehicle rate ±S.E.M. for each transduction condition. Asterisks indicate a significant difference from vector-transduced control, *p<0.03, **p<0.01, one-way ANOVA with Dunnett's multiple comparison test, n=4-7. **E.** Pirl1-induced DAT internalization rates expressed as %vehicle rate ±S.E.M. for each transduction condition. Asterisks indicate a significant difference from vector-transduced control, *p<0.02, **p<0.01, one-way ANOVA with Dunnett's multiple comparison test, n=4-7.
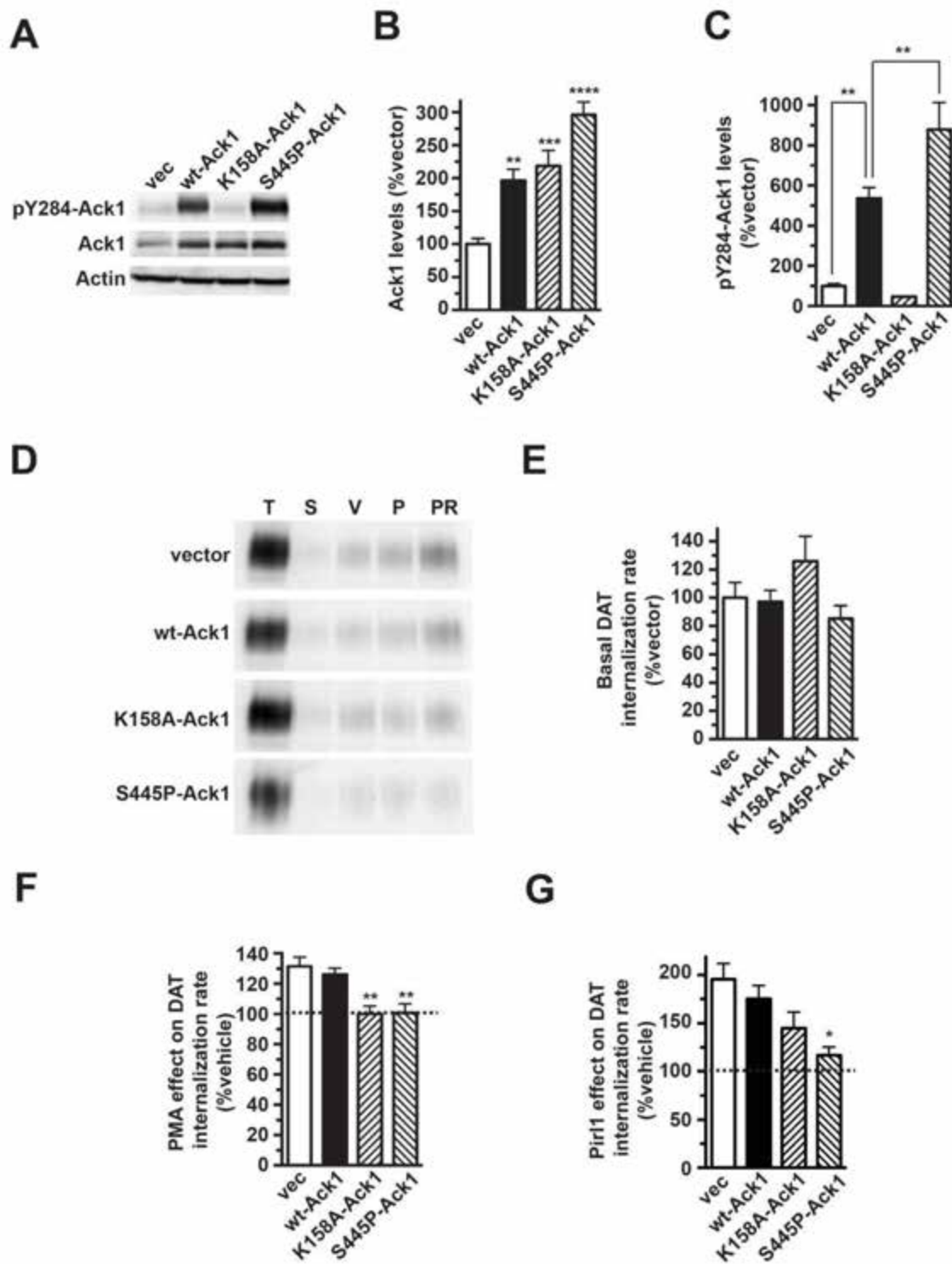
Figure II-7. Ack1 inactivation is required for stimulated DAT endocytosis.
A. Representative immunoblots showing pY284-Ack1, total Ack1, and actin
levels in lysates from cells cotransfected with DAT and either vector, wt-Ack1,
K158A-Ack1, or S445P-Ack1. **B.** Average total Ack1 levels expressed as
percent vector-transfected levels ± SEM (normalized to actin loading control).
Asterisks indicate a significant difference from vector-transfected control, one
way ANOVA with Dunnett's multiple comparisons test, **P < 0.01, ***P <
0.005, ****P < 0.0001, n = 6. **C.** Average pY284-Ack1 levels expressed as
percent vector-transfected levels ± SEM (normalized to total Ack1 levels). **P
< 0.01 compared with vector-transfected control, one-way ANOVA with
Bonferroni's multiple comparisons test, n = 6. **D-G** *Internalization assays:* SK-
N-MC cells were co-transfected with the indicated DAT and Ack1 isoforms and
DAT internalization rates were measured during treatment ±1µM PMA or
20µM pirl1 as described in *Methods.* A-D. Wildtype DAT co-transfected with
the indicated Ack1 cDNAs. **D**. Representative immunoblots showing total
surface DAT at t=0 (T), strip control (S), and internalized DAT during vehicle
(V), 1µM PMA (P) or 20µM pirl1 (PR) treatments. **E.** Average basal DAT
internalization rate expressed as %vector co-transfected rate ±S.E.M., one-
way ANOVA, p=0.10, n=8-9. **F.** Average PKC-stimulated DAT internalization
rate expressed as %vector co-transfected rate ±S.E.M. **Significantly different
from vector control, p<0.01, one-way ANOVA with Dunnett's multiple
comparison test, n=8-9. **G.** Average pirl1-stimulated DAT internalization rates
expressed as %vector co-transfected rate ±S.E.M. *Significantly different from
vector, p<0.02, one-way ANOVA with Dunnett's multiple comparison test, n=8-
9.
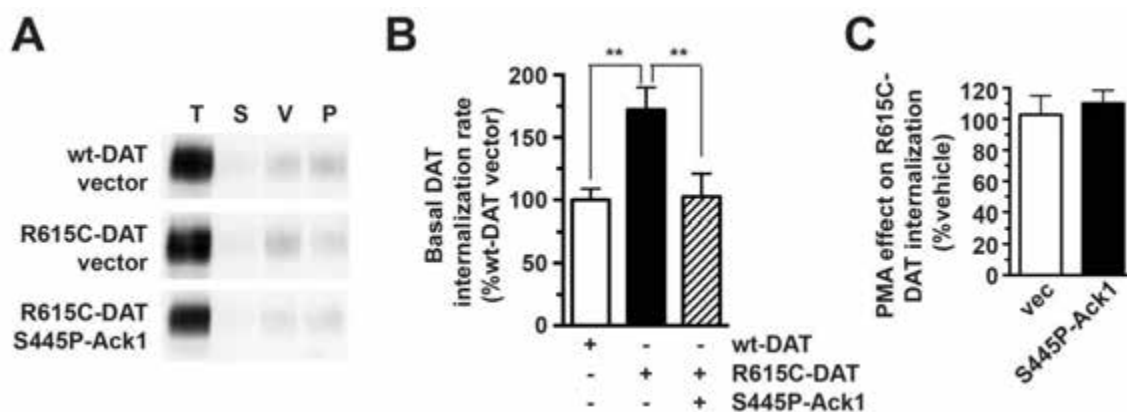
Figure II-8. Constitutive Ack1 activation rescues ADHD DAT coding variant R615C endocytic dysfunction. DAT vs. DAT(R615) internalization rates ±S445P-Ack1. **A**. Representative immunoblots. **B.** Average DAT internalization rates, expressed as %wildtype DAT control rate ±S.E.M., **Significantly different from indicated sample, p<0.01, one-way ANOVA with Bonferroni's multiple comparison test, n=8-11. **C.** Constitutively Ack1 activation does not rescue PKC-stimulated DAT(R615C) internalization. *Internalization assay:* DAT(R615C) was coexpressed in SK-N-MC cells with either vector or S445P-Ack1 and internalization rates were measured ±1 µM PMA (see Fig.I-10 for representative immunoblot). Average PMA-stimulated DAT(R615C) internalization rates expressed as percent vehicle-treated ± SEM, P = 0.33, Student's t test, n = 5–7.
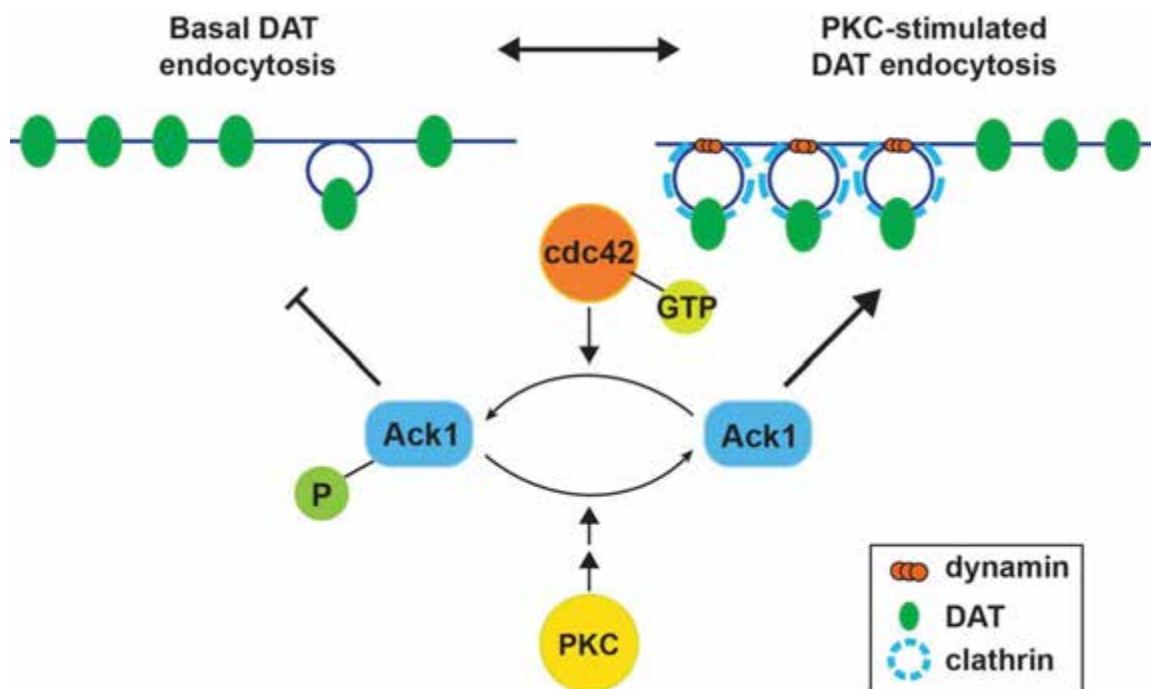
Figure II-9. Model for a PKC-sensitive, Ack1-mediated DAT endocytic brake. Under basal conditions, the cdc42-activated Ack1 pool imposes an endocytic brake upon the plasma membrane DAT population, permitting slow, clathrin- and dynamin-independent DAT endocytosis. PKC activation inactivates Ack1 and releases the DAT endocytic brake, facilitating rapid, clathrin- and dynamin-dependent, DAT internalization and intracellular sequestration.

PREFACE TO CHAPTER III

This chapter is unpublished and in preparation for submission

Author contributions:

Wu S and Melikian HE designed research.

Wu S performed research.

Lifshitz LM and Fogarty KE contributed analytic tools.

Uttamapinant C and Ting AY contributed new reagents

Wu S and Melikian HE analyzed data.

Wu S and Melikian HE wrote the paper.

CHAPTER III

The Dopamine Transporter Recycles Via A Retromer-Dependent Post-Endocytic

Mechanism: Tracking Studies Using A Novel Fluorophore-Coupling Approach

III.A Introduction

Dopamine (DA) neurotransmission is responsible for vital functions in the central nervous system such as locomotion, reward and sleep/arousal (Iversen and Iversen, 2007). Dysregulation of DA neurotransmission is coupled to multiple neurological and psychiatric disorders such as Parkinson's disease, schizophrenia, ADHD and bipolar disorder (Snyder, 2002; Chen et al., 2004; Sulzer, 2007; Sharma and Couture, 2014). The presynaptic dopamine transporter (DAT) expresses exclusively in DA neurons and mediates high-affinity reuptake of synaptically released DA, thus temporally and spatially restraining DA neurotransmission (Gether et al., 2006). DAT is the primary target for widely abused psychostimulants, cocaine and amphetamine, as well as therapeutic agents such as methylphenidate (Ritalin) (Torres and Amara, 2007; Kristensen et al., 2011). Loss-of-function DAT coding variants cause dopamine transporter deficiency syndrome, which is a Parkinsonism/dystonia subtype (Kurian et al., 2009; Kurian et al., 2011). Altered DAT function has also been associated with attention deficit hyperactivity disorder (ADHD), autism spectrum disorders (ASD) and adult Parkinsonism (Mazei-Robison et al., 2008; Sakrikar et al., 2012; Hamilton et al., 2013; Hansen et al., 2014). Thus, regulatory

mechanisms that control DAT function may exert impactful consequences on DA neurotransmission and DA homeostasis.

Numerous studies demonstrate that DAT function is acutely regulated by membrane trafficking, which provides a potential means to acutely enhance or diminish DA signaling (Melikian, 2004; Eriksen et al., 2010a; Bermingham and Blakely, 2016). DAT constitutively internalizes and acute stimuli such as PKC activation and amphetamine exposure accelerate DAT endocytosis, resulting in decreased DAT surface expression and function (Huff et al., 1997; Daniels and Amara, 1999; Melikian and Buckley, 1999; Torres et al., 2003a; Eriksen et al., 2009). Considerable effort has been directed towards understanding DAT's post-endocytic fate. Function studies in heterologous expression systems have demonstrated that DAT recycles back to the plasma membrane under basal and regulated conditions (Loder and Melikian, 2003; Sorkina et al., 2005; Boudanova et al., 2008a; Chen et al., 2013; Richardson et al., 2016). Paradoxically, DAT post-endocytic tracking studies in heterologous cells and primary neuronal cultures using either antibody feeding or fluorescent cocaine analogs, reported that DAT targets to pre-lysosomal and lysosomal pathways, but not to classical recycling compartments (Eriksen et al., 2010b), while results from an antibody feeding assay showed that DAT recycled back to the plasma membrane in heterologous cells and primary culture (Rao et al., 2011; Hong and Amara, 2013). Moreover, a recent antibody feeding study performed in acute mouse brain slices reported little surface DAT internalization, in either DAergic terminals or

somatodendritic areas of DA neurons (Block et al., 2015). These discrepancies prompted us to 1) interrogate the DAT post-endocytic itinerary in absence of inhibitor analog or bound antibodies; 2) identify the molecular mechanisms that mediate DAT post-endocytic sorting.

The retromer complex mediates cargo export from endosomes to either the trans-Golgi network (TGN; retrograde transport) or back to the plasma membrane (recycling) (Seaman, 2012; Burd and Cullen, 2014). Multiple neuronal proteins, such as β2-adrenergic receptor, AMPA-type glutamate receptor, wntless and Alzheimer-associated sortilin-related receptor 1 recycle back to the plasma membrane mediated in a retromer-dependent manner (Rogaeva et al., 2007; Zhang et al., 2012; Choy et al., 2014; Loo et al., 2014; Varandas et al., 2016). Moreover, retromer disruption is closely linked to multiple neurological disorders, including Alzheimer's and Parkinson's diseases (Tsika et al., 2014; Dhungel et al., 2015; Small and Petsko, 2015).

In the current study, we took advantage of Protein Incorporation Mediated by Enzyme (PRIME) labeling to directly couple a small (~700 dalton) fluorophore to the DAT surface population, and subsequently tracked DAT's temporal-spatial post-endocytic itinerary in immortalized mesencephalic cells. Taken together, our data demonstrate that internalized DAT targets to a retromer-positive endocytic compartment, and that retromer is required to maintain DAT surface levels. Moreover, our results demonstrate that DAT recycling via retromer requires a C-terminal PDZ-binding motif.

III.B Materials and methods

Materials: Picolyl azide (pAz) and Bis[(tertbutyltriazoyl)methyl]-[(2-carboxymethyltriazoyl)methyl]-amine were synthesized as previously reported (Uttamapinant et al., 2010; Uttamapinant et al., 2012). Rat anti-DAT antibody (MAB369) was from EMD Millipore and mouse anti-actin antibody (sc-56459) was from Santa Cruz Biotechnology. Mouse anti-EEA1 (610456) and mouse anti-rab11 (610656) antibodies were from BD Transduction. Rabbit anti-rab7 antibody (D95F2) was from Cell Signaling Technology and goat anti-Vps35 antibody (NB100-1397) was from Novus Biologicals. Horseradish peroxidase-conjugated secondary antibodies were from EMD Millipore (goat anti-rat), Jackson ImmunoReseach (donkey anti-goat, minimal cross-reaction to mouse serum proteins) and Pierce (goat anti-mouse). Alexa488-conjugated secondary antibodies were from Invitrogen (goat anti-mouse, goat anti-rabbit, goat anti-rat and donkey anti-goat (minimal cross-reaction to mouse serum proteins) Alexa Fluor488) and donkey anti-rat Alexa Fluor594 (minimal cross-reaction to mouse serum proteins) was from Jackson ImmunoResearch. Alkyne-conjugated Alexa Fluor594 was from Invitrogen. [^{3}H]DA (dihydroxyphenylethylamine 3,4-[ring-2,5,6-^{3}H]) was from Perkin Elmer. Sulfo-NHS-SS-biotin, Tris(2-carboxyethyl)phosphine hydrochloride (TECP), and streptavidin agarose were purchased from Thermo Fisher Scientific. Phorbol 12-myristate 13-acetate (PMA), AIM-100 and GBR12909 were from Tocris Bioscience. All other chemicals and

reagents were from Thermo Fisher Scientific or Sigma-Aldrich and were of highest grade possible.

cDNA Constructs and Mutagenesis: To generate LAP-hDAT-pcDNA3.1(+), hDAT was subcloned into pBS-SKII⁻ as a shuttle vector, and degenerate mutations were introduced into hDAT codons corresponding to amino acids 193 and 204, adding BsaBI and HpaI sites (Quickchange mutagenesis kit, Agilent Technologies). Sense and anti-sense oligonucleotides encoding the LAP-peptide sequence, flanked by linkers (GSSGSSG<u>GFEIDKVWHDFPA</u>GSSGSSG; LAP peptide sequence is underlined), were annealed and ligated into the blunt BsaBI/HpaI site, and the final LAP-DAT cDNA was subcloned into pcDNA3.1(+) at HindIII/XbaI sites. LAP-DAT-AAA-pcDNA3.1(+) was generated by mutating the last three amino acids of hDAT into alanines (LKV to AAA) using a Quickchange mutagenesis kit (Agilent Technologies). All DNA sequences were determined by the dideoxy chain termination (Genewiz, New Jersey).

Cell Culture and Transfections: The rat mesencephalic cell line 1Rb3AN27 was a kind gift from Dr. Alexander Sorkin (University of Pittsburgh, Pittsburgh, PA) and was maintained in RPMI1640 supplemented with 10% fetal bovine serum, 2mM glutamine and 100 units/ml penicillin/streptomycin, 37°C, 5% CO_2. Pooled stable AN27 cell lines expressing either wild-type hDAT, LAP-hDAT or LAP-hDAT-AAA, respectively, were generated by transfecting 2×10^5 cells/well in 6-well culture plate with 1µg plasmid DNA using Lipofectamine 2000, at lipid:DNA ratio of 2:1 (w/w). Stably transfected cells were selected with 200 µg/ml G418

(Invitrogen) and resistant cells were pooled and maintained under selective pressure in 80 μg/ml G418. SK-N-MC cells were from American Type Culture Collection (ATCC) and were maintained in MEM (Sigma-Aldrich M2279) supplemented with 10% fetal bovine serum (Invitrogen), 2mM L-glutamine, 10^2 U/ml penicillin/streptomycin, 37°C, 5% CO_2. Pooled #14 stable SK-N-MC cell lines expressing hDAT was generated by transfecting 1×10^6 cells/well in 6-well culture plate with 3 μg plasmid DNA using Lipofectamine 2000, at lipid:DNA ratio of 2:1 (w/w). Stably transfected cells were selected in 500 μg/ml G418 (Invitrogen) and resistant cells were pooled and maintained under selective pressure in 200 μg/ml G418.

[^{3}H]DA Uptake Assay: DAT-AN27 and LAP-DAT-AN27 cells were seeded onto 24-well plates at 8×10^4 cells per well one day before performing assays. Cells were washed twice with KRH buffer (120mM NaCl, 4.7 mM KCl, 2.2 mM $CaCl_2$, 1.2 mM $MgSO_4$, 1.2 mM KH_2PO_4, 10mM HEPES, pH 7.4) and preincubated in KRH buffer supplemented with 0.18% glucose, 0.1% BSA at 37°C for 30min in the presence of either vehicle or the indicated drugs. Uptake was initiated by adding 1 μM [^{3}H]DA containing 10^{-5} M pargyline and 10^{-5} M ascorbic acid and proceeded for 10 min, 37°C. Assays were terminated by rapidly washing cells thrice with ice-cold KRH buffer. Cells were solubilized in scintillation fluid, and accumulated radioactivity was measured by liquid scintillation counting in a Wallac Microbeta plate counter. Non-specific uptake was defined in the presence of 10 μM GBR12909.

Endocytic Rate Measurements by Reversible Biotinylation: Stable DAT-AN27 and LAP-DAT-AN27 cells were plated at $3x10^5$ cells per well in 6-well plate 24 hours prior to conducting experiments. Cells were washed three times with ice-cold PBS^{2+} (phosphate-buffered saline, pH 7.4, supplemented with 1mM $MgCl_2$ and 0.1mM $CaCl_2$), surface proteins were biotinylated twice, 15 min, 4°C, with 2.5 mg/mL sulfo-NHS-SS-biotin, and were quenched twice, 15 min, 4°C with 100 mM glycine/PBS^{2+}. Internalization was initiated by washing cells rapidly with three times with pre-warmed (37°C) PBS^{2+}/0.18% glucose/0.1% BSA (IgG/protease free) containing either vehicle or the indicated drugs, and incubating 10 min, 37°C. Zero timepoint and strip controls were kept at 4°C in parallel. Endocytosis was arrested by rapidly washing cells with ice-cold NT buffer (150 mM NaCl, 20mM Tris, pH 8.6, 1.0mM EDTA, pH 8.0, 0.2% protease free/IgG free BSA). Residual surface biotin was stripped by reducing twice with 50 mM TCEP/NT buffer, 25 min, 4°C, followed by three washes with PBS^{2+}. Cells were lysed in RIPA containing protease inhibitors and protein concentrations were determined by BCA protein assay (Thermo) comparing BSA standards. Biotinylated proteins were isolated from equivalent amounts of total cellular protein by streptavidin-agarose affinity chromatography. Samples were analyzed by SDS-PAGE and DAT was detected using a monoclonal rat anti-DAT antibody (MAB369; EMD Millipore). Non-saturating DAT bands were detected using a VersaDoc gel documentation system and were quantified using Quantity One

software (Bio-Rad). Internalization rates were calculated as %biotinylated DAT recovered as compared to DAT surface levels at t= 0.

[W37V]LplA expression and purification: Expression and purification of His_6-tagged [W37V]LplA was described in detail at (Uttamapinant et al., 2013). Briefly, pYFJ16-His_6-[W37V]LplA plasmid was transformed into BL21 *E. Coli* and bacteria were incubated at 37°C, with shaking until they attained log phase growth. Protein expression was induced by adding 100 µg/ml isopropyl-β-D-thiogalactopyranoside (IPTG) and proceeded for 8 hrs at room temperature. Bacteria were lysed and His_6-[W37V]LplA was purified by nickel-affinity chromatography. Eluted protein was dialyzed for 8 hours, twice, against 20 mM Tris base, 1 mM DTT, 10% (v/v) glycerol, pH 7.5, at 4 ºC, and protein concentrations were determined by A_{280} absorbance using NanoDrop (Thermo Scientific) using an extinction coefficient of 46250 $M^{-1}cm^{-1}$. Ligase aliquots were stored at -80ºC.

Probe Incorporation Mediated by Enzymes (PRIME) Labeling and Post-Endocytic Tracking Studies: Live AN27 cells stably expressing the indicated LAP-DAT constructs were covalently labeled with alkyne-Alexa as described previously (Uttamapinant et al., 2013). Briefly, cells were seeded onto glass coverslips in 24-well plates at a density of $8x10^4$ cell/well, one day prior to assaying. A picolyl azide (PAz) ligation mixture was prepared, containing 10 µM [W37V]LplA, 200 µM pAz, 1 mM ATP and 5 mM $MgCl_2$ in PBS/3%BSA and cells incubated with Paz ligation mixture, 20min, room temperature, followed by three washes with PBS^{2+}.

A low Cu^{2+} click labeling solution containing 10 mM $CuSO_4$, 50 mM BTTAA and 100 mM sodium ascorbate and was prepared and incubated with cells at room temperature,10min in a closed tube. The labeling solution was diluted 200X with PBS^{2+}, alkyne-Alexa594 was added to a final concentration of 20 μM and incubated with cells for 10 min, room temperature. Cells were washed three times with room temperature PBS^{2+} and internalization was initiated by rapidly washing cells and incubating in pre-warmed (37°C) PBS^{2+}/g/BSA (PBS^{2+}, 0.18% glucose, 0.1% IgG/protease-free BSA) containing the indicated drugs. Cells were fixed at the indicated post-endocytic timepoints in 4% paraformaldehyde for 10 min, room temperature and were subsequently blocked, permeabilized and stained with indicated primary antibodies and Alexa488-conjugated secondary antibodies as previously described (Navaroli et al., 2011). Note that all of the antibodies directed against endosomal markers were carefully vetted for specificity: 1. By their ability to recognize native and GFP-tagged proteins via immunoblot, and 2) by their ability to co-stain GFP-tagged markers *in situ*. Dried coverslips were mounted in ProLong Gold with DAPI to stain and were dried prior to performing imaging.

Wide Field Microscopy and Image Analysis: Cells were visualized with a Zeiss Axiovert 200M microscope using a 63X, 1.4 N.A. oil immersion objective and 0.2 μm optical sections were captured through the z-axis with a Retiga-1300R cooled CCD camera (Qimaging). For image presentation, 3-D z-stack images were deconvolved with a constrained iterative algorithm using measured point spread

functions for each fluorescent channel using Slidebook 5.0 software (Intelligent Imaging Innovations). All representative images shown are single 0.2 µm planes through the center of each cell. To quantify the percentage of LAP-DAT that co-localized with different endosomal markers (by volume, i.e. counting voxel), the DAT image was used to identify 1) an extracellular background region-of-interest (ROI) for background fluorescence estimation, and 2) the range of contiguous optical sections (z-axis planes) having infocus DAT information (i.e. the cell). The sample fields imaged were chosen to contain at least one extracellular region of at least 5 µm across. This background region was automatically determined by first taking the maximum intensity projection (in Z) of the DAT stack. Then the (x,y) position of the 2-D region (x±radius, y±radius) having the lowest average intensity within this projection was saved. The radius used was nominally 20 pixels (±2 µm). For each of the color image stacks, at each z plane the average intensity of this 2-D region was subtracted from all pixels of the plane, leaving as positive signal the fluorescence greater than the extracellular background. The outline of the box containing this background region was superimposed on the DAT maximum projection image, as well as the maximum projections of the other color stacks, for visual inspection and verification before proceeding with the analysis. The infocus DAT data planes were also automatically determined, by first calculating the normalized total energy $\hat{E}$ of each Z plane, defined as

$$E(z) = (\Sigma\Sigma I([x,y],z)^2 - n(z)\cdot\bar{I}(z)^2) / n(z)\cdot I(z)^2$$

And $\hat{E}(z) = (E(z)-E_{min})/(E_{max}-E_{min})$, where $I([x,y],z)$ is a pixel intensity at position [x,y] in plane z, $\bar{I}(z)$ is the average intensity of plane z, and $n(z)$ is the total number of pixels in plane z. Starting from the bottom of the stack (1st z plane) and moving up, the first infocus plane z_{bot} was defined as the z plane where $\hat{E}(z)$ exceeds $\hat{E}_T$=0.5. Similarly, starting from the top (last z plane) and moving down, the last infocus plane z_{top} is where $\hat{E}(z)$ exceeds the threshold $\hat{E}T$. This was generally a conservative threshold, keeping a few out-of-focus planes at the top and the bottom. The planes z_{bot} to z_{top} are extracted from the background-corrected multi-color stacks for deconvolution. The point spread function of the microscope system was determined from images of slides of 4 color, 175 nm diameter beads (PS-Speck Microscope Point Source Kit, Thermo Fisher Scientific Inc.) All images were subjected to regularized, constrained, iterative deconvolution with the same smoothness parameter ($a=5 \cdot 10^{-5}$) and iterated until the algorithm reached convergence (0.001 level).

Image segmentation (i.e., identification of signal) was performed on each restored image (each wavelength separately) via a manually set threshold. Each 3-D restored image was projected (via maximum intensity projection) to 2-D and then displayed using a false color scale manually adjusted for each displayed image to maximize contrast between signal and background. Three different thresholds were then chosen for each image: the lower threshold allowed some diffused background fluorescence, the middle threshold removed all the diffused background and the higher threshold eliminated edges of the labeled structures.

Pixels above threshold were kept while those below threshold were set to 0. Colocalization of DAT with a second protein was calculated by counting the number of positive (>0) pixels in the 3-D DAT image which were also positive in the corresponding position of the second protein image, and dividing by the number of positive DAT pixels. The low and high thresholds were used to evaluate whether conclusions drawn from the colocalization results for the best (middle) thresholds were dependent on the threshold chosen and the best threshold was used for the data presentation and analysis. All image processing and analysis was performed using custom software.

Initial time points of EEA1 and Vps35 data as well as Rab7 data was fit to a linear regression equation $Y = kx + a$, where Y = % DAT colocalized with endosomal markers, x is the time (min), k is slope and a is %DAT with endosomal markers at time zero.

Brain Slice Immunohistochemistry and Confocal Microscopy: All animals were handled according to University of Massachusetts Medical School IACUC protocol A1506 (H.E.M.). Adult C57/B6 mice were transcardially perfused with 4% paraformaldehyde and brains were removed and post-fixed for one day at 4°C, followed by dehydration in PBS/30% sucrose, 4°C, 2-3 days. 25 µm coronal sections were taken through the striatum and midbrain using a sliding microtome (Leica) and slices were blocked in PBS with 0.2% TritonX-100, 5% normal donkey serum and 1% H_2O_2. For DAT and Vps35 immunofluorescence, sections were co-incubated overnight with rat anti-DAT (1:2000) and goat anti-Vps35

(1:500) in PBS with 0.2% TritonX-100, 5% normal donkey serum and 1% H_2O_2. Slices were rinsed in PBS, and incubated with donkey anti-goat and donkey anti-mouse Alexa Fluor (1:2000 each) for 1hr at room temperature. Unbound secondary antibodies were washed in PBS and slices were mounted onto glass slides, dried and coverslipped in Prolong Gold mounting medium containing DAPI (Invitrogen). Images were acquired with a Leica TCS SP5 II laser scanning confocal microscope (Cell and Developmental Biology Core, University of Massachusetts Medical School) with either a 20X, 0.7 N.A. objective (HCX PL APO CS 20.0x0.70 IMM, Leica) or a 63X, 1.4 N.A. oil immersion objective (HCX PL APO CS 63.0x1.40 OIL, Leica). 0.4 µm optical sections were captured through the z-axis and 3-D z-stack images were imported into ImageJ using Bio-Format Importer plugin. All images shown are single representative 0.4 µm planes.

shRNA, Lentiviral Production and Transduction: Human Vps35-targeted short hairpin RNA (shRNA), cloned into the pGIPZ lentiviral vector, were from GE Healthcare Dharmacon, and were purchased from University of Massachusetts Medical School RNAi Core.

Full length hairpin sequences were as follows:

Non-silencing (Luciferase 693):

TGCTGTTGACAGTGAGCGCTCTAAGAACGTTGTATTTATATAGTGAAGCCAC
AGATGTATATAAATACAACGTTCTTAGATTGCCTACTGCCTCGGA

hVps35 sh#32:

TGCTGTTGACAGTGAGCGACTGACAGATGAGTTTGCTAAATAGTGAAGCCA

CAGATGTATTTAGCAAACTCATCTGTCAGGTGCCTACTGCCTCGGA

Initial shRNA efficacies were determined by immunoblotting cell lysates obtained from HEK293T cells transiently transfected (Lipofectamine 2000) with the indicated pGIPZ-shRNA vs. control vectors. Replication incompetent lentiviral particles were produced as previously described by our laboratory (Wu et al., 2015) and titers were determined 48 hrs post-transfection by counting GFP-positive cells in transduced HEK293T cells.

<u>For Lentiviral Transduction</u>: $5x10^5$ DAT SK-N-MC cells/well were seeded into 6-well plate one day prior to viral transduction and were infected with 5ml of the indicated crude lentivirus supplemented with 8µg/ml polybrene. Virus was removed 24 hours post-infection and transduced cells were enriched by selecting with 1µg/ml puromycin. Cells were assayed 96 hours post-infection.

Cell Surface Biotinylation: DAT surface levels in SK-N-MC cells were determined by steady state biotinylation as previously described (Navaroli et al., 2011; Gabriel et al., 2013; Wu et al., 2015). Briefly, cells were labeled twice, 15 min, 4°C with 1.0 mg/ml sulfo-NHS-SS-biotin in PBS^{2+} and excess biotinylation reagent was quenched twice, 15 min, 4°C with PBS^{2+}/100mM glycine. Excess glycine was removed by washing three times in ice-cold PBS^{2+} and cells were lysed in RIPA buffer (10mM Tris, pH 7.4, 150mM NaCl, 1mM EDTA, 0.1%SDS, 1%Triton-X-100, 1% sodium deoxycholate) containing protease inhibitors. Lysates were cleared by centrifugation and protein concentrations were

determined by BCA protein assay kit (Pierce). Biotinylated proteins from equivalent amount of cellular protein were recovered by batch streptavidin affinity chromatography (overnight, 4°C) and bound proteins were eluted in denaturing SDS-PAGE sample buffer, 30 min, room temperature with rotation. Samples were analyzed by SDS-PAGE and indicated proteins were detected by immunoblotting with the indicated antibodies. Immunoreactive bands were detected with SuperSignal West Dura (Pierce) and were captured using the VersaDoc Imaging station (Biorad). Non-saturating bands were quantified using Quantity One software (Biorad).

Statistical Analysis: Data were presented as means of results from each experimental condition, as indicated in figure legends. For experiments in which two conditions were compared, data were analyzed using an unpaired, two-tailed Student's t test. For experiments in which three or more conditions were evaluated, statistical significance was calculated using either a one-way or two-day ANOVA followed by either Tukey's or Bonferroni's multiple comparison test as indicated in the figure legends. All time course data sets passed normality test. Statistical analyses were performed using GraphPad Prism 6.0 software.

III.C Results

DAT expression, function and trafficking tolerate LAP peptide incorporation into extracellular loop 2

Previous studies investigating DAT post-endocytic trafficking have relied primarily on either antibody feeding or fluorescent competitive DAT inhibitors, both of which could potentially target DAT to a physiologically irrelevant post-endocytic pathway. Therefore, we aimed to track DAT's post-endocytic itinerary by covalently labeling the DAT cell surface population with small fluorophores, thereby creating a "fluorescent DAT". To accomplish this, we took advantage of the recently reported Protein Incorporation Mediated by Enzyme (PRIME) labeling approach (Uttamapinant et al., 2013). This method covalently couples fluorophore to cell surface proteins that encode an extracellular ligase acceptor peptide (LAP), which is a substrate for bacterial lipoic acid ligase. The PRIME strategy for labeling cell surface DAT is illustrated in Figure III-1A. We replaced hDAT residues 193-204 in the 2nd extracellular loop (EL2) with a twenty-seven amino acid peptide sequence containing LAP, flanked by linker sequence. We first tested the specificity of this labeling approach by stably expressing LAP-DAT in the rat mesencephalic cell line, 1Rb3AN27, and subsequently performing PRIME labeling followed by immunocytochemistry on fixed, permeabilized cells using an anti-DAT antibody, to detect total LAP-DAT expression. Alkyne-Alexa594 coupled specifically to the surface of cells expressing LAP-DAT, whereas nearby LAP-DAT-negative cells (identified using DAPI staining) were not labeled (Fig.III-1B). Moreover, the alkyne-Alexa594 signal overlapped with the anti-DAT antibody signal at the cell surface. These results demonstrate that PRIME labeling is both highly efficacious and specific for LAP-DAT. We also

performed PRIME labeling on cells expressing wild-type DAT (wt-DAT), and observed no labeling (data not shown). Of note, we observed that the requirement of a linker between the DAT polypeptide backbone and the LAP peptide was absolutely required in order to achieve high efficiency labeling, and earlier attempts at labeling LAP-DAT constructs, either without linkers or with shorter linkers, failed to efficiently label cells (data not shown).

We next asked whether LAP-DAT expressed, functioned and downregulated comparable to wt-DAT. Immunoblot analysis revealed that LAP-DAT expressed at levels comparable to wt-DAT, with a similar ratio of mature (~75kDa) to immature (~55kDa) biosynthetic species (Fig.III-1C). LAP-DAT was also subjected to PKC-induced function downregulation. PKC activator PMA significantly decreased wt-DAT and LAP-DAT function to 68.70 ± 3.42% and 58.15 ± 7.49% control levels, respectively (Fig.III-1C). To test whether LAP-DAT undergoes regulated endocytosis, we stimulated DAT internalization by inhibiting Ack1 with 20μM AIM-100, as previously reported (Wu et al., 2015). Basal LAP-DAT internalization rates were not significantly different from wt-DAT (p=0.2) and AIM-100 treatment similarly increased both LAP-DAT (134.48 ± 5.33% of control levels) and wt-DAT (162.57 ± 16.8% control levels) internalization rates (Fig.III-1D). Thus, appending DAT with the LAP peptide did not deleteriously impact DAT biosynthesis, function or endocytic trafficking.

Tracking DAT temporal-spatial post-endocytic trafficking via PRIME labeling

We next used LAP-DAT to temporally track DAT's post-endocytic fate by fluorescently labeling the surface DAT population at room temperature (18°C - 22°C; conditions of minimal endocytosis), stimulating internalization by shifting cells to 37°C, and fixing/staining cells at various post-endocytic time points to measuring DAT co-localization with several endosomal markers (see schematic, Fig.III-2A). As a proof of principle, we first characterized DAT trafficking from the plasma membrane to early endosomes, given multiple reports that DAT co-localizes to EEA1/rab5-positive vesicles shortly following internalization (Daniels and Amara, 1999; Melikian and Buckley, 1999; Eriksen et al., 2009). At time zero, 4.01 ± 0.21% of the LAP-DAT signal co-localized with EEA1 (Fig.III-2C). This low-level co-localization was observed between DAT and all endocytic markers investigated throughout the study, and we attributed this to low-level basal DAT internalization that occurred during the room temperature labeling procedure. Under basal conditions, DAT/EEA1 co-localization rapidly and significantly increased over the first 10 minutes of internalization and peaked at 21.29 ±1.37%, which translates to a 430.9% enhancement over baseline. DAT/EEA1 co-localization plateaued at subsequent time points, although there was a trend for decreased DAT/EEA1 colocalization at the 60 minute time point as compared to the 10 minute peak (Fig.III-2C; p=0.08) Treatment with AIM-100 to stimulate DAT internalization also significantly increased DAT/EEA1 colocalization over time,

although the initial rate of entry into EEA1-positives was significantly slower as compared to vehicle conditions (slope = veh: 1.73±0.41 vs. AIM-100: 0.87±0.11, p<.03, Student's t test, n=30), with co-localization peaking at 20 minutes post-endocytosis. We likewise observed no significant decrease in DAT/EEA1 co-localization after the 20 minute peak. These results demonstrate that the PRIME labeling strategy is effective for tracking DAT from the cell surface to endosomal destinations. Note that in the interest of space, we have only presented DAT internalization images under control conditions, as any AIM-100-induced differences are not markedly different by visual inspection.

Following internalization and localization to early endosomes, proteins are targeted to either degradative, recycling, or retrograde (i.e. TGN) pathways. Given that DAT recycling and rapid delivery to the plasma membrane has been reported by our laboratory and others (Loder and Melikian, 2003; Lee et al., 2007; Gabriel et al., 2013; Richardson et al., 2016), we next asked whether DAT is targeted to the conventional rab11 recycling endosome (Welz et al., 2014). Under basal conditions, we observed no significant DAT/rab11 co-localization over baseline at either 5 or 10 minute time points, and a small, but significant amount of DAT/rab11 co-localization (7.36 ± 0.42% co-localization; Fig.III-3B) that translated to 46.3% over baseline at 20 minutes post-endocytosis, and plateaued across all subsequent time points. During AIM-100 treatment, there was no significant co-localization with rab11 at early time points, but DAT significantly co-localized with rab11 at 45 min and 60 min, as compared to

baseline and early time points (Fig.III-3B). Moreover, at 60 min post-endocytosis, there was significantly more DAT co-localized with rab11 under AIM-100 treatment as compared to vehicle treatment. These results indicate although the majority of DAT does not go through conventional recycling pathway, a small but significant DAT population enters rab11-positive endosomes, and this is increased when DAT endocytosis is stimulated by acute Ack1 inhibition.

Given that the majority of internalized DAT did not co-localize with a rab11-positive endosome, we next asked whether DAT sorted to degradation by staining late endosomes, using rab7 as a marker. Under basal conditions, DAT exhibited a slow, significant, linear (r^2=0.95) increase in rab7 co-localization over time, with 22.11 ± 0.97% DAT/rab7 co-localization observed at the 45 minute timepoint, which translated to a 295.5% elevation over baseline (Fig.III-3D). AIM-100 treatment had no effect on the rate of DAT/rab7 co-localization (slope = vehicle: 0.34 ±0.04 vs. AIM-100: 0.31 ±0.04, p=0.62, Student's t test, n=30). These results suggest that a fraction of DAT moves into rab7-positive endosomes following internalization, with no difference between the kinetics of basal vs. stimulated DAT endocytosis.

DAT targets to retromer-positive endosomes

Given that DAT expression is quite stable, we questioned whether DAT post-endocytic sorting to a rab7-positive compartment was indicative of immediate post-endocytic targeting to the degradative pathway. Recent studies indicate that rab7 is also part of the cargo-selective trimer (Vps35-Vps29-Vps26) that recruits

proteins to the retromer complex from the endosomal membrane (Rojas et al., 2008; Seaman et al., 2009). Therefore, we hypothesized that DAT may recycle to the plasma membrane via a retromer-mediated mechanism. To test this hypothesis, we asked whether internalized DAT entered a retromer-positive endosome, as indicated by co-localization with Vps35, a retromer core protein for cargo recognition (Seaman, 2012; Burd and Cullen, 2014). Under basal conditions, DAT/Vps35 co-localization rapidly and significantly increased over time, peaking at 24.01 ±0.88% co-localization at 15 minutes post-endocytosis, which translates to 413.0% enhanced co-localization over baseline (Fig.III-4B). Moreover, DAT/Vps35 co-localization was significantly reduced by 45min compared with 15min, likely reflecting DAT exiting from Vps35-positive endosomes over time. During AIM-100 stimulation, DAT/Vps35 co-localization likewise increased significantly over time (Fig.III-4B). However, the rate of DAT/Vps35 increased co-localization was significantly lower in AIM-100 vs. vehicle-treated cells (slope = veh: 1.24±0.28 vs. AIM-100: 0.63±0.14, p<.04, one-tailed Student's t test, n=24-30). However, in contrast to vehicle-treated cells, DAT/Vps35 co-localization continued to increase at later time points (Fig.III-4B). These results suggested that DAT is targeted to the retromer complex following either basal or stimulated endocytosis.

We further asked whether native DAT co-localized with Vps35 *in situ* in bona fide DAergic neurons. Immunocytochemistry performed on coronal mouse brain slices revealed DAT/Vps35 co-localization in perinuclear regions of substantia

nigra DAergic neurons (Fig. 4C). We also observed discrete DAT/Vps35-positive puncta in a subset of DAergic terminals in the dorsal striatum (Fig. 4D), consistent with DAT targeting to retromer complex. Taken together with our cellular LAP-DAT studies, these results indicate that DAT co-localizes with retromer in both AN27 cells and intact DA neurons, raising the possibility that internalized DAT is sorted and recycled via a retromer-dependent mechanism.

Retromer complex is required to maintain DAT surface levels

We next tested whether intact retromer activity was required to recycle DAT back to the plasma membrane following internalization. We reasoned that if retromer were required for DAT recycling, retromer disruption would decrease DAT surface levels, and potentially target DAT to degradation if it were unable to recycle back to the plasma membrane. To test this hypothesis, we used shRNA to knock down Vps35, an approach previously reported to perturb retromer function (Choy et al., 2014; Varandas et al., 2016). We screened several human Vps35-targeted shRNA constructs and found that shRNA#32 significantly reduced Vps35 expression to 35.17 ± 4.82% of control levels (Fig.III-5A). In DAT-SK-N-MC cells, Vps35 loss resulted in a significant decrease in DAT surface levels (54.90 ±6.43% of control; Fig.III-5B), consistent with a role of retromer in maintaining DAT surface expression. Moreover, total DAT levels were also reduced to 54.40 ±4.72% control levels following Vps35 knockdown (Fig.III-5C), suggesting that compromised retromer activity drives DAT to degradation. Taken

together, these results demonstrate that retromer is required to maintain DAT surface levels, and implicates retromer as the DAT recycling mechanism.

DAT exit from retromer is dependent of its C-terminal PDZ-binding motif

We next asked whether a specific domain targeted to and/or recruited DAT from retromer. Many proteins target to retromer via PDZ binding motifs (Lauffer et al., 2010; Clairfeuille et al., 2016; McGarvey et al., 2016). Interestingly, DAT encodes a C-terminal PDZ-binding motif (-LKV), and multiple reports indicate that DAT surface stability is dependent upon this motif (Torres et al., 2001; Bjerggaard et al., 2004; Rickhag et al., 2013). To test whether the DAT C-terminal PDZ-binding motif was required for targeting to the retromer complex, we mutagenized the DAT C-terminus within the LAP-DAT background (LAP-DAT-AAA) and tested whether DAT retromer targeting was maintained. As seen in Figure III-6B, both wildtype LAP-DAT and LAP-DAT-AAA were robustly targeted to Vps35 compartment. However, there was a significant difference between WT-DAT and DAT-AAA co-localization with Vps35 at the 45 minute time point, suggesting that the DAT –LKV sequence is necessary to exit retromer-associated endosomes.

III.D Discussion

Neurons utilize energy-demanding mechanisms to organize and maintain functional and plastic presynaptic terminals. DAT is expressed in midbrain dopaminergic cell bodies, and is biosynthetically trafficked to distant presynaptic boutons in the dorsal and ventral striata, respectively, where it is properly

organized adjacent to active release sites. Given the large energy expenditure required to construct DAergic terminals, it is evolutionarily advantageous to maintain these complex structures as efficiently as possible. Endocytic recycling rapidly modulates the synapse, bypassing the requirement for either biosynthesis or degradative burden. Evidence from multiple laboratories supports that DAT is subject to constitutive and regulated internalization (Melikian, 2004; Bermingham and Blakely, 2016). However, DAT's post-endocytic fate has long been debated, with numerous reports demonstrating measurable DAT recycling (Loder and Melikian, 2003; Boudanova et al., 2008a; Chen et al., 2013; Richardson et al., 2016). In contrast, several tracking studies found that DAT targets to degradative vesicles (Miranda et al., 2005; Eriksen et al., 2010b). These seemingly disparate findings may have arisen from the broad variety of approaches used to interrogate the DAT trafficking itinerary, including antibody tracking (Hong and Amara, 2013; Block et al., 2015), fluorescent high-affinity DAT ligands (Eriksen et al., 2009) and DAT-reporter fusion proteins (Eriksen et al., 2010b). Moreover, previous studies reported steady-state findings following extended labeling times, which might unintentionally overlook early post-endocytic trafficking events. It is worth noting that although our studies were highly feasible in the cell line utilized, LAP-DAT expression was compromised in both SK-N-MC and SH-SY5Y cell lines, possibly due to cleavage of LAP peptide by endogenous transmembrane proteases.

Consistent with previous results, we observed robust, rapid DAT entry into EEA1-positive endosomes within 5-10 minutes post-endocytosis. Surprisingly, when we stimulated DAT endocytosis by acutely inhibiting Ack1, we did not observe more rapid or enhanced DAT entry into EEA1-positive endosomes. Rather, we observed significantly less DAT/EEA1 colocalization at 5min and 10min, compared to vehicle controls (Fig.III-2C). Basal DAT internalization is both clathrin- and dynamin-independent (Gabriel et al., 2013; Wu et al., 2015), whereas PKC- and AIM-100 stimulated DAT internalization are both clathrin and dynamin-dependent (Gabriel et al., 2013; Wu et al., 2015). Thus, a DAT subpopulation may target to an EEA1-negative (Hayakawa et al., 2006; Lakadamyali et al., 2006; Kalaidzidis et al., 2015) early endosomes following stimulated endocytosis. Alternatively, enhanced DAT internalization may saturate the early endosomal machinery, and thereby stall entry kinetics into EEA1-positive early endosomes.

Although DAT recycling and rab11-dependent DAT delivery to the plasma membrane have been reported (Loder and Melikian, 2003; Furman et al., 2009a; Sakrikar et al., 2012; Richardson et al., 2016), previous DAT tracking studies have not observed robust DAT entry into classic rab11-positive recycling endosomes (Eriksen et al., 2010b; Hong and Amara, 2013). We observed a small, but significant, enhancement in DAT/rab11 co-localization under basal conditions, that increased in response to stimulated DAT endocytosis (Fig.III-3A, 4B). However, DAT/rab11 co-localization over baseline was relatively modest

over time (~46%), did not account for the robust DAT population that entered early endosomes (~500% enhanced co-localization over baseline). In contrast, we observed robust and significant DAT co-localization in Vps35-positive vesicles, that peaked between 15-20 minutes post internalization (Fig.III-4A, 4B), with an enhancement of 513% over baseline, comparable to what we observed for DAT entry into early endosomes. These data suggest that the majority of internalized DAT targets to the retromer complex. Retromer and rab11-dependence are not necessarily mutually exclusive, as several reports suggest that rab11 may function in consort with retromer to facilitate recycling (van Weering et al., 2012; Hsiao et al., 2015). Likewise, several reports suggest that rab7 is required for retromer recruitment, both in yeast and mammalian cells, and acts in consort with rab5 (Rojas et al., 2008; Seaman et al., 2009). Thus, both our results, and those from other groups, indicating significant DAT post-endocytic trafficking through a rab7-positive compartment may also be indicative the retromer-mediated recycling mechanism. We cannot, however, rule out the possibility that a fraction of DAT is sorted to late endosomes for degradation. Indeed, we observed a decrease in total and surface DAT in response to retromer disruption, consistent with targeted degradation. However, dissimilar to previous reports (Miranda et al., 2005; Hong and Amara, 2013), we did not observe any enhanced targeting to rab7-positive endosomes in response to stimulated DAT internalization (Fig.III-3C, 3D).

Steady state DAT/Vps35 co-localization was detected in perinuclear regions of DAergic soma (Fig.III-4C). This could indicate potential DAT recycling in somatodendritic compartments via the perinuclear recycling compartment. Alternatively, given that retromer is responsible for retrograde transport from the plasma membrane to the TGN, DAT/Vps35 co-localization may simply reflect close opposition between DAT biosynthesis and retrogradely targeted proteins in the TGN. Although DAT expression is strikingly robust in DAergic terminal regions, we only detected DAT/Vps35 co-localization in a small subset of DAT puncta (Fig.III-4D). Thus, DAT recycling may only occur in the small subset of actively releasing terminals. Consistent with this premise, we observe only modest, but significant, losses in DAT surface expression following PKC activation in *ex vivo* mouse striatal slices (Gabriel et al., 2013), which could reflect larger losses in individual active boutons averaged with a static DAT population in the inactive DA terminal population. Future studies should better illuminate this possibility.

Retromer complex was originally identified as mediating cargo recruitment for retrograde trafficking from plasma membrane to the TGN (Seaman et al., 1997; Seaman et al., 1998). However, recent studies have revealed that retromer plays an equally important role in recruiting membrane protein cargo from endosomes for recycling (Seaman, 2012; Choy et al., 2014). Importantly, retromer disruption via shRNA-mediated Vps35 knockdown resulted in marked DAT depletion from the plasma membrane (Fig.III-5C), consistent with a requirement of retromer to

recycle constitutively internalizing DAT and maintain DAT surface expression. However, retromer disruption did not completely deplete DAT surface expression over a 96 hour knockdown window. Given that we only achieved a partial Vps35 knockdown, there was likely still some active retromer complex available. Moreover, given that some DAT targets to rab11-positive endosomes, there could have remained some additional recycling via this endosomal route.

Retromer-mediated cargo recruitment from the endosomal membrane frequently requires interaction of sorting nexin 27 (SNX27) with a PDZ-binding motif on cargo proteins (Lauffer et al., 2010). DAT encodes a distal C-terminal PDZ binding motif (-LKV), and previous studies implicate this motif in stabilizing mature DAT in DAergic terminals (Torres et al., 2001; Bjerggaard et al., 2004; Rickhag et al., 2013). We found that DAT required the –LKV signal in order to efficiently exit from Vps35-positive endosomes (Fig.III-6B), consistent with retromer-mediated DAT recruitment from endosomes for recycling. Retromer endosome fission away is promoted by Vps1, a dynamin-related protein in yeast (Chi et al., 2014; Arlt et al., 2015), which is consistent with our previous finding that DAT endocytic recycling relies on a dynamin-dependent mechanism (Gabriel et al., 2013). While we do not currently known whether other SLC6 transporters rely upon retromer, a recent proteomic screen identified multiple potential members of the retromer interactome (McMillan et al., 2016), including the DAT SLC6 homolog, GLYT2 (SLC6A9). GLYT2 also encodes a C-terminal PDZ binding site, which is required for stable plasma membrane expression (Armsen

et al., 2007). In contrast, serotonin transporter expression and stability are insensitive to C-terminal perturbations (El-Kasaby et al., 2010).

In summary, we used PRIME labeling to track DAT post-endocytic fate, both during constitutive and stimulated internalization. Our results provide compelling evidence that DAT surface stability relies upon retromer-mediated endocytic recycling. Moreover, these findings coalesce several seemingly disparate previous reports, all of which are consistent with a retromer-mediated mechanism governing DAT's post-endocytic fate.
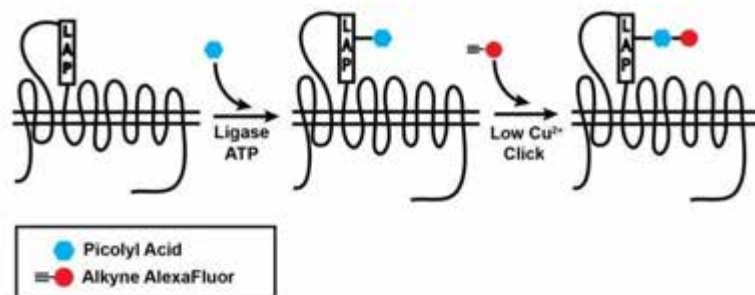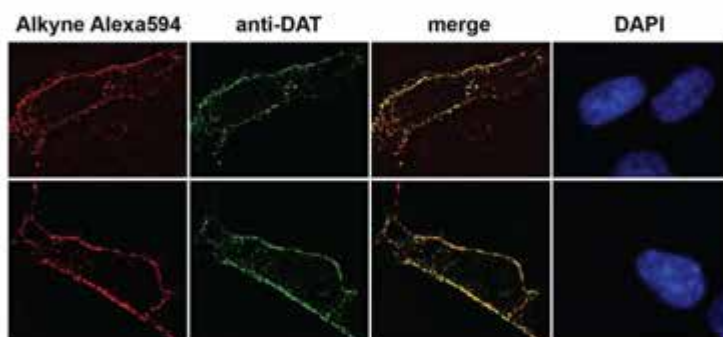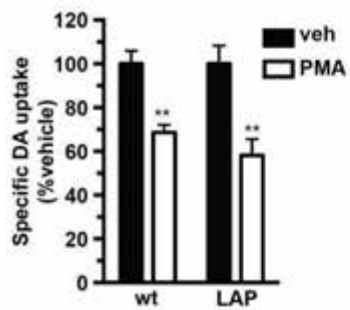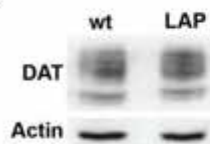
A

Picolyl Acid
Alkyne AlexaFluor

B

Alkyne Alexa594   anti-DAT   merge   DAPI

C

wt   LAP

DAT

Actin

D

T   S   V   A

wt-DAT

LAP-DAT
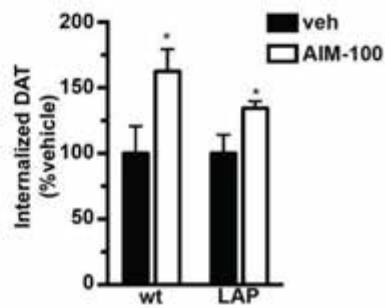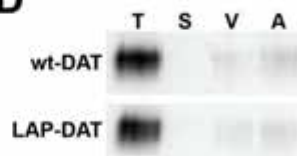
Figure III-1. DAT expression, function and trafficking tolerate LAP peptide incorporation into extracellular loop 2. A. *PRIME strategy for labeling surface DAT*. A ligase acceptor peptide (LAP) was engineered into the DAT 2nd extracellular loop. Picolyl azide (PAz) is coupled to surface DAT encoding LAP peptide (LAP-DAT), followed by alkyne-Alexa594 conjugation, resulting in fluorescent surface DAT. **B.** *LAP-DAT labeling.* Stable LAP-DAT AN27 cells were labeled with alkyne Alexa594 as described in *Materials and Methods,* followed by fixation and staining for DAT, in parallel. Two representative cells are shown, and all cells in the field are indicated by DAPI staining. **C.** *LAP-DAT immunoblots and [^{3}H]DA uptake assays. Top:* Representative immunoblots showing expression of wt-DAT and LAP-DAT in AN27 cells. *Bottom:* [^{3}H]-DA uptake assay. Stable wt-DAT AN27 or LAP-DAT AN27 cells were treated $\pm$1µM PMA, 30 min, 37°C and [^{3}H]-DA uptake was measured as described in *Material and Methods*. Average data are presented, expressed as %vehicle-treated control uptake ±SEM. **p<0.01, Student's t test, n=4. **D.** *Internalization assay:* wt-DAT and LAP-DAT internalization rates were measured in AN27 cells $\pm$20µM AIM-100, as described in *Material and Methods. Top*: Representative immunoblots showing the total surface protein at t=0 (T), strip controls (S), and internalized protein during either vehicle (V) or AIM-100 (A) treatments. *Bottom:* Average internalization rates expressed as percent vehicle-treated internalization ±SEM, *p<0.05, Student's t test, n=6 (wt-DAT) n=10 (LAP-DAT).
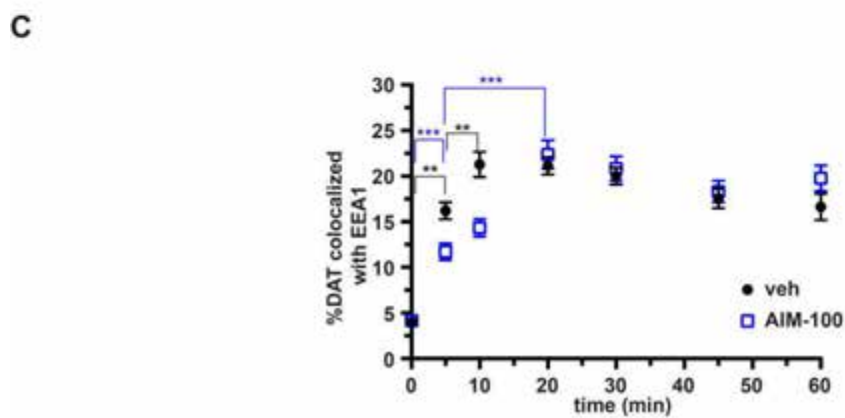
A

LAP labeling RT

Internalization 37 ℃

Fixation Ab staining

B

LAP-DAT EEA1

0'

5'

10'

20'

45'

60'

C

%DAT colocalized with EEA1
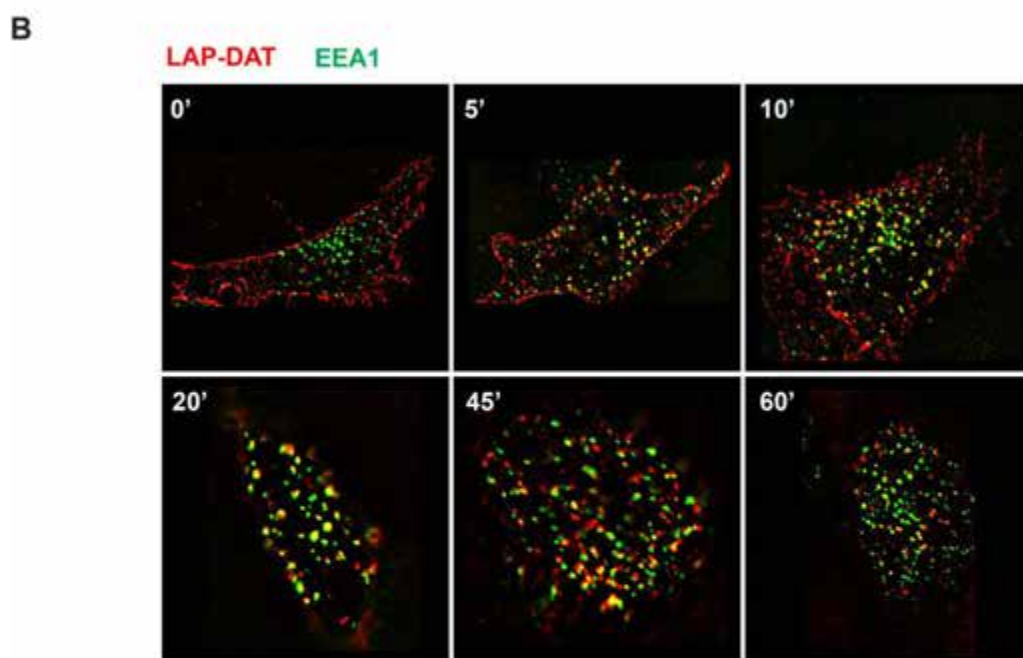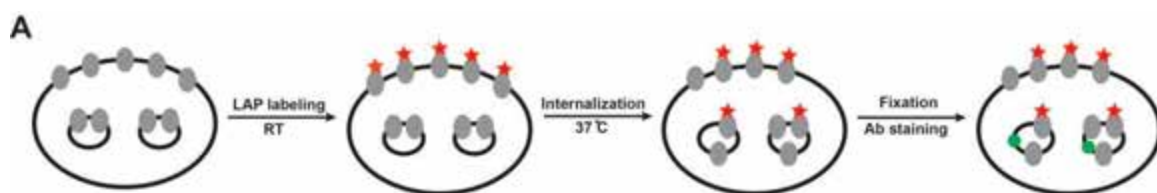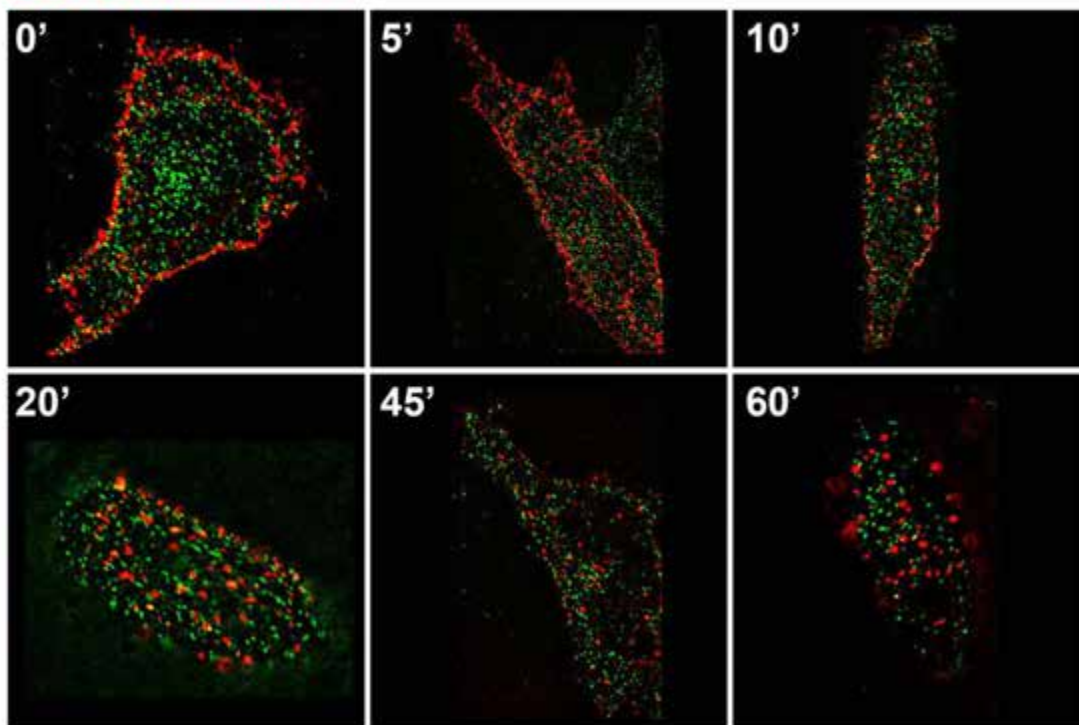
time (min)

● veh
□ AIM-100

Figure III-2. LAP-DAT labeling is highly specific and facilitates DAT post-endocytic tracking A. *Strategy for tracking DAT post-endocytic routes using PRIME labeling.* Live LAP-DAT AN27 cells were labeled at room temperature using the PRIME labeling approach, as described in *Material and Methods*. Internalization was induced by shifting cells to 37°C, ±20μM AIM-100 to induce internalization. Cells were then fixed, permeabilized and stained for endosomal markers using specific antibodies. **B.** Representative images showing LAP-DAT (red) and early endosome marker EEA1 (green) at the indicated time points (vehicle-treated). **C**. Average data expressed as %DAT signal co-localized with EEA1 signals ±SEM. * indicates significant difference, **p<0.005, ***p<0.001, two-way ANOVA with multiple comparison Tukey's and Bonferroni's test, n=19-49 cells, imaged across three independent experiments.

A

B

C

LAP-DAT Rab7

D

Figure III-3. A small DAT fraction targets to rab11- and rab-7 positive endosomes. A-D. *PRIME labeling on live cells.* Live LAP-DAT AN27 cells were labeled using PRIME labeling approach at room temperature, internalized for indicated time, fixed and stained for indicated markers as described in *Material and Methods*. **A and C.** Representative images showing LAP-DAT (red) with recycling endosome marker rab11 (green, **A**) or late endosome marker rab7 (green, **C**) at the indicated time points. **B and D.** Average data expressed as %DAT signal that co-localized with either rab11 signal (**B**) or rab7 signal (**D**) ±SEM. * indicates significant difference *p<0.05, **p<0.005, ***p<0.001, two-way ANOVA with multiple comparison Tukey's and Bonferroni's test, n=28-30 cells (C), n=30 cells (D), imaged over three independent experiments.

A

LAP-DAT VPS35

B

C

| DAT | VPS35 | merge |

substantia nigra

D

| DAT | VPS35 | merge |

dorsal striatim
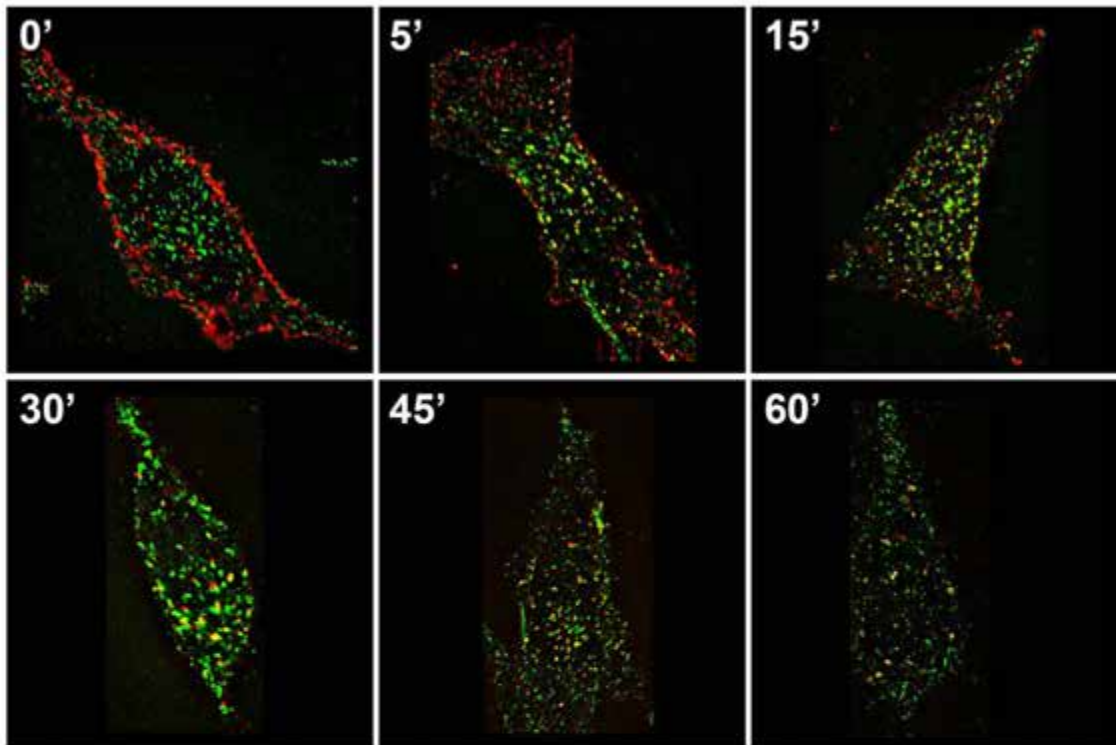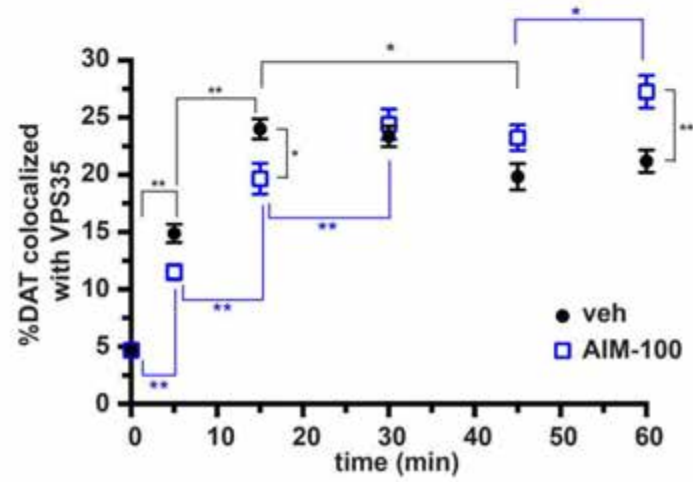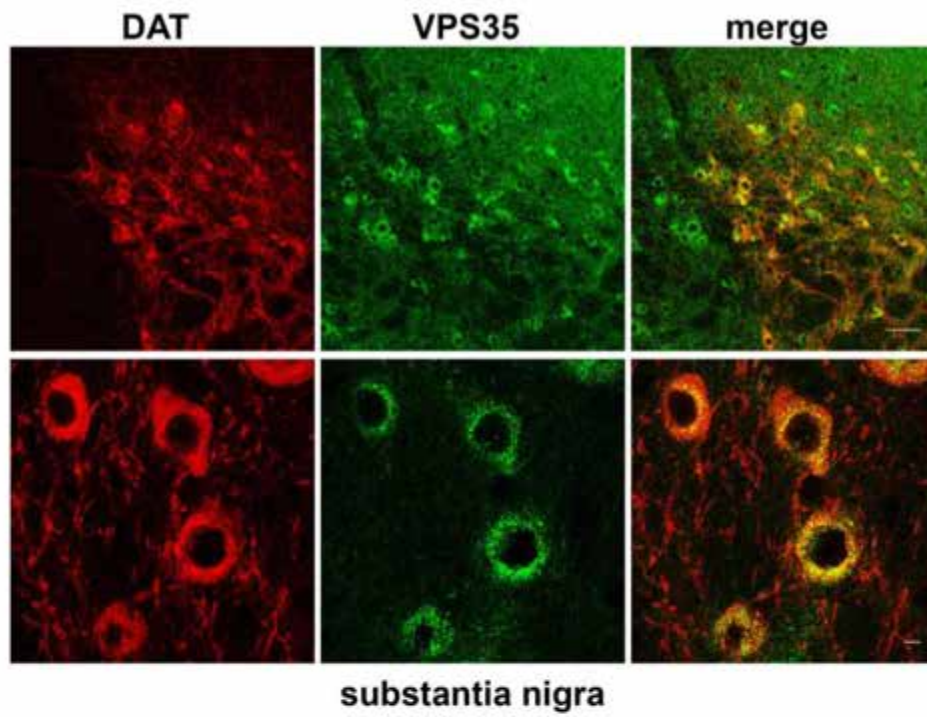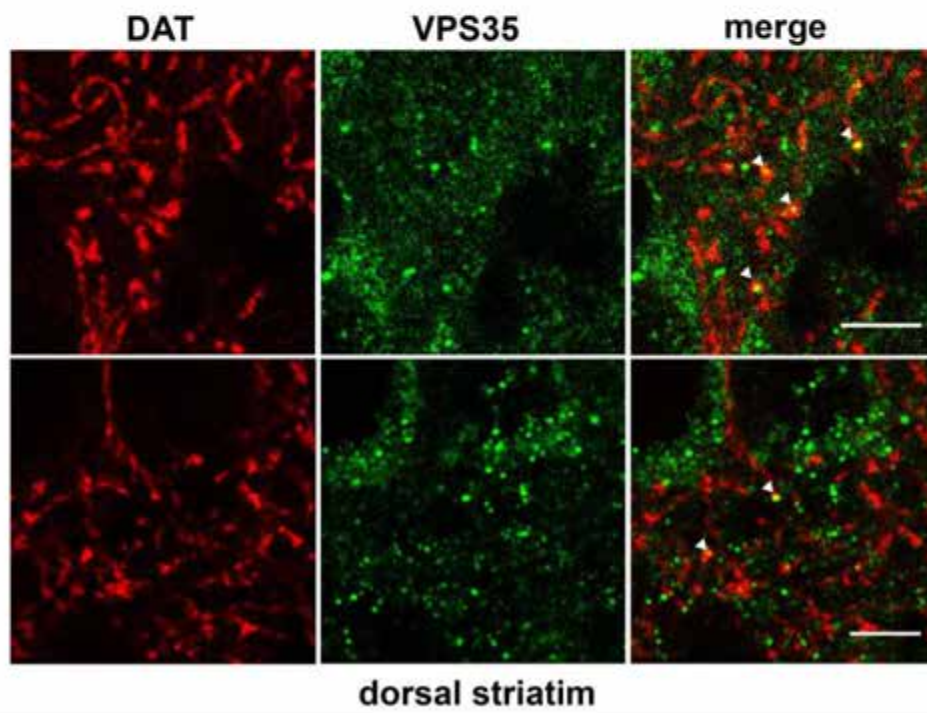
Figure III-4. DAT is targeted to retromer positive endosomes. A-B. LAP-DAT is sorted to retromer in AN27 cells**.** *PRIME labeling on live cells.* **A.** Representative images showing LAP-DAT (red) and retromer marker Vps35 (green) at the indicated time points. **B.** Average data expressed as %DAT-positive objects that co-localized with Vps35 signal ±SEM. All later time points were significant different from baseline; * indicates significant difference under basal condition, *p<0.05, **p<0.001, two-way ANOVA with multiple comparison Tukey's and Bonferroni's test,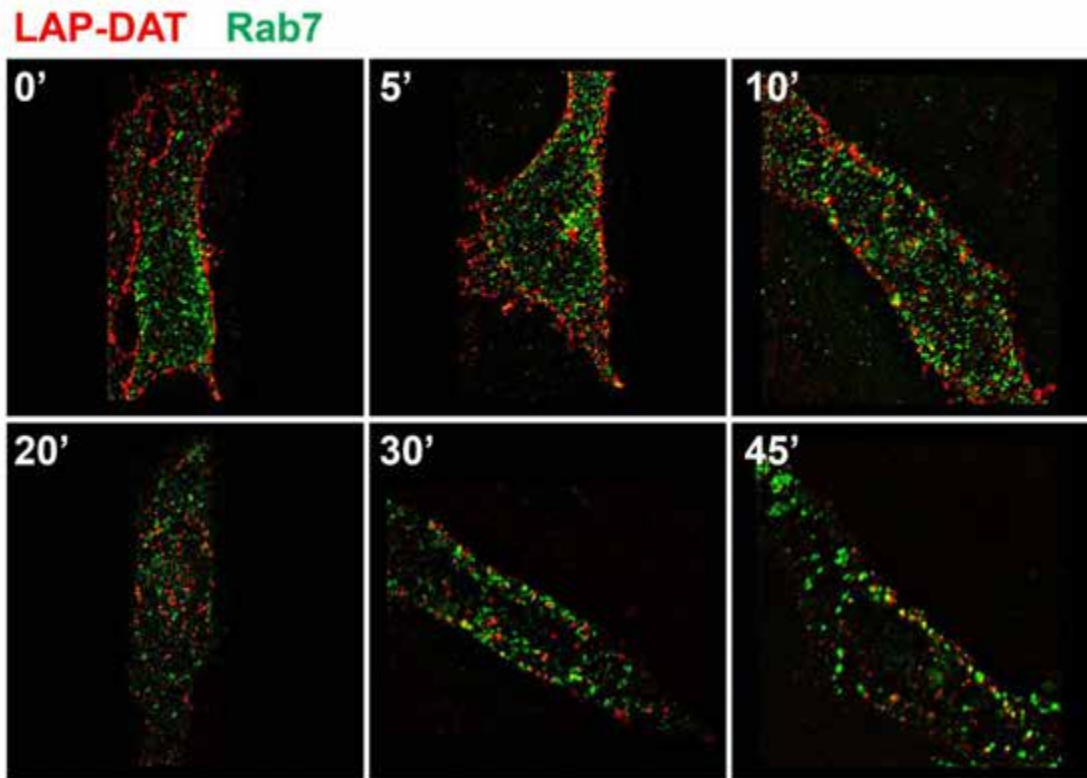 n=2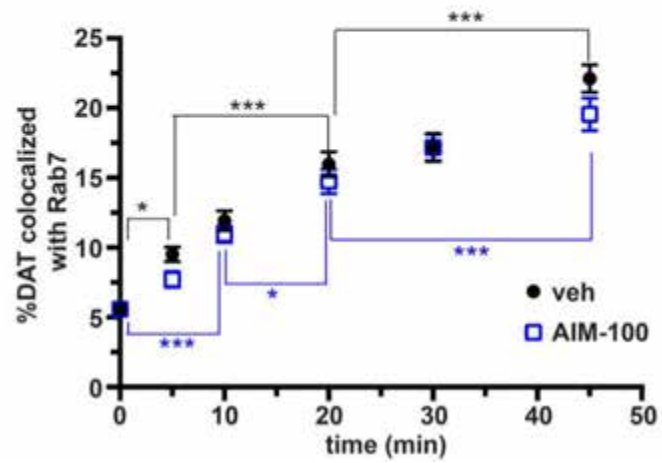4-30 cells, imaged over three independent experiments. **C-D.** *DAT/Vps35 co-localization in mouse DAergic neurons.* Brains from perfused mice were fixed and stained for DAT and Vps35 as described in *Material and Methods*. **C.** Representative confocal images showing DAT (red) and Vps35 (green) expression in DA neuronal cell bodies in substantial nigra, scale bar, 50 μm (top) and 5 μm (bottom). **D.** Representative confocal images showing DAT (red) and Vps35 (green) expression in DA terminals in dorsal striatum. Scale bar: 5 μm. White arrowheads indicate DAT/Vps35 co-localized puncta.
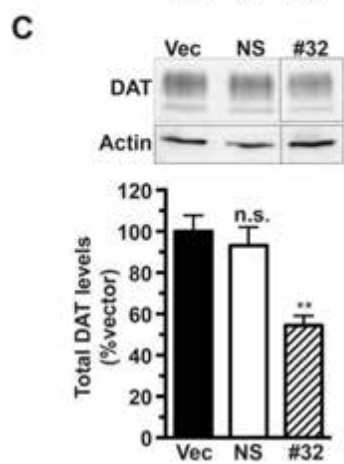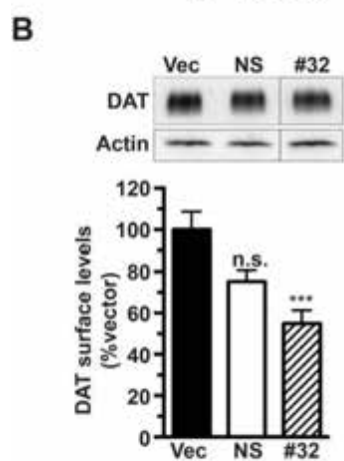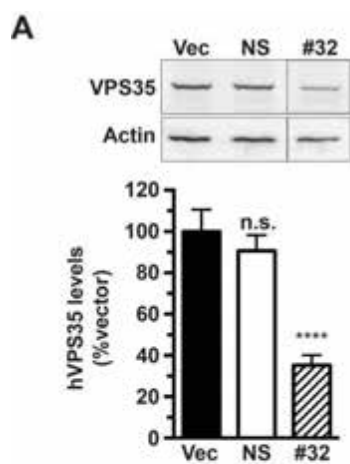
Figure III-5.Retromer complex is required to maintain DAT surface levels.
A. *Lentiviral-mediated hVps35 knockdown in SK-N-MC cells.* DAT SK-N-MC cells were transduced with the indicated lentiviral particles and hVps35 protein expression was measured 96 h posttransduction. *Top:* Representative immunoblots showing endogenous hVps35 levels in lysates from cell transduced with lentiviral particles expression either pGIPZ vector (vec), nonsilencing shRNA (NS), hVps35 #32 (#32). *Bottom:* Average hVps35 protein levels expressed as %vector-transduced hVps35 levels ±SEM. ****$p < 0.001$, one-way ANOVA with post-hoc Dunnett's test, n=7. **B.** *Cell surface biotinylation.* DAT SK-N-MC cells were transduced with indicated lentiviral particles and relative DAT surface levels were measured by biotinylation as described in *Material and Methods. Top:* Representative immunoblots. *Bottom:* Average DAT surface levels expressed as %vector levels ±SEM (normalized to actin levels). ***$p < 0.005$, One-way ANOVA with post-hoc Bonferroni's test, n=6. **C.** DAT SK-N-MC cells were transduced with indicated lentiviral particles and total DAT levels were quantified by immunoblotting normalized to actin loading controls. *Top:* Representative immunoblots. *Bottom:* Average total DAT levels expressed as %vector levels ±SEM (normalized to actin levels). **$p < 0.01$, One-way ANOVA with post-hoc Bonferroni's test, n=5.
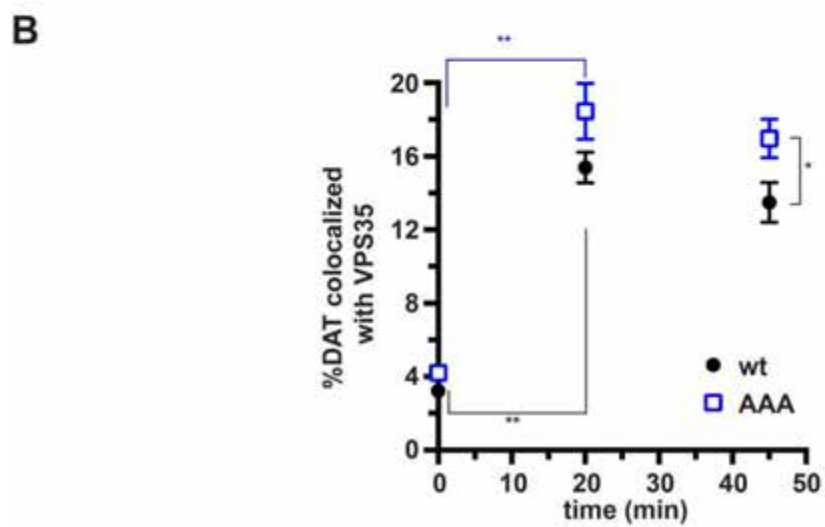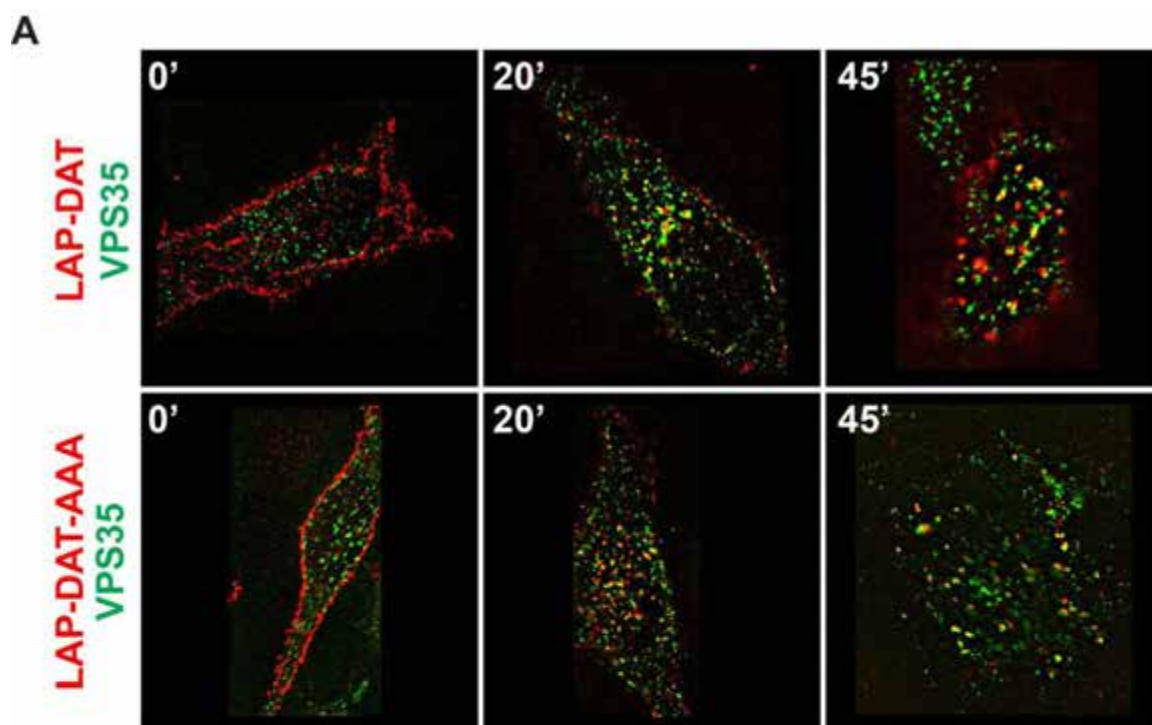
Figure III-6. DAT exit from retromer is dependent upon its C-terminal PDZ-binding motif. A. Representative images showing wt-LAP-DAT or LAP-DAT-AAA (red) with retromer marker Vps35 (green) at indicated time points. **C.** Average data expressed as %DAT objects co-localized with Vps35 signals ±SEM.* indicates significant difference, *p<0.05, **p<0.001, two-way ANOVA with multiple comparison Tukey's and Bonferroni's test, n= 29-30 cells, imaged over two independent experiments.

CHAPTER IV

Investigating Dopamine Transporter Endocytic Trafficking In *Ex Vivo* Slice

Preparations Using A Direct Fluorophore Coupling Approach

IV.A Introduction

DAT robustly traffics to and from the plasma membrane via the endocytic pathways. Numerous stimuli, including PKC activation and amphetamine exposure acutely decreased DAT plasma membrane availability in dopaminergic terminals by promoting DAT endocytosis. However, DAT's post-endocytic fate is unclear and conflicting studies report that DAT targets to either recycling or degradative endocytic compartments, or that DAT may not traffic in bona fide DAergic neurons. In the previous chapter, using PRIME labeling in a neuronal cell line, I generated a temporal-spatial profile of DAT movement along the endosomal pathways. To further expand these findings in bona fide DAergic neurons, I attempted to use the LAP-DAT construct to examine the DAT endocytic trafficking in *ex vivo* brain slices.

IV.B Material And Methods

Material: HA tag from HA-hDAT-pcDNA3.1(+) was cloned into LAP-hDAT-pcDNA3.1(+) using HindIII and BamHI sites. The resulting construct, HA-LAP-hDAT-pcDNA3.1(+) was put into pAAV-EF1α-DIO-WPRE vector using the BamHI cloning site, generating pAAV-EF1α-DIO-HA-LAP-hDAT-WPRE. Rat anti-

HA was from Roche. Rat anti-rat (MAB369) and mouse anti-TH were from EMD Millipore. Horseradish peroxidase (HRP)-conjugated goat anti-rat was from EMD Millipore. Alexa fluorophore-conjugated secondary antibodies were from Jackson ImmunoResearch (cross absorbed goat anti-rat Alexa 594, cross absorbed goat anti-rat Alexa 488, goat anti-mouse Alexa 488, goat anti-mouse Dylight 405). pAz and BTTAA were kindly provided by Dr. Alice Ting (Stanford University, Stanford CA). Alkyne-conjugated Alexa Fluor594 was from Invitrogen.

Viruses and Stereotaxic Intracranial Injection: Conditional expression of HA-LAP-hDAT in Cre-containing neurons were achieved using recombinant adeno-associated viruses 2 (AAV2s) encoding a double-floxed inverted open reading frame (DIO) of HA-LAP-hDAT. Plasmid DNA was packaged in the viral core of University of Massachusetts Medical School. All animals were handled according to University of Massachusetts Medical School IACUC protocol A-1506 (H.E.M.). P21-30 male C57/B6 mice were anesthetized with 100mg/kg ketamine 10mg/kg xylazine and placed in a digital stereotaxic frame (Stoelting). After puncturing the skull under aseptic conditions, AAV2 viral particles were injected (1µL total volume) unilaterally through a microliter syringe (Hamilton) at a rate of 0.2µL/min. Injection coordinates were -3.08mm anterior/posterior, 1.0mm medial/lateral and 4.5mm dorsal/ventral for the Substantia Nigra Pars Compacta (SNpc). After surgical procedures, mice were returned to their home cage for >21 days to allow for maximal gene expression.

Immunohistochemistry for floating sections: Viral injected TH-Cre C57/B6 mice were transcardially perfused with 4% paraformaldehyde for fixation. Brains were post-fixed overnight at 4°C, followed by dehydration in PBS/30% sucrose, 2-3 days prior to sectioning at 25 µm on a sliding microtome (Leica). Coronal sections at SNc or striatum were incubated overnight at 4°C with rat anti-HA (1:2000) and mouse anti-TH (1:1000) in PBS with 0.2% TritonX-100, 5% normal goat serum, 1%BSA (protease and IgG free) and 1% H_2O_2. Slices were rinsed in PBS, and incubated with goat anti-rat and goat anti-mouse Alexa Fluor (1:500 each) for 1hr at room temperature. Excess secondary antibodies were washed in PBS and slices were mounted onto glass slides, dried and coverslipped in Prolong Gold mounting medium containing DAPI (Invitrogen).

Ex vivo Mouse Striatal Slice PRIME labeling: Viral injected TH-cre C57BL/6 mice were sacrificed by cervical dislocation and decapitation. Mouse brains were rapidly removed and chilled in ice cold sucrose- and kynurenic acid (1mM)-supplemented artificial CSF (SACSF) (2.5mM KCl, 1.2mM NaH_2PO_4, 1.2mM $MgCl_2$, 2.4mM $CaCl_2$, 26mM $NaHCO_3$, 11mM glucose, 250mM sucrose) saturated with 95% O_2/5% CO_2. Brains were mounted on Leica VT1200S Vibratome and 300µm coronal sections were obtained at both striatal regions and midbrain regions. Slices recovered for 40min, at 31°C in 95%O_2/5%CO_2-saturated ACSF (125mM NaCl, 2.5mM KCl, 1.2mM NaH_2PO_4, 1.2mM $MgCl_2$, 2.4mM $CaCl_2$, 26mM $NaHCO_3$, 11mM glucose) containing 1mM kynurenic acid. Surface DAT was labeled using the PRIME method as described in Chapter III.

Briefly, a pAz ligation mix was prepared in ACSF with 10 µM ^{W37V}LplA, 200 µM pAz, 1 mM ATP and 5 mM MgCl$_2$ and was incubated with slices, 20min, room temperature. Slices were rinsed three times with ACSF. A low Cu^{2+} click labeling solution containing 10 mM CuSO$_4$, 50 mM BTTAA and 100 mM sodium ascorbate was prepared in ACSF and incubated at room temperature for 10min in a closed tube. Labeling solution was diluted 200X with ACSF and alkyne-Alexa594 was added to a final concentration of 20 µM. The labeling solution was added to slices and incubated for 10 min, room temperature followed by three rinses with room temperature ACSF. 95% O$_2$/5% CO$_2$ was provided to slices at all labeling steps. Slices were then fixed in 4% paraformaldehyde overnight, 4°C, dehydrated in PBS/30%sucrose and further sectioned into 12 µm subslices. Subslices were blocked, permeabilized and stained with indicated antibodies and Alexa fluorophore-conjugated secondary antibodies. Floating slices were mounted onto glass slides, dried and coverslipped in Prolong Gold mounting medium containing DAPI (Invitrogen).

Wide field microscopy: Brain slices were visualized with a Zeiss Axiovert 200M microscope using either a 20X, 0.75 N.A. objective or a 63X, 1.4 N.A. oil immersion objective and images were captured with a Retiga-1300R cooled CCD camera (Qimaging). For images captured with a 63X objective, 0.4 µm optical sections were obtained through the z-axis and 3D z-stack images were deconvolved with a constrained iterative algorithm using measured point spread

functions for each fluorescent channel using Slidebook 5.0 software (Intelligent Imaging Innovations). All images shown are single representative 0.4 µm planes.

IV.C Results

HA-LAP-DAT expresses as a mature protein and is targeted to DAergic terminals in the dorsal striatum

We first asked whether the AAV2 virus containing HA-LAP-DAT conditionally expressed in DA neurons of TH-Cre mice. Western blots showed that DAT protein was expressed in the DAergic terminals in the dorsal striatum and less in the midbrain somatodendritic compartments (Fig. IV-1A). Note that only mature (~75 KDa) DAT protein was detected in the terminals whereas both mature (~75KDa) and immature (~55 KDa) DAT was expressed in the midbrain. The HA-LAP-DAT construct was only detected in the injected hemisphere, but not in the control hemisphere and mature HA-LAP-DAT was robustly expressed in the DAergic terminals. Immunostaining further confirmed that viral expression was exclusively in DA neurons shown by colocalization between HA and TH staining and readily detected in both dorsal striatum and substantial nigra (Fig. IV-1B, IV-1C). These results suggest that LAP-DAT expresses as a mature protein and is targeted to DAergic terminals in the dorsal striatum.

HA-LAP-DAT cannot efficiently be labeled in ex vivo midbrain slices using the PRIME approach

We next asked whether surface expressed HA-LAP-DAT could be labelled using the PRIME approach in *ex vivo* midbrain slices. The PRIME strategy for labeling surface DAT on ex vivo slices and subsequent immunostainings is illustrated in Figure IV-2A. Acute 300 µm mouse midbrain slices were subjected to PRIME labeling and subsequent immunohistochemistry in parallel to identify DA neurons, as wells as expression of the HA-LAP-DAT construct. As shown in Figure IV-2B, HA-LAP-DAT was expressed in DA neuron cell bodies whereas alkyne-Alexa594 failed to be coupled to the surface of DA neurons expressing HA-LAP-DAT.

IV.D Discussion

In this study, we generated AAV2 virus expressing DIO-HA-LAP-DAT that enables selective expression of this transgene in DA neurons in an intact animal. LAP-DAT expressed as a mature protein and was targeted to the DAergic terminals in the dorsal striatum (Fig. IV-1). Despite the fact that we successfully tracked DAT post-endocytic itinerary using the PRIME labeling in neuronal cell lines, we were unable to efficiently label LAP-DAT in *ex vivo* midbrain slices, making it not feasible to assess DAT post-endocytic targeting in bona fide DA neurons (Fig. IV-2). A possible reason for our negative result is that the 38kDa lipoic acid ligase may not be able to efficiently permeate a 300 µm brain slice. A recent comprehensive study from Sorkin and colleagues used antibody feeding to characterize DAT endocytic trafficking in a knock-in mouse expressing DAT with an extracellular HA epitope, and found little antibody localization with

endosomal markers in dopaminergic terminal regions (Block et al., 2015). It is possible that this result is due to challenges in permeating a relatively thick brain slice (1.0 mm) with a large, globular antibody, similar to what we encountered with LplA-mediated LAP-DAT labeling. Moreover, it is unclear whether internalized DAT bound to a large immunoglobulin would accurately reflect native DAT endocytic targeting, particularly in light of recent studies demonstrating that antibody binding targets membrane proteins to degradation, despite their endogenous endocytic route (St Pierre et al., 2011; Bien-Ly et al., 2014).

A

B
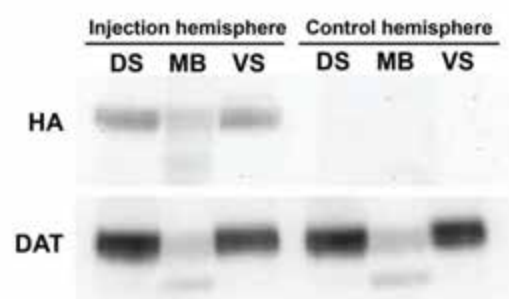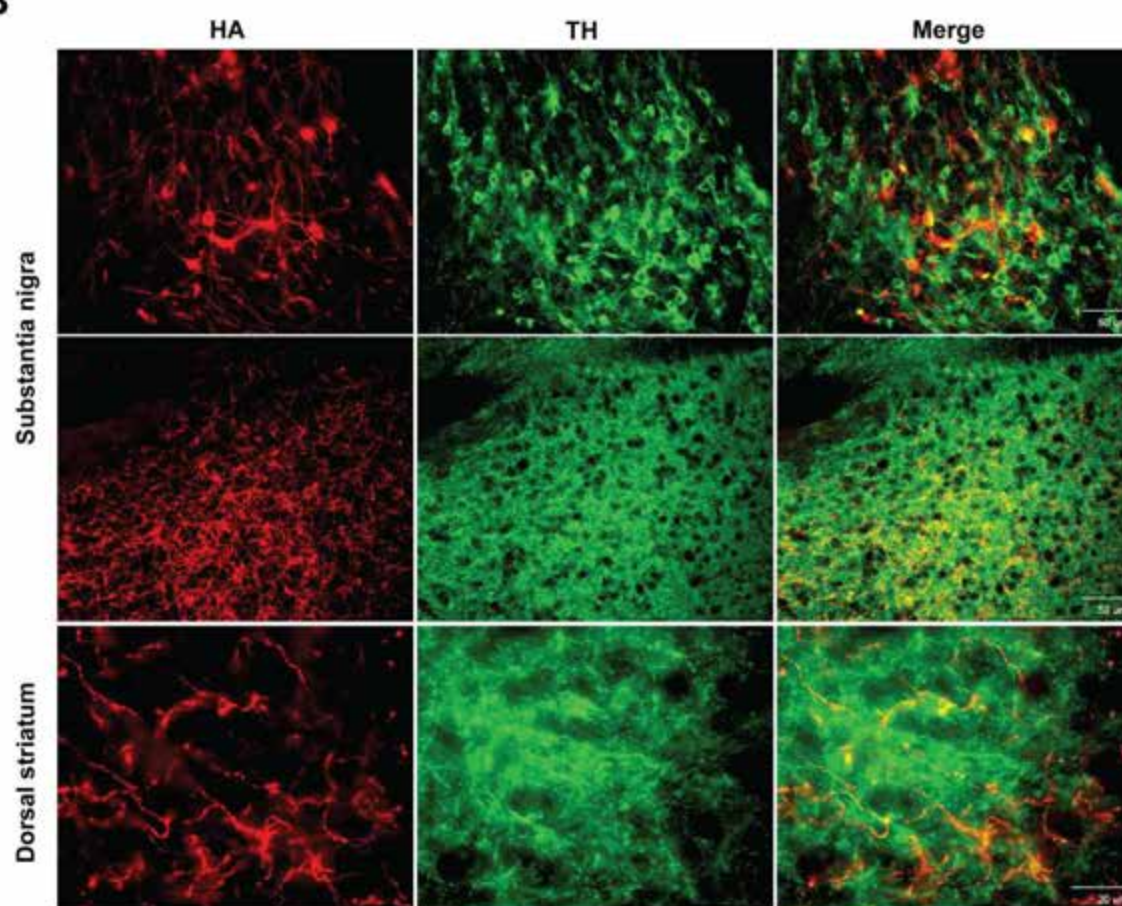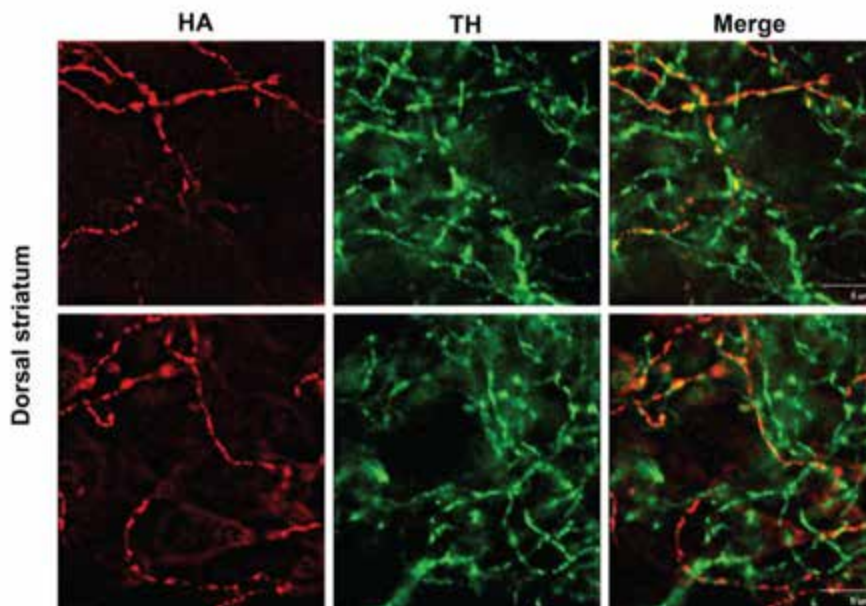
Figure IV-1. HA-LAP-hDAT expresses as a mature protein and is targeted to DAergic terminals in the dorsal striatum. A. Representative blots showing HA-LAP-DAT expression in dorsal striatum (DS), midbrain (MB) and ventral striatum (VS) 3 weeks after intracranial viral injection as described in *Methods*. Note no HA expression was detected in the non-injected hemisphere. **B and C.** Representative immunohistochemistry images showing HA-LAP-DAT expression exclusively in DA neurons in substantia nigra and dorsal striatum. **B.** *Top:* representative HA (red) and DA neuron marker TH (green) staining in substantia nigra under 20X objective, *Middle and Bottom:* representative HA (red) and TH (green) staining in dorsal striatum under 20X objective (middle) and 63X objective (bottom). **C.** Representative HA (red) and TH (green) stainings in dorsal striatum, an enlarged view.
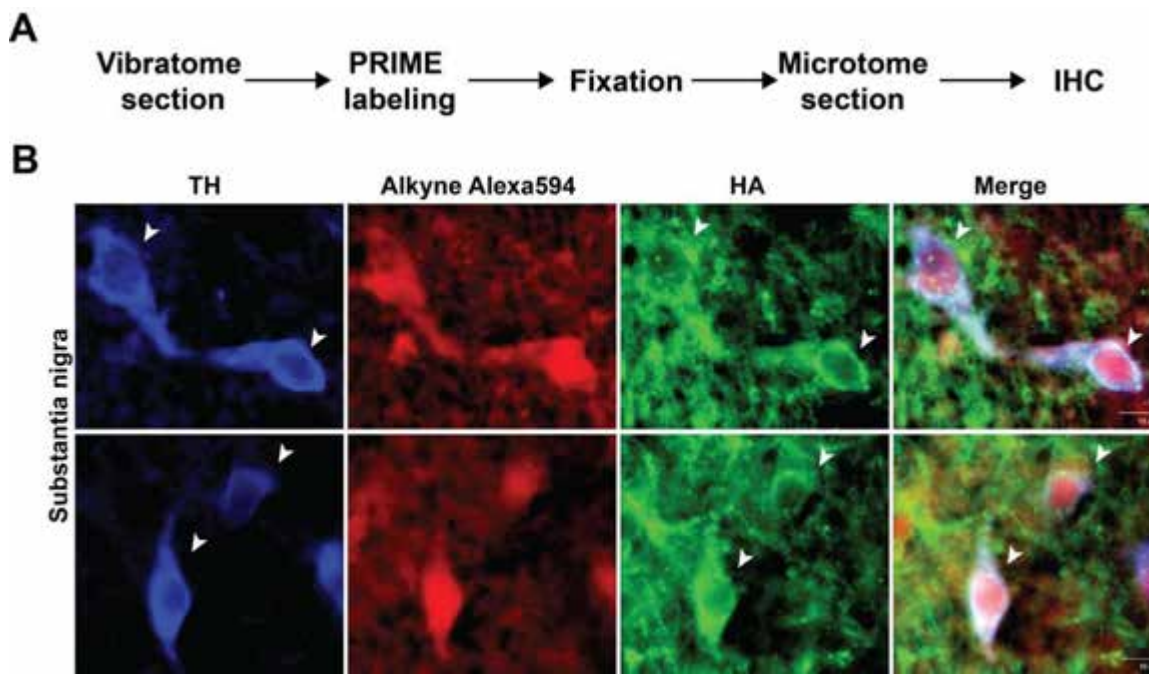
Figure IV-2. HA-LAP-hDAT cannot efficiently be labeled in *ex vivo* midbrain slices using PRIME approach. A. *Strategy for labeling surface DAT in ex vivo midbrain slices using the PRIME approach.* Live acute 300 μm midbrain slices were labeled using PRIME approach at room temperature as described in *Methods*. Slices were fixed, dehydrated and subject to microtome sectioning into 12 μm subslices. Subslices were permeabilized and stained for TH to identify DA neurons. **B.** Representative images showing LAP-DAT (red), DA neuron marker TH (blue) and HA-LAP-DAT contruct expression (green). White arrow heads indicate expression of HA-LAP-DAT in TH positive DA neurons. Note no specific Alkyne Alexa conjugation to the surface DAT.

CHAPTER V

CONCLUSION, DISCUSSION AND FUTURE DIRECTIONS

DA neurotransmission modulates key brain functions such as voluntary movement, reward and desire (Iversen and Iversen, 2007). Dysregulation of DA neurotransmission leads to various neuropsychiatric disorders that affect millions of people worldwide (Snyder, 2002; Sulzer, 2007). DAT-mediated high-affinity reuptake of synaptic DA is the primary mechanism to modulate DA neurotransmission and maintain DA homeostasis in the CNS (Rudnick et al., 2014; Bermingham and Blakely, 2016). DAT is the primary target for the wildly abused psychostimulants cocaine and amphetamine (Amara and Sonders, 1998). Loss-of-function DAT mutations cause dopamine transporter deficiency syndrome, a subtype of parkinsonism dystonia (Kurian et al., 2009). Multiple DAT coding variants are associated with ADHD, ASD, schizophrenia and adult parkinsonism (Mazei-Robison et al., 2008; Sakrikar et al., 2012; Hamilton et al., 2013; Hansen et al., 2014). All three lines of evidence support that changes in DAT function could exert impactful consequences on DA neurotransmission and behavior.

Numerous studies have worked on molecular mechanisms that regulate DAT function. Among them, molecular mechanisms of DAT endocytic trafficking are the primary interest of our lab. DAT plasma membrane expression is requisite for efficacious synaptic DA removal and replenishing of presynaptic DA.

Mechanisms that govern DAT membrane trafficking enable acute modulation of DAT plasma membrane availability, providing means of diminishing or enhancing DA neurotransmission.

V.A DAT Endocytosis: Ack1 as an Endocytic Brake Molecule

We and others have shown that DAT is subject to constitutive and regulated endocytosis (Daniels and Amara, 1999; Melikian and Buckley, 1999; Loder and Melikian, 2003; Sorkina et al., 2005). Stimuli such as PKC and amphetamine promote DAT endocytosis that results in a loss of DAT membrane availability and function. A negatively regulatory mechanism, or an "endocytic brake", controls DAT plasma membrane availability. PKC activation releases the endocytic brake, stimulating DAT endocytosis. Both the intracellular N- and C-termini are required for this negative regulatory mechanism (Boudanova et al., 2008b; Sorkina et al., 2009), however, cellular factors that control the DAT endocytic brake are completely undefined.

In Chapter II, through a candidate gene approach, I discovered that a non-receptor tyrosine kinase, Ack1, negatively controls DAT endocytosis (Fig. II-2). Tyrosine kinases caught interest in the field years ago when Zahniser's group used a non-selective tyrosine kinase inhibitor, genistein, to acutely block tyrosine kinase activity in either Xenopus oocytes or rat synaptosomes and reported decrease of DAT function (Doolen and Zahniser, 2001; Hoover et al., 2007). Our

findings demonstrated that Ack1's effect was specific to DAT and that SERT, a SLC6 DAT homolog, was not subject to Ack1 controlled endocytosis (Fig. II-2).

Using pharmacological and genetic approaches, I further showed that Ack1 inactivation was required to release the DAT endocytic brake, downstream of PKC and cdc42 (Fig. II-7). PKC activation decreased Ack1 activity in both SK-N-MC cells and mouse striatum (Fig. II-1), but PKC does not directly phosphorylate Ack1 (Linseman et al., 2001). Thus, it is likely that another signaling molecule exists between PKC and Ack1, probably an Ack1-targeted protein tyrosine phosphatase that can be activated by PKC. How Ack1 stabilizes DAT at the plasma membrane also remains unclear. I showed that when Ack1 is inactivated, DAT internalizes through clathrin-mediated endocytosis (Fig. II-4). Since Ack1 directly interacts with clathrin (Teo et al., 2001; Yang et al., 2001), it is possible that Ack1 controls the DAT endocytic brake through interaction with clathrin machinery. Another tentative hypothesis is that Ack1 interacts directly with DAT, so that when Ack1 is inactivated, its disassociation from DAT triggers DAT endocytosis. Our lab tested this hypothesis by co-IP and found no association between Ack1 and plasma membrane DAT (Sweeney and Melikian, unpublished result). We also did not observe any DAT/Ack1 co-localization using immunohistochemistry, arguing against a DAT/Ack1 complex (Marshall and Melikian, unpublished result). Future studies elucidating molecular mechanisms of how Ack1 stabilizes DAT on the plasma membrane will provide us more information on the Ack1-controlled DAT endocytic brake.

Another intriguing question is whether Ack1 inactivation is also required for amphetamine-stimulated DAT endocytosis. To test that, I overexpressed constitutively active form of Ack1 (S445P-Ack1) and measured DAT internalization rate in presence of 10 µM amphetamine. Preliminary results showed that overexpressing S445P-Ack1 mutants had a trend to revert the amphetamine-induced increase in DAT endocytosis (p=0.055, n=3), suggesting Ack1 may also negatively regulate amphetamine-stimulated DAT endocytosis.

By identifying Ack1 as a DAT endocytic brake molecule, I was able to restore normal trafficking to a DAT coding variant (R615C) identified in an ADHD proband by constitutively activating Ack1 (Fig. II-10). These findings support the idea that targeting DAT regulatory mechanism may be a viable approach to treat trafficking dysregulated DAT. Other than the DAT-R615C mutant, the DAT-A559V mutant, that is associated with ADHD and ASD, is insensitive to amphetamine-induced cell surface redistribution (Bowton et al., 2014). Given that Ack1 may also negatively regulate amphetamine-stimulated DAT endocytosis, Future studies should test whether inhibiting Ack1 activity or knocking down Ack1 would rescue amphetamine's effect on DAT-A559V.

V.B DAT Endocytosis: Differential Dependence on Clathrin

There have been conflicting results in the field about the requirement of clathrin in basal and regulated DAT endocytosis. Both clathrin-dependent and –independent mechanisms have been implicated in heterologous cell lines as well

as primary cultured DA neurons (Daniels and Amara, 1999; Sorkina et al., 2005; Cremona et al., 2011). However, they either used non-selective clathrin inhibitors or shRNAs to chronically deplete clathrin over days, which could globally disrupt both clathrin-dependent and –independent endocytic mechanisms. Using a selective dynamin inhibitor, our laboratory recently demonstrated in intact mouse DA neuron terminals that PKC-stimulated DAT endocytosis was dynamin-dependent while basal DAT endocytosis did not require dynamin (Gabriel et al., 2013). These results suggested that constitutive and PKC-stimulated DAT internalization might also be differentially dependent on clathrin. In Chapter II, I used a selective clathrin inhibitor, Pitstop2, to test this hypothesis, and found that PKC-stimulated DAT endocytosis was clathrin-dependent, whereas basal DAT endocytosis was clathrin-independent (Fig. II-5). Furthermore, when directly visualizing DAT surface dynamics using TIRF microscopy, I observed little/no co-localization between DAT and clathrin, supporting that basal DAT endocytosis does not require clathrin (Fig. II-5). However, mechanisms mediating basal DAT endocytosis remain unclear.

A number of endocytic pathways internalize cargos independent of clathrin. Understandings of these pathways mainly came from morphology studies using electron microscopy, pharmacology studies examining sensitivity to pharmacological agents or biochemical and cell biology studies determining their dependence on certain kinases and GTPases. Key proteins have been identified to mediate clathrin-independent endocytosis. Lipid raft residing integral

transmembrane proteins caveolin and flotillin mediate caveolin- and flotillin-dependent endocytosis, respectively (Parton, 2003; Glebov et al., 2006). DAT has been shown to distribute in both lipid raft and non-raft microdomains within the plasma membrane and is associated with flotillin-1 (Adkins et al., 2007; Foster et al., 2008; Cremona et al., 2011; Navaroli et al., 2011). Lipid raft microdomains were reported to constrain DAT lateral mobility (Adkins et al., 2007; Sorkina et al., 2013) and influence DAT conformation (Hong and Amara, 2010). Moreover, an ADHD-linked DAT coding variant, R615C, displayed reduced flotillin-1 association and lipid raft localization (Sakrikar et al., 2012). Given that this DAT mutant has enhanced endocytic trafficking rates, lipid raft localization probably stabilizes DAT at the plasma membrane. Consistent with this, using TIRF to measure DAT plasma membrane distribution, our lab showed that PKC activation significantly decreased raft localized DAT, suggesting that PKC-stimulated DAT endocytosis occurs in the non-raft microdomain (Gabriel et al., 2013). Whether basal DAT endocytosis preferentially occurs in the lipid raft microdomains and the molecular mechanisms behind it remains to be elucidated.

There are also phagocytosis and macropinocytosis that involve uptake of larger membrane areas than clathrin- or caveolin-dependent pathways (Chimini and Chavrier, 2000; Dharmawardhane et al., 2000; Shao et al., 2002). Fundamental questions such as how membrane invagination is formed and how endocytic pits are pinched off the plasma membrane are unclear for some of these clathrin-independent pathways. The BIN/amphiphysin/Rvs (BAR) domain-containing

protein endophilin has recently been shown to control a fast-acting tubulovesicular endocytic pathway that is independent of clathrin and its accessary protein AP2 (Boucrot et al., 2015; Renard et al., 2015). Multiple G-protein coupled receptors such as β1-adrenergic, dopamine D3 and D4 receptors, muscarinic acetylcholine receptor 4, the receptor tyrosine kinases EGFR, PDGFR as well as interleukin-2 receptor all require endophilin for their ligand-induced internalization. Thus, future studies investigating these different clathrin-independent endocytosis pathways would shed light on basal DAT endocytosis mechanisms.

V.C DAT post-endocytic sorting: retromer-mediated recycling

Multiple investigators aiming to elucidate DAT's endocytic fate generated disparate results. Functional studies demonstrated that the DA D2 receptor activation promoted surface expression of DAT, supporting the idea of an endocytic DAT pool that is readily inserted into the plasma membrane (Bolan et al., 2007; Lee et al., 2007). Our lab has shown that globally blocking endocytic recycling using either lower temperature (18ºC) or vacuolar H^+ ATPase inhibitor monensin decreased DAT surface levels, suggesting a constitutive recycling process (Loder and Melikian, 2003; Gabriel et al., 2013). More recently, Richardson et al. reported that changes in membrane potential alone can rapidly drive DAT endocytosis and reinsertion into the plasma membrane. However, dynamic imaging studies visualizing which compartments DAT go through using

either inhibitor analog or bulky antibodies implicated both degradation and recycling pathways (Eriksen et al., 2010b; Hong and Amara, 2013; Block et al., 2015). Multiple groups reported that PKC activation drove DAT to lysosomal degradation (Daniels and Amara, 1999; Miranda et al., 2005; Hong and Amara, 2013). In Chapter III, I took advantage of a small molecule labeling technique called PRIME to directly couple fluorophore to DAT that minimally disturbs DAT expression and function (Fig. III-1). This labeling technique enables selective labeling of the cell surface population of DAT. Instead of tracking DAT with endosomal markers following steady state redistribution of labeled DAT, as previously described, I generated a temporal profile of DAT with distinct endosomal markers to track its movement along the endocytic pathways.

Rather than observing entry and exit into the endocytic vesicles, I observed enhanced DAT colocalization with early endosome marker (i.e. EEA1-positive) that plateaued over time. This suggests that cell surface population of DAT did not internalize simultaneously but reached steady-state distribution over time (Fig. III-2). The majority of DAT does not recycle through the conventional (i.e. rab11-positive) recycling endosomes, although I did observe a small, but significant, entry into rab11-positive vesicles (Fig. III-3). In contrast, DAT showed robust colocalization with retromer marker Vps35, suggesting DAT was targeted to retromer (Fig. III-4). Further Vps35 knockdown experiments in intact cells showed that impairing retromer function significantly reduced both cell surface DAT levels as well as total DAT levels (Fig. III-5), indicating retromer mediates

DAT recycling back to the plasma membrane. I also observed a slow, but linear increase, of DAT movement into Rab7-positive vesicles (Fig. III-3). Retromer and rab7-targeting are not mutually exclusive since Rab7 has also been reported to recruit retromer complex core proteins for cargo sorting (Rojas et al., 2008; Seaman et al., 2009). However, this study does not rule out the possibility that a fraction of DAT is sorted to late endosomes for degradation. The fact that impairing retromer function reduced total DAT levels indicating targeted degradation. Future experiments using lysosome marker such as lysoTracker are needed to test this possibility.

Using the PDZ-binding domain mutant DAT (DAT-AAA), I showed that this mutant did not exit retromer as efficiently as wt-DAT, suggesting DAT PDZ-binding motif in retromer-mediated DAT recycling. However, the molecular mechanisms mediating this process remain unknown. The first question that needs to be tested is whether DAT also direct binds SNX27 for retromer recruitment like β2-adrenergic receptors (Lauffer et al., 2010). Also, given that both degradation and recycling pathways have been indicated in this study, what are the signal sequences/motifs in DAT that determines the distinct post-endocytic sorting destinations (recycling vs, degradation)? To answer these questions, high resolution microscopy and robust image quantification techniques are required to direct visualize DAT sorting at the endosomes and distinguish the retromer exit domain from the sorting endosomes.

Study in Chapter III tested DAT post-endocytic route under basal and Ack1-controlled conditions and I observed similar targeting but distinct colocalzation kinetics for EEA1, Vps35 and rab11. Hong et al. showed that DAT was targeted to different destinations under PKC- or amphetamine- regulated endocytosis (Hong and Amara, 2013). Therefore, future studies using the PRIME labeling-based single cell endocytosis assay will elucidate what happens in PKC- and amphetamine- stimulated DAT endocytosis and whether retromer still mediates DAT recycling under these conditions.

Mutations in retromer core protein Vps35 have been identified in autosomal dominant, late-onset Parkinson's disease (Vilarino-Guell et al., 2011; Zimprich et al., 2011). Since retromer is important for the post-endocytic sorting of many proteins including DAT, DAT membrane trafficking may also be altered under pathological conditions such as Parkinson's disease.

V.D Studying DAT Endocytic Trafficking *in vivo*:
Challenges and Future Directions

Majority of studies on DAT membrane trafficking have been performed using non-neuronal heterologous expression systems rather than intact DA neurons. The reason is that it is notoriously difficult to obtain neuronal cultures that contain a high faction of DA neurons. In dissociated postnatal midbrain neuron culture, 50% or less neurons were dopaminergic (Rayport et al., 1992) and even so,

these cultured DA neurons are not suitable for biochemical assays. The intracellularly located N- and C- termini make it technically challenging to introduce tags in the extracellular domain without perturbation of the transporter expression and function. Sorkin and colleagues first successfully incorporated a HA tag to DAT EL2 without altering DAT function (Sorkina et al., 2006). They further generated a KI mouse line that expressed HA-EL2-DAT to track DAT membrane trafficking in *ex vivo* brain slices and reported a very low level of basal DAT endocytic trafficking in the striatum and no amphetamine-regulated DAT trafficking (Block et al., 2015). However, their experiments lack inherent controls for the overall healthiness of the acute sagittal brain slices during the labeling procedure. Our lab and others used biochemical analysis on acute coronal brain slices that are enriched in DAergic nerve terminals and reported significant DAT surface reduction in response to PKC and amphetamine (Cremona et al., 2011; Gabriel et al., 2013; Wu et al., 2015).

To resolve these controversial results and gain insight of how DAT membrane trafficking is regulated *in vivo*, I proposed to express the LAP-DAT containing AAV2 virus selectively in the adult DA neurons in mouse brain and track the DAT endocytic itinerary in both somatodendritic and terminal parts of DA neurons. Althrough the LAP-DAT containing AAV2 virus expressed in adult DA neurons and was targeted to terminals, the PRIME labeling was not successful in acute brain slices, probably due to insufficient penetration of the lipoic acid ligase, the 38kDa enzyme necessary for the first labeling step (Fig. IV1, IV2). These results

additionally raise the possibility that lack of robust labeling in the studies by Block et al. may be due to difficulty in achieving efficient antibody permeation of their thicker, 1 mm acute slices. Therefore, alternative approaches are needed to study DAT endocytic trafficking *in vivo*.

Combining *in vivo* DAT approach with the latest microscopy techniques such as super-resolution microscopy would enable us to investigate some of the fundamental questions regarding DAT membrane trafficking at individual synapses. It is well established that receptor membrane trafficking at the postsynaptic membrane is a key mechanism underlying different forms of postsynaptic plasticity (Kennedy and Ehlers, 2006). An intriguing question, then, is whether there is a relationship between DAT endocytic trafficking and DA synaptic vesicle release/recycling. It is already reported that changes in membrane potential alone rapidly altered DAT endocytic trafficking (Richardson et al., 2016), raising the possibility that DAT endocytic trafficking is acutely regulated during DA neurotransmission and this could be an essential mechanism to maintain presynaptic DA homeostasis.

To address this question, the first step would be to test whether DAT membrane trafficking occurs in every DA synapses. A recent study using a Fluorescent False Neurotransmitters (FFN) that resolves individual DA synapses revealed that less than 20% of labeling DA synapses was able to release DA in response to stimulation, suggesting that the majority of DA synapses were silent synapses

(Pereira et al., 2016). Testing this question requires simultaneously measuring DAT membrane trafficking and DA vesicle release at the same synapse.

Since synaptic vesicle recycling and regulated DAT endocytosis both utilize clathrin machineries, the next intriguing question is whether these two processes occur at the same presynaptic membrane domain. In other words, is the presynaptic membrane compartmentalized into active zone and endocytic zone? DAT has been shown to locate at the perisynaptic zone, adjacent to the active synaptic vesicle release zone (Nirenberg et al., 1997b; Nirenberg et al., 1997a), supporting the idea of presynaptic membrane compartmentalization. However, considering DAT is highly mobile on the membrane (Eriksen et al., 2009), it is also possible that a fraction of DAT transiently moves into the active zone though lateral diffusion. I attempted to investigate DAT surface dynamics using PRIME labeling and TIRF microscopy but could not obtain quantifiable images, mostly due to the diffuse DAT surface distribution. Considering that the individual DA synapse is extremely fine (~0.3 µm in diameter), super resolution microscopy techniques will be necessary to test these hypotheses in real time.

Other than the DA nerve terminals, DAT is also expressed in somatodendritic compartments and it is not clear what DAT function is there and whether DAT regulatory mechanisms are the same compared with DAT in the terminals. The LAP-DAT expressing AAV2 virus had very little mature DAT expression in the midbrain, suggesting very little DAT would be inserted in the somatodendritic

plasma membrane (Fig. IV1). Our lab has begun to investigate brain region specific membrane trafficking of DAT. The first question is whether regulated DAT endocytic trafficking is different between dorsal striatum and ventral striatum (NAc). To test that, coronal striatal slices will be dissected into dorsal and ventral (NAc) subslices and PKC- or amphetamine-stimulated DAT endocytosis will be examined using steady-state biotinylation on acute coronal brain slices. Similarly, to test whether DAT undergoes regulated endocytosis in somatodentritic compartments, acute coronal brain slices containing substantial nigra or VTA will be treated with PKC activator PMA or amphetamine and DAT surface levels will be assessed using *ex vivo* slice biotinylation.

Functional importance of DAT membrane trafficking *in vivo* is also poorly resolved. How does altered DAT membrane trafficking affect DA neurotransmission and behavior? What happens in psychostimulant addicted brain? Does DAT trafficking contribute to these pathological conditions? It is recently reported that Vav2, a Rho family guanine nucleotide exchange factor protein, negatively regulated DAT surface levels and that Vav2 KO mice selectively increased DAT function in NAc and diminished cocaine-induced locomotor and reward behavior response, suggesting DAT endocytic regulatory mechanisms contribute to cocaine response in rodents (Zhu et al., 2015). Our lab has started to look into some of these questions by manipulating proteins required for stimulated DAT endocytosis such as Ack1 and Rin in intact mouse brain and correlating data of DAT surface level, DA release and DA-related

behavior. By doing so, we aim to get a comprehensive understanding of DAT endocytic trafficking mechanisms and their functional importance *in vivo*.

BIBLIOGRAPHY

Adkins EM, Samuvel DJ, Fog JU, Eriksen J, Jayanthi LD, Vaegter CB, Ramamoorthy S, Gether U (2007) Membrane mobility and microdomain association of the dopamine transporter studied with fluorescence correlation spectroscopy and fluorescence recovery after photobleaching. Biochemistry 46:10484-10497.

Alexander GE, Crutcher MD, DeLong MR (1990) Basal ganglia-thalamocortical circuits: parallel substrates for motor, oculomotor, "prefrontal" and "limbic" functions. Prog Brain Res 85:119-146.

Amara SG, Kuhar MJ (1993) Neurotransmitter transporters: recent progress. Annu Rev Neurosci 16:73-93.

Amara SG, Sonders MS (1998) Neurotransmitter transporters as molecular targets for addictive drugs. Drug Alcohol Depend 51:87-96.

Anden NE, Hfuxe K, Hamberger B, Hokfelt T (1966) A quantitative study on the nigro-neostriatal dopamine neuron system in the rat. Acta Physiol Scand 67:306-312.

Arbuthnott GW (1974) Proceedings: Spontaneous activity of single units in the striatum after unilateral destruction of the dopamine input. J Physiol 239:121P-122P.

Arlt H, Reggiori F, Ungermann C (2015) Retromer and the dynamin Vps1 cooperate in the retrieval of transmembrane proteins from vacuoles. J Cell Sci 128:645-655.

Armsen W, Himmel B, Betz H, Eulenburg V (2007) The C-terminal PDZ-ligand motif of the neuronal glycine transporter GlyT2 is required for efficient synaptic localization. Mol Cell Neurosci 36:369-380.

Assmann BE, Robinson RO, Surtees RA, Brautigam C, Heales SJ, Wevers RA, Zschocke J, Hyland K, Sharma R, Hoffmann GF (2004) Infantile Parkinsonism-dystonia and elevated dopamine metabolites in CSF. Neurology 62:1872-1874.

Axelrod J (2003) Journey of a late blooming biochemical neuroscientist. J Biol Chem 278:1-13.

Axelrod J, Tomchick R (1958) Enzymatic O-methylation of epinephrine and other catechols. J Biol Chem 233:702-705.

Axelrod J, Laroche MJ (1959) Inhibitor of O-methylation of epinephrine and norepinephrine in vitro and in vivo. Science 130:800.

Bauer B, Ehinger B, Aberg L (1980) [3H]-dopamine release from the rabbit retina. Albrecht Von Graefes Arch Klin Exp Ophthalmol 215:71-78.

Bauman AL, Apparsundaram S, Ramamoorthy S, Wadzinski BE, Vaughan RA, Blakely RD (2000) Cocaine and antidepressant-sensitive biogenic amine transporters exist in regulated complexes with protein phosphatase 2A. J Neurosci 20:7571-7578.

Bermingham DP, Blakely RD (2016) Kinase-dependent Regulation of Monoamine Neurotransmitter Transporters. Pharmacol Rev 68:888-953.

Bien-Ly N, Yu YJ, Bumbaca D, Elstrott J, Boswell CA, Zhang Y, Luk W, Lu Y, Dennis MS, Weimer RM, Chung I, Watts RJ (2014) Transferrin receptor (TfR) trafficking determines brain uptake of TfR antibody affinity variants. J Exp Med 211:233-244.

Binda F, Dipace C, Bowton E, Robertson SD, Lute BJ, Fog JU, Zhang M, Sen N, Colbran RJ, Gnegy ME, Gether U, Javitch JA, Erreger K, Galli A (2008) Syntaxin 1A interaction with the dopamine transporter promotes amphetamine-induced dopamine efflux. Mol Pharmacol 74:1101-1108.

Bjerggaard C, Fog JU, Hastrup H, Madsen K, Loland CJ, Javitch JA, Gether U (2004) Surface targeting of the dopamine transporter involves discrete epitopes in the distal C terminus but does not require canonical PDZ domain interactions. J Neurosci 24:7024-7036.

Bjorklund A, Falck B, Hromek F, Owman C, West KA (1970) Identification and terminal distribution of the tubero-hypophyseal monoamine fibre systems in the rat by means of stereotaxic and microspectrofluorimetric techniques. Brain Res 17:1-23.

Blakely RD, Berson HE, Fremeau RT, Jr., Caron MG, Peek MM, Prince HK, Bradley CC (1991) Cloning and expression of a functional serotonin transporter from rat brain. Nature 354:66-70.

Block ER, Nuttle J, Balcita-Pedicino JJ, Caltagarone J, Watkins SC, Sesack SR, Sorkin A (2015) Brain Region-Specific Trafficking of the Dopamine Transporter. J Neurosci 35:12845-12858.

Bloom FE (1975) Monoaminergic neurotoxins: are they selective? J Neural Transm 37:183-187.

Blum D, Torch S, Lambeng N, Nissou M, Benabid AL, Sadoul R, Verna JM (2001) Molecular pathways involved in the neurotoxicity of 6-OHDA, dopamine and MPTP: contribution to the apoptotic theory in Parkinson's disease. Prog Neurobiol 65:135-172.

Bolan EA, Kivell B, Jaligam V, Oz M, Jayanthi LD, Han Y, Sen N, Urizar E, Gomes I, Devi LA, Ramamoorthy S, Javitch JA, Zapata A, Shippenberg TS (2007) D2 receptors regulate dopamine transporter function via an extracellular signal-regulated kinases 1 and 2-dependent and phosphoinositide 3 kinase-independent mechanism. Mol Pharmacol 71:1222-1232.

Bonanno G, Raiteri M (1987) Coexistence of carriers for dopamine and GABA uptake on a same nerve terminal in the rat brain. Br J Pharmacol 91:237-243.

Bonifacino JS, Traub LM (2003) Signals for sorting of transmembrane proteins to endosomes and lysosomes. Annu Rev Biochem 72:395-447.

Boucrot E, Ferreira AP, Almeida-Souza L, Debard S, Vallis Y, Howard G, Bertot L, Sauvonnet N, McMahon HT (2015) Endophilin marks and controls a clathrin-independent endocytic pathway. Nature 517:460-465.

Boudanova E, Navaroli DM, Melikian HE (2008a) Amphetamine-induced decreases in dopamine transporter surface expression are protein kinase C-independent. Neuropharmacology 54:605-612.

Boudanova E, Navaroli DM, Stevens Z, Melikian HE (2008b) Dopamine transporter endocytic determinants: carboxy terminal residues critical for basal and PKC-stimulated internalization. Mol Cell Neurosci 39:211-217.

Bourne JA (2003) Intracerebral microdialysis: 30 years as a tool for the neuroscientist. Clin Exp Pharmacol Physiol 30:16-24.

Bowton E, Saunders C, Reddy IA, Campbell NG, Hamilton PJ, Henry LK, Coon H, Sakrikar D, Veenstra-VanderWeele JM, Blakely RD, Sutcliffe J, Matthies HJ, Erreger K, Galli A (2014) SLC6A3 coding variant Ala559Val found in two autism probands alters dopamine transporter function and trafficking. Transl Psychiatry 4:e464.

Braz JM, Rico B, Basbaum AI (2002) Transneuronal tracing of diverse CNS circuits by Cre-mediated induction of wheat germ agglutinin in transgenic mice. Proc Natl Acad Sci U S A 99:15148-15153.

Broer S, Gether U (2012) The solute carrier 6 family of transporters. Br J Pharmacol 167:256-278.

Buchmayer F, Schicker K, Steinkellner T, Geier P, Stubiger G, Hamilton PJ, Jurik A, Stockner T, Yang JW, Montgomery T, Holy M, Hofmaier T, Kudlacek O, Matthies HJ, Ecker GF, Bochkov V, Galli A, Boehm S, Sitte HH (2013) Amphetamine actions at the serotonin transporter rely on the availability of phosphatidylinositol-4,5-bisphosphate. Proc Natl Acad Sci U S A 110:11642-11647.

Budygin EA, John CE, Mateo Y, Jones SR (2002) Lack of cocaine effect on dopamine clearance in the core and shell of the nucleus accumbens of dopamine transporter knock-out mice. J Neurosci 22:RC222.

Burd C, Cullen PJ (2014) Retromer: a master conductor of endosome sorting. Cold Spring Harb Perspect Biol 6.

Carboni E, Spielewoy C, Vacca C, Nosten-Bertrand M, Giros B, Di Chiara G (2001) Cocaine and amphetamine increase extracellular dopamine in the nucleus accumbens of mice lacking the dopamine transporter gene. J Neurosci 21:RC141: 141-144.

Carneiro AM, Ingram SL, Beaulieu JM, Sweeney A, Amara SG, Thomas SM, Caron MG, Torres GE (2002) The multiple LIM domain-containing adaptor protein Hic-5 synaptically colocalizes and interacts with the dopamine transporter. J Neurosci 22:7045-7054.

Carvelli L, McDonald PW, Blakely RD, DeFelice LJ (2004) Dopamine transporters depolarize neurons by a channel mechanism. Proc Natl Acad Sci U S A 101:16046-16051.

Carvelli L, Moron JA, Kahlig KM, Ferrer JV, Sen N, Lechleiter JD, Leeb-Lundberg LM, Merrill G, Lafer EM, Ballou LM, Shippenberg TS, Javitch JA, Lin RZ, Galli A (2002) PI 3-kinase regulation of dopamine uptake. J Neurochem 81:859-869.

Cass WA, Gerhardt GA, Mayfield RD, Curella P, Zahniser NR (1992) Differences in dopamine clearance and diffusion in rat striatum and nucleus accumbens following systemic cocaine administration. J Neurochem 59:259-266.

Chan W, Tian R, Lee YF, Sit ST, Lim L, Manser E (2009) Down-regulation of active ACK1 is mediated by association with the E3 ubiquitin ligase Nedd4-2. J Biol Chem 284:8185-8194.

Chen N, Ferrer JV, Javitch JA, Justice JB, Jr. (2000) Transport-dependent accessibility of a cytoplasmic loop cysteine in the human dopamine transporter. J Biol Chem 275:1608-1614.

Chen NH, Reith ME, Quick MW (2004) Synaptic uptake and beyond: the sodium- and chloride-dependent neurotransmitter transporter family SLC6. Pflugers Arch 447:519-531.

Chen R, Furman CA, Zhang M, Kim MN, Gereau RWt, Leitges M, Gnegy ME (2009) Protein kinase Cbeta is a critical regulator of dopamine transporter trafficking and regulates the behavioral response to amphetamine in mice. J Pharmacol Exp Ther 328:912-920.

Chen R, Daining CP, Sun H, Fraser R, Stokes SL, Leitges M, Gnegy ME (2013) Protein kinase Cbeta is a modulator of the dopamine D2 autoreceptor-activated trafficking of the dopamine transporter. J Neurochem 125:663-672.

Chen R, Tilley MR, Wei H, Zhou F, Zhou FM, Ching S, Quan N, Stephens RL, Hill ER, Nottoli T, Han DD, Gu HH (2006) Abolished cocaine reward in mice with a cocaine-insensitive dopamine transporter. Proc Natl Acad Sci U S A 103:9333-9338.

Chi L, Reith ME (2003) Substrate-induced trafficking of the dopamine transporter in heterologously expressing cells and in rat striatal synaptosomal preparations. J Pharmacol Exp Ther 307:729-736.

Chi RJ, Liu J, West M, Wang J, Odorizzi G, Burd CG (2014) Fission of SNX-BAR-coated endosomal retrograde transport carriers is promoted by the dynamin-related protein Vps1. J Cell Biol 204:793-806.

Chimini G, Chavrier P (2000) Function of Rho family proteins in actin dynamics during phagocytosis and engulfment. Nat Cell Biol 2:E191-196.

Choy RW, Park M, Temkin P, Herring BE, Marley A, Nicoll RA, von Zastrow M (2014) Retromer mediates a discrete route of local membrane delivery to dendrites. Neuron 82:55-62.

Clague MJ, Liu H, Urbe S (2012) Governance of endocytic trafficking and signaling by reversible ubiquitylation. Dev Cell 23:457-467.

Clairfeuille T, Mas C, Chan AS, Yang Z, Tello-Lafoz M, Chandra M, Widagdo J, Kerr MC, Paul B, Merida I, Teasdale RD, Pavlos NJ, Anggono V, Collins BM (2016) A molecular code for endosomal recycling of phosphorylated cargos by the SNX27-retromer complex. Nat Struct Mol Biol 23:921-932.

Cook EH, Jr., Stein MA, Krasowski MD, Cox NJ, Olkon DM, Kieffer JE, Leventhal BL (1995) Association of attention-deficit disorder and the dopamine transporter gene. Am J Hum Genet 56:993-998.

Copeland BJ, Vogelsberg V, Neff NH, Hadjiconstantinou M (1996) Protein kinase C activators decrease dopamine uptake into striatal synaptosomes. J Pharmacol Exp Ther 277:1527-1532.

Cremona ML, Matthies HJ, Pau K, Bowton E, Speed N, Lute BJ, Anderson M, Sen N, Robertson SD, Vaughan RA, Rothman JE, Galli A, Javitch JA, Yamamoto A (2011) Flotillin-1 is essential for PKC-triggered endocytosis and membrane microdomain localization of DAT. Nat Neurosci 14:469-477.

Curran S, Mill J, Tahir E, Kent L, Richards S, Gould A, Huckett L, Sharp J, Batten C, Fernando S, Ozbay F, Yazgan Y, Simonoff E, Thompson M, Taylor E, Asherson P (2001) Association study of a dopamine transporter polymorphism and attention deficit hyperactivity disorder in UK and Turkish samples. Mol Psychiatry 6:425-428.

Daniels GM, Amara SG (1999) Regulated trafficking of the human dopamine transporter. Clathrin-mediated internalization and lysosomal degradation in response to phorbol esters. J Biol Chem 274:35794-35801.

Dauer W, Przedborski S (2003) Parkinson's disease: mechanisms and models. Neuron 39:889-909.

Dauer W, Kholodilov N, Vila M, Trillat AC, Goodchild R, Larsen KE, Staal R, Tieu K, Schmitz Y, Yuan CA, Rocha M, Jackson-Lewis V, Hersch S, Sulzer D, Przedborski S, Burke R, Hen R (2002) Resistance of alpha -synuclein null mice to the parkinsonian neurotoxin MPTP. Proc Natl Acad Sci U S A 99:14524-14529.

Daws LC, Callaghan PD, Moron JA, Kahlig KM, Shippenberg TS, Javitch JA, Galli A (2002) Cocaine increases dopamine uptake and cell surface expression of dopamine transporters. Biochem Biophys Res Commun 290:1545-1550.

Dempsey EC, Newton AC, Mochly-Rosen D, Fields AP, Reyland ME, Insel PA, Messing RO (2000) Protein kinase C isozymes and the regulation of diverse cell responses. Am J Physiol Lung Cell Mol Physiol 279:L429-438.

Dharmawardhane S, Schurmann A, Sells MA, Chernoff J, Schmid SL, Bokoch GM (2000) Regulation of macropinocytosis by p21-activated kinase-1. Mol Biol Cell 11:3341-3352.

Dhungel N, Eleuteri S, Li LB, Kramer NJ, Chartron JW, Spencer B, Kosberg K, Fields JA, Stafa K, Adame A, Lashuel H, Frydman J, Shen K, Masliah E, Gitler AD (2015) Parkinson's disease genes VPS35 and EIF4G1 interact genetically and converge on alpha-synuclein. Neuron 85:76-87.

Dickinson SD, Sabeti J, Larson GA, Giardina K, Rubinstein M, Kelly MA, Grandy DK, Low MJ, Gerhardt GA, Zahniser NR (1999) Dopamine D2 receptor-deficient mice exhibit decreased dopamine transporter function but no changes in dopamine release in dorsal striatum. J Neurochem 72:148-156.

Doherty GJ, McMahon HT (2009) Mechanisms of endocytosis. Annu Rev Biochem 78:857-902.

Doolen S, Zahniser NR (2001) Protein tyrosine kinase inhibitors alter human dopamine transporter activity in Xenopus oocytes. J Pharmacol Exp Ther 296:931-938.

Doolen S, Zahniser NR (2002) Conventional protein kinase C isoforms regulate human dopamine transporter activity in Xenopus oocytes. FEBS Lett 516:187-190.

Dougherty DD, Bonab AA, Spencer TJ, Rauch SL, Madras BK, Fischman AJ (1999) Dopamine transporter density in patients with attention deficit hyperactivity disorder. Lancet 354:2132-2133.

Dutta D, Williamson CD, Cole NB, Donaldson JG (2012) Pitstop 2 is a potent inhibitor of clathrin-independent endocytosis. PLoS One 7:e45799.

Egana LA, Cuevas RA, Baust TB, Parra LA, Leak RK, Hochendoner S, Pena K, Quiroz M, Hong WC, Dorostkar MM, Janz R, Sitte HH, Torres GE (2009) Physical and functional interaction between the dopamine transporter and the synaptic vesicle protein synaptogyrin-3. J Neurosci 29:4592-4604.

Eiden LE, Schafer MK, Weihe E, Schutz B (2004) The vesicular amine transporter family (SLC18): amine/proton antiporters required for vesicular accumulation and regulated exocytotic secretion of monoamines and acetylcholine. Pflugers Arch 447:636-640.

El-Kasaby A, Just H, Malle E, Stolt-Bergner PC, Sitte HH, Freissmuth M, Kudlacek O (2010) Mutations in the carboxyl-terminal SEC24 binding motif of the serotonin transporter impair folding of the transporter. J Biol Chem 285:39201-39210.

Eriksen J, Jorgensen TN, Gether U (2010a) Regulation of dopamine transporter function by protein-protein interactions: new discoveries and methodological challenges. J Neurochem 113:27-41.

Eriksen J, Bjorn-Yoshimoto WE, Jorgensen TN, Newman AH, Gether U (2010b) Postendocytic sorting of constitutively internalized dopamine transporter in cell lines and dopaminergic neurons. J Biol Chem 285:27289-27301.

Eriksen J, Rasmussen SG, Rasmussen TN, Vaegter CB, Cha JH, Zou MF, Newman AH, Gether U (2009) Visualization of dopamine transporter trafficking in live neurons by use of fluorescent cocaine analogs. J Neurosci 29:6794-6808.

Falck B, Torp A (1962) New evidence for the localization of noradrenalin in the adrenergic nerve terminals. Med Exp Int J Exp Med 6:169-172.

Fattakhova G, Masilamani M, Borrego F, Gilfillan AM, Metcalfe DD, Coligan JE (2006) The high-affinity immunoglobulin-E receptor (FcepsilonRI) is endocytosed by an AP-2/clathrin-independent, dynamin-dependent mechanism. Traffic 7:673-685.

Ferris RM, Tang FL, Maxwell RA (1972) A comparison of the capacities of isomers of amphetamine, deoxypipradrol and methylphenidate to inhibit the uptake of tritiated catecholamines into rat cerebral cortex slices,

synaptosomal preparations of rat cerebral cortex, hypothalamus and striatum and into adrenergic nerves of rabbit aorta. J Pharmacol Exp Ther 181:407-416.

Fog JU, Khoshbouei H, Holy M, Owens WA, Vaegter CB, Sen N, Nikandrova Y, Bowton E, McMahon DG, Colbran RJ, Daws LC, Sitte HH, Javitch JA, Galli A, Gether U (2006) Calmodulin kinase II interacts with the dopamine transporter C terminus to regulate amphetamine-induced reverse transport. Neuron 51:417-429.

Foster JD, Pananusorn B, Vaughan RA (2002) Dopamine transporters are phosphorylated on N-terminal serines in rat striatum. J Biol Chem 277:25178-25186.

Foster JD, Adkins SD, Lever JR, Vaughan RA (2008) Phorbol ester induced trafficking-independent regulation and enhanced phosphorylation of the dopamine transporter associated with membrane rafts and cholesterol. J Neurochem 105:1683-1699.

Foster JD, Yang JW, Moritz AE, Challasivakanaka S, Smith MA, Holy M, Wilebski K, Sitte HH, Vaughan RA (2012) Dopamine transporter phosphorylation site threonine 53 regulates substrate reuptake and amphetamine-stimulated efflux. J Biol Chem 287:29702-29712.

Fountaine TM, Wade-Martins R (2007) RNA interference-mediated knockdown of alpha-synuclein protects human dopaminergic neuroblastoma cells from MPP(+) toxicity and reduces dopamine transport. J Neurosci Res 85:351-363.

Freyberg Z et al. (2016) Mechanisms of amphetamine action illuminated through optical monitoring of dopamine synaptic vesicles in Drosophila brain. Nat Commun 7:10652.

Furman CA, Lo CB, Stokes S, Esteban JA, Gnegy ME (2009a) Rab 11 regulates constitutive dopamine transporter trafficking and function in N2A neuroblastoma cells. Neurosci Lett 463:78-81.

Furman CA, Chen R, Guptaroy B, Zhang M, Holz RW, Gnegy M (2009b) Dopamine and amphetamine rapidly increase dopamine transporter trafficking to the surface: live-cell imaging using total internal reflection fluorescence microscopy. J Neurosci 29:3328-3336.

Gabriel LR, Wu S, Kearney P, Bellve KD, Standley C, Fogarty KE, Melikian HE (2013) Dopamine transporter endocytic trafficking in striatal dopaminergic neurons: differential dependence on dynamin and the actin cytoskeleton. J Neurosci 33:17836-17846.

Galisteo ML, Yang Y, Urena J, Schlessinger J (2006) Activation of the nonreceptor protein tyrosine kinase Ack by multiple extracellular stimuli. Proc Natl Acad Sci U S A 103:9796-9801.

Garcia BG, Wei Y, Moron JA, Lin RZ, Javitch JA, Galli A (2005) Akt is essential for insulin modulation of amphetamine-induced human dopamine transporter cell-surface redistribution. Mol Pharmacol 68:102-109.

Garris PA, Wightman RM (1994) In vivo voltammetric measurement of evoked extracellular dopamine in the rat basolateral amygdaloid nucleus. J Physiol 478 (Pt 2):239-249.

Gauthier NC, Monzo P, Kaddai V, Doye A, Ricci V, Boquet P (2005) Helicobacter pylori VacA cytotoxin: a probe for a clathrin-independent and Cdc42-dependent pinocytic pathway routed to late endosomes. Mol Biol Cell 16:4852-4866.

Gether U, Andersen PH, Larsson OM, Schousboe A (2006) Neurotransmitter transporters: molecular function of important drug targets. Trends Pharmacol Sci 27:375-383.

Giros B, Jaber M, Jones SR, Wightman RM, Caron MG (1996) Hyperlocomotion and indifference to cocaine and amphetamine in mice lacking the dopamine transporter. Nature 379:606-612.

Glebov OO, Bright NA, Nichols BJ (2006) Flotillin-1 defines a clathrin-independent endocytic pathway in mammalian cells. Nat Cell Biol 8:46-54.

Goeders NE, Smith JE (1983) Cortical dopaminergic involvement in cocaine reinforcement. Science 221:773-775.

Gorentla BK, Moritz AE, Foster JD, Vaughan RA (2009) Proline-directed phosphorylation of the dopamine transporter N-terminal domain. Biochemistry 48:1067-1076.

Grace AA, Bunney BS (1984a) The control of firing pattern in nigral dopamine neurons: burst firing. J Neurosci 4:2877-2890.

Grace AA, Bunney BS (1984b) The control of firing pattern in nigral dopamine neurons: single spike firing. J Neurosci 4:2866-2876.

Granas C, Ferrer J, Loland CJ, Javitch JA, Gether U (2003) N-terminal truncation of the dopamine transporter abolishes phorbol ester- and substance P receptor-stimulated phosphorylation without impairing transporter internalization. J Biol Chem 278:4990-5000.

Greenfield JG, Bosanquet FD (1953) The brain-stem lesions in Parkinsonism. J Neurol Neurosurg Psychiatry 16:213-226.

Greengard P (2001) The neurobiology of slow synaptic transmission. Science 294:1024-1030.

Guastella J, Nelson N, Nelson H, Czyzyk L, Keynan S, Miedel MC, Davidson N, Lester HA, Kanner BI (1990) Cloning and expression of a rat brain GABA transporter. Science 249:1303-1306.

Hamilton PJ, Belovich AN, Khelashvili G, Saunders C, Erreger K, Javitch JA, Sitte HH, Weinstein H, Matthies HJ, Galli A (2014) PIP2 regulates psychostimulant behaviors through its interaction with a membrane protein. Nat Chem Biol 10:582-589.

Hamilton PJ, Campbell NG, Sharma S, Erreger K, Herborg Hansen F, Saunders C, Belovich AN, Consortium NAAS, Sahai MA, Cook EH, Gether U, McHaourab HS, Matthies HJ, Sutcliffe JS, Galli A (2013) De novo mutation in the dopamine transporter gene associates dopamine dysfunction with autism spectrum disorder. Mol Psychiatry 18:1315-1323.

Hansen FH et al. (2014) Missense dopamine transporter mutations associate with adult parkinsonism and ADHD. J Clin Invest 124:3107-3120.

Hastrup H, Karlin A, Javitch JA (2001) Symmetrical dimer of the human dopamine transporter revealed by cross-linking Cys-306 at the extracellular end of the sixth transmembrane segment. Proc Natl Acad Sci U S A 98:10055-10060.

Hayakawa A, Leonard D, Murphy S, Hayes S, Soto M, Fogarty K, Standley C, Bellve K, Lambright D, Mello C, Corvera S (2006) The WD40 and FYVE domain containing protein 2 defines a class of early endosomes necessary for endocytosis. Proc Natl Acad Sci U S A 103:11928-11933.

Heikkila RE, Orlansky H, Cohen G (1975a) Studies on the distinction between uptake inhibition and release of (3H)dopamine in rat brain tissue slices. Biochem Pharmacol 24:847-852.

Heikkila RE, Orlansky H, Mytilineou C, Cohen G (1975b) Amphetamine: evaluation of d- and l-isomers as releasing agents and uptake inhibitors for 3H-dopamine and 3H-norepinephrine in slices of rat neostriatum and cerebral cortex. J Pharmacol Exp Ther 194:47-56.

Heimer L, Alheid GF, de Olmos JS, Groenewegen HJ, Haber SN, Harlan RE, Zahm DS (1997) The accumbens: beyond the core-shell dichotomy. J Neuropsychiatry Clin Neurosci 9:354-381.

Hersch SM, Yi H, Heilman CJ, Edwards RH, Levey AI (1997) Subcellular localization and molecular topology of the dopamine transporter in the striatum and substantia nigra. J Comp Neurol 388:211-227.

Hertting G, Axelrod J (1961) Fate of tritiated noradrenaline at the sympathetic nerve-endings. Nature 192:172-173.

Hertting G, Axelrod J, Kopin IJ, Whitby LG (1961) Lack of uptake of catecholamines after chronic denervation of sympathetic nerves. Nature 189:66.

Hill TA, Gordon CP, McGeachie AB, Venn-Brown B, Odell LR, Chau N, Quan A, Mariana A, Sakoff JA, Chircop M, Robinson PJ, McCluskey A (2009) Inhibition of dynamin mediated endocytosis by the dynoles--synthesis and functional activity of a family of indoles. J Med Chem 52:3762-3773.

Hoebel BG, Monaco AP, Hernandez L, Aulisi EF, Stanley BG, Lenard L (1983) Self-injection of amphetamine directly into the brain. Psychopharmacology (Berl) 81:158-163.

Hokfelt T, Halasz N, Ljungdahl A, Johansson O, Goldstein M, Park D (1975) Histochemical support for a dopaminergic mechanism in the dendrites of certain periglomerular cells in the rat olfactory bulb. Neurosci Lett 1:85-90.

Holton KL, Loder MK, Melikian HE (2005) Nonclassical, distinct endocytic signals dictate constitutive and PKC-regulated neurotransmitter transporter internalization. Nat Neurosci 8:881-888.

Hong WC, Amara SG (2010) Membrane cholesterol modulates the outward facing conformation of the dopamine transporter and alters cocaine binding. J Biol Chem 285:32616-32626.

Hong WC, Amara SG (2013) Differential targeting of the dopamine transporter to recycling or degradative pathways during amphetamine- or PKC-regulated endocytosis in dopamine neurons. FASEB J 27:2995-3007.

Hoover BR, Everett CV, Sorkin A, Zahniser NR (2007) Rapid regulation of dopamine transporters by tyrosine kinases in rat neuronal preparations. J Neurochem 101:1258-1271.

Hornykiewicz O (1966) Dopamine (3-hydroxytyramine) and brain function. Pharmacol Rev 18:925-964.

Hsiao JC, Chu LW, Lo YT, Lee SP, Chen TJ, Huang CY, Ping YH, Chang W (2015) Intracellular Transport of Vaccinia Virus in HeLa Cells Requires WASH-VPEF/FAM21-Retromer Complexes and Recycling Molecules Rab11 and Rab22. J Virol 89:8365-8382.

Huff RA, Vaughan RA, Kuhar MJ, Uhl GR (1997) Phorbol esters increase dopamine transporter phosphorylation and decrease transport Vmax. J Neurochem 68:225-232.

Hyman SE, Malenka RC, Nestler EJ (2006) Neural mechanisms of addiction: the role of reward-related learning and memory. Annu Rev Neurosci 29:565-598.

Ingram SL, Prasad BM, Amara SG (2002) Dopamine transporter-mediated conductances increase excitability of midbrain dopamine neurons. Nat Neurosci 5:971-978.

Iversen L (2000) Neurotransmitter transporters: fruitful targets for CNS drug discovery. Mol Psychiatry 5:357-362.

Iversen L (2006) Neurotransmitter transporters and their impact on the development of psychopharmacology. Br J Pharmacol 147 Suppl 1:S82-88.

Iversen LL (1971) Role of transmitter uptake mechanisms in synaptic neurotransmission. Br J Pharmacol 41:571-591.

Iversen SD, Iversen LL (2007) Dopamine: 50 years in perspective. Trends Neurosci 30:188-193.

Johnson LA, Furman CA, Zhang M, Guptaroy B, Gnegy ME (2005) Rapid delivery of the dopamine transporter to the plasmalemmal membrane upon amphetamine stimulation. Neuropharmacology 49:750-758.

Jones KT, Zhen J, Reith ME (2012) Importance of cholesterol in dopamine transporter function. J Neurochem 123:700-715.

Jones SR, Garris PA, Kilts CD, Wightman RM (1995) Comparison of dopamine uptake in the basolateral amygdaloid nucleus, caudate-putamen, and nucleus accumbens of the rat. J Neurochem 64:2581-2589.

Jones SR, Gainetdinov RR, Wightman RM, Caron MG (1998a) Mechanisms of amphetamine action revealed in mice lacking the dopamine transporter. J Neurosci 18:1979-1986.

Jones SR, Gainetdinov RR, Jaber M, Giros B, Wightman RM, Caron MG (1998b) Profound neuronal plasticity in response to inactivation of the dopamine transporter. Proc Natl Acad Sci U S A 95:4029-4034.

Jones SR, Gainetdinov RR, Hu XT, Cooper DC, Wightman RM, White FJ, Caron MG (1999) Loss of autoreceptor functions in mice lacking the dopamine transporter. Nat Neurosci 2:649-655.

Jonsson G, Fuxe K, Hokfelt T (1972) On the catecholamine innervation of the hypothalamus, with special reference to the median eminence. Brain Res 40:271-281.

Kalaidzidis I, Miaczynska M, Brewinska-Olchowik M, Hupalowska A, Ferguson C, Parton RG, Kalaidzidis Y, Zerial M (2015) APPL endosomes are not obligatory endocytic intermediates but act as stable cargo-sorting compartments. J Cell Biol 211:123-144.

Kawarai T, Kawakami H, Yamamura Y, Nakamura S (1997) Structure and organization of the gene encoding human dopamine transporter. Gene 195:11-18.

Kennedy MJ, Ehlers MD (2006) Organelles and trafficking machinery for postsynaptic plasticity. Annu Rev Neurosci 29:325-362.

Kilty JE, Lorang D, Amara SG (1991) Cloning and expression of a cocaine-sensitive rat dopamine transporter. Science 254:578-579.

Kim HJ, Im JH, Yang SO, Moon DH, Ryu JS, Bong JK, Nam KP, Cheon JH, Lee MC, Lee HK (1997) Imaging and quantitation of dopamine transporters with iodine-123-IPT in normal and Parkinson's disease subjects. J Nucl Med 38:1703-1711.

Kitayama S, Dohi T, Uhl GR (1994) Phorbol esters alter functions of the expressed dopamine transporter. Eur J Pharmacol 268:115-119.

Kitayama S, Shimada S, Xu H, Markham L, Donovan DM, Uhl GR (1992) Dopamine transporter site-directed mutations differentially alter substrate transport and cocaine binding. Proc Natl Acad Sci U S A 89:7782-7785.

Kovtun O, Sakrikar D, Tomlinson ID, Chang JC, Arzeta-Ferrer X, Blakely RD, Rosenthal SJ (2015) Single-quantum-dot tracking reveals altered membrane dynamics of an attention-deficit/hyperactivity-disorder-derived dopamine transporter coding variant. ACS Chem Neurosci 6:526-534.

Kristensen AS, Andersen J, Jorgensen TN, Sorensen L, Eriksen J, Loland CJ, Stromgaard K, Gether U (2011) SLC6 neurotransmitter transporters: structure, function, and regulation. Pharmacol Rev 63:585-640.

Kurian MA, Zhen J, Cheng SY, Li Y, Mordekar SR, Jardine P, Morgan NV, Meyer E, Tee L, Pasha S, Wassmer E, Heales SJ, Gissen P, Reith ME, Maher ER (2009) Homozygous loss-of-function mutations in the gene encoding the dopamine transporter are associated with infantile parkinsonism-dystonia. J Clin Invest 119:1595-1603.

Kurian MA et al. (2011) Clinical and molecular characterisation of hereditary dopamine transporter deficiency syndrome: an observational cohort and experimental study. Lancet Neurol 10:54-62.

Laakso A, Hietala J (2000) PET studies of brain monoamine transporters. Curr Pharm Des 6:1611-1623.

Laasonen-Balk T, Kuikka J, Viinamaki H, Husso-Saastamoinen M, Lehtonen J, Tiihonen J (1999) Striatal dopamine transporter density in major depression. Psychopharmacology (Berl) 144:282-285.

Lakadamyali M, Rust MJ, Zhuang X (2006) Ligands for clathrin-mediated endocytosis are differentially sorted into distinct populations of early endosomes. Cell 124:997-1009.

Lauffer BE, Melero C, Temkin P, Lei C, Hong W, Kortemme T, von Zastrow M (2010) SNX27 mediates PDZ-directed sorting from endosomes to the plasma membrane. J Cell Biol 190:565-574.

LaVail JH, LaVail MM (1972) Retrograde axonal transport in the central nervous system. Science 176:1416-1417.

Lee FJ, Liu F, Pristupa ZB, Niznik HB (2001) Direct binding and functional coupling of alpha-synuclein to the dopamine transporters accelerate dopamine-induced apoptosis. FASEB J 15:916-926.

Lee FJ, Pei L, Moszczynska A, Vukusic B, Fletcher PJ, Liu F (2007) Dopamine transporter cell surface localization facilitated by a direct interaction with the dopamine D2 receptor. EMBO J 26:2127-2136.

Lee KH, Kim MY, Kim DH, Lee YS (2004) Syntaxin 1A and receptor for activated C kinase interact with the N-terminal region of human dopamine transporter. Neurochem Res 29:1405-1409.

Lees AJ (2007) Unresolved issues relating to the shaking palsy on the celebration of James Parkinson's 250th birthday. Mov Disord 22 Suppl 17:S327-334.

Lew R, Vaughan R, Simantov R, Wilson A, Kuhar MJ (1991) Dopamine transporters in the nucleus accumbens and the striatum have different apparent molecular weights. Synapse 8:152-153.

Li LB, Chen N, Ramamoorthy S, Chi L, Cui XN, Wang LC, Reith ME (2004) The role of N-glycosylation in function and surface trafficking of the human dopamine transporter. J Biol Chem 279:21012-21020.

Lin Q, Wang J, Childress C, Yang W (2012) The activation mechanism of ACK1 (activated Cdc42-associated tyrosine kinase 1). Biochem J 445:255-264.

Lin Z, Wang W, Kopajtic T, Revay RS, Uhl GR (1999) Dopamine transporter: transmembrane phenylalanine mutations can selectively influence dopamine uptake and cocaine analog recognition. Mol Pharmacol 56:434-447.

Lindvall O, Bjorklund A (1974) The glyoxylic acid fluorescence histochemical method: a detailed account of the methodology for the visualization of central catecholamine neurons. Histochemistry 39:97-127.

Linseman DA, Heidenreich KA, Fisher SK (2001) Stimulation of M3 muscarinic receptors induces phosphorylation of the Cdc42 effector activated Cdc42Hs-associated kinase-1 via a Fyn tyrosine kinase signaling pathway. J Biol Chem 276:5622-5628.

Little KY, Elmer LW, Zhong H, Scheys JO, Zhang L (2002) Cocaine induction of dopamine transporter trafficking to the plasma membrane. Mol Pharmacol 61:436-445.

Loder MK, Melikian HE (2003) The dopamine transporter constitutively internalizes and recycles in a protein kinase C-regulated manner in stably transfected PC12 cell lines. J Biol Chem 278:22168-22174.

Loland CJ, Norregaard L, Litman T, Gether U (2002) Generation of an activating Zn(2+) switch in the dopamine transporter: mutation of an intracellular tyrosine constitutively alters the conformational equilibrium of the transport cycle. Proc Natl Acad Sci U S A 99:1683-1688.

Loo LS, Tang N, Al-Haddawi M, Dawe GS, Hong W (2014) A role for sorting nexin 27 in AMPA receptor trafficking. Nat Commun 5:3176.

Lord C, Ferro-Novick S, Miller EA (2013) The highly conserved COPII coat complex sorts cargo from the endoplasmic reticulum and targets it to the golgi. Cold Spring Harb Perspect Biol 5.

Lyness WH, Friedle NM, Moore KE (1979) Destruction of dopaminergic nerve terminals in nucleus accumbens: effect on d-amphetamine self-administration. Pharmacol Biochem Behav 11:553-556.

Mahajan K, Challa S, Coppola D, Lawrence H, Luo Y, Gevariya H, Zhu W, Chen YA, Lawrence NJ, Mahajan NP (2010) Effect of Ack1 tyrosine kinase inhibitor on ligand-independent androgen receptor activity. Prostate 70:1274-1285.

Mahajan NP, Whang YE, Mohler JL, Earp HS (2005) Activated tyrosine kinase Ack1 promotes prostate tumorigenesis: role of Ack1 in polyubiquitination of tumor suppressor Wwox. Cancer Res 65:10514-10523.

Marks MJ, Stitzel JA, Romm E, Wehner JM, Collins AC (1986) Nicotinic binding sites in rat and mouse brain: comparison of acetylcholine, nicotine, and alpha-bungarotoxin. Mol Pharmacol 30:427-436.

Marsden CA, Joseph MH, Kruk ZL, Maidment NT, O'Neill RD, Schenk JO, Stamford JA (1988) In vivo voltammetry--present electrodes and methods. Neuroscience 25:389-400.

Massol P, Montcourrier P, Guillemot JC, Chavrier P (1998) Fc receptor-mediated phagocytosis requires CDC42 and Rac1. EMBO J 17:6219-6229.

Matsumoto M, Weickert CS, Akil M, Lipska BK, Hyde TM, Herman MM, Kleinman JE, Weinberger DR (2003) Catechol O-methyltransferase mRNA expression in human and rat brain: evidence for a role in cortical neuronal function. Neuroscience 116:127-137.

Mazei-Robison MS, Couch RS, Shelton RC, Stein MA, Blakely RD (2005) Sequence variation in the human dopamine transporter gene in children with attention deficit hyperactivity disorder. Neuropharmacology 49:724-736.

Mazei-Robison MS, Bowton E, Holy M, Schmudermaier M, Freissmuth M, Sitte HH, Galli A, Blakely RD (2008) Anomalous dopamine release associated

with a human dopamine transporter coding variant. J Neurosci 28:7040-7046.

McElvain JS, Schenk JO (1992) A multisubstrate mechanism of striatal dopamine uptake and its inhibition by cocaine. Biochem Pharmacol 43:2189-2199.

McGarvey JC, Xiao K, Bowman SL, Mamonova T, Zhang Q, Bisello A, Sneddon WB, Ardura JA, Jean-Alphonse F, Vilardaga JP, Puthenveedu MA, Friedman PA (2016) Actin-Sorting Nexin 27 (SNX27)-Retromer Complex Mediates Rapid Parathyroid Hormone Receptor Recycling. J Biol Chem 291:10986-11002.

McMillan KJ, Gallon M, Jellett AP, Clairfeuille T, Tilley FC, McGough I, Danson CM, Heesom KJ, Wilkinson KA, Collins BM, Cullen PJ (2016) Atypical parkinsonism-associated retromer mutant alters endosomal sorting of specific cargo proteins. J Cell Biol 214:389-399.

Melikian HE (2004) Neurotransmitter transporter trafficking: endocytosis, recycling, and regulation. Pharmacol Ther 104:17-27.

Melikian HE, Buckley KM (1999) Membrane trafficking regulates the activity of the human dopamine transporter. J Neurosci 19:7699-7710.

Melikian HE, Ramamoorthy S, Tate CG, Blakely RD (1996) Inability to N-glycosylate the human norepinephrine transporter reduces protein stability, surface trafficking, and transport activity but not ligand recognition. Mol Pharmacol 50:266-276.

Mergy MA, Gowrishankar R, Gresch PJ, Gantz SC, Williams J, Davis GL, Wheeler CA, Stanwood GD, Hahn MK, Blakely RD (2014) The rare DAT coding variant Val559 perturbs DA neuron function, changes behavior, and alters in vivo responses to psychostimulants. Proc Natl Acad Sci U S A 111:E4779-4788.

Miranda M, Sorkina T, Grammatopoulos TN, Zawada WM, Sorkin A (2004) Multiple molecular determinants in the carboxyl terminus regulate dopamine transporter export from endoplasmic reticulum. J Biol Chem 279:30760-30770.

Miranda M, Wu CC, Sorkina T, Korstjens DR, Sorkin A (2005) Enhanced ubiquitylation and accelerated degradation of the dopamine transporter mediated by protein kinase C. J Biol Chem 280:35617-35624.

Molinoff PB, Axelrod J (1971) Biochemistry of catecholamines. Annu Rev Biochem 40:465-500.

Moore RY, Bloom FE (1978) Central catecholamine neuron systems: anatomy and physiology of the dopamine systems. Annu Rev Neurosci 1:129-169.

Moritz AE, Rastedt DE, Stanislowski DJ, Shetty M, Smith MA, Vaughan RA, Foster JD (2015) Reciprocal Phosphorylation and Palmitoylation Control Dopamine Transporter Kinetics. J Biol Chem 290:29095-29105.

Moron JA, Brockington A, Wise RA, Rocha BA, Hope BT (2002) Dopamine uptake through the norepinephrine transporter in brain regions with low levels of the dopamine transporter: evidence from knock-out mouse lines. J Neurosci 22:389-395.

Moron JA, Zakharova I, Ferrer JV, Merrill GA, Hope B, Lafer EM, Lin ZC, Wang JB, Javitch JA, Galli A, Shippenberg TS (2003) Mitogen-activated protein kinase regulates dopamine transporter surface expression and dopamine transport capacity. J Neurosci 23:8480-8488.

Moszczynska A, Saleh J, Zhang H, Vukusic B, Lee FJ, Liu F (2007) Parkin disrupts the alpha-synuclein/dopamine transporter interaction: consequences toward dopamine-induced toxicity. J Mol Neurosci 32:217-227.

Navaroli DM, Stevens ZH, Uzelac Z, Gabriel L, King MJ, Lifshitz LM, Sitte HH, Melikian HE (2011) The plasma membrane-associated GTPase Rin interacts with the dopamine transporter and is required for protein kinase C-regulated dopamine transporter trafficking. J Neurosci 31:13758-13770.

Navaroli DM, Bellve KD, Standley C, Lifshitz LM, Cardia J, Lambright D, Leonard D, Fogarty KE, Corvera S (2012) Rabenosyn-5 defines the fate of the transferrin receptor following clathrin-mediated endocytosis. Proc Natl Acad Sci U S A 109:E471-480.

Nicholson C (1995) Interaction between diffusion and Michaelis-Menten uptake of dopamine after iontophoresis in striatum. Biophys J 68:1699-1715.

Nirenberg MJ, Chan J, Vaughan RA, Uhl GR, Kuhar MJ, Pickel VM (1997a) Immunogold localization of the dopamine transporter: an ultrastructural study of the rat ventral tegmental area. J Neurosci 17:5255-5262.

Nirenberg MJ, Chan J, Pohorille A, Vaughan RA, Uhl GR, Kuhar MJ, Pickel VM (1997b) The dopamine transporter: comparative ultrastructure of dopaminergic axons in limbic and motor compartments of the nucleus accumbens. J Neurosci 17:6899-6907.

Nomikos GG, Damsma G, Wenkstern D, Fibiger HC (1990) In vivo characterization of locally applied dopamine uptake inhibitors by striatal microdialysis. Synapse 6:106-112.

Olds J, Milner P (1954) Positive reinforcement produced by electrical stimulation of septal area and other regions of rat brain. J Comp Physiol Psychol 47:419-427.

Pacholczyk T, Blakely RD, Amara SG (1991) Expression cloning of a cocaine- and antidepressant-sensitive human noradrenaline transporter. Nature 350:350-354.

Parker EM, Cubeddu LX (1986) Effects of d-amphetamine and dopamine synthesis inhibitors on dopamine and acetylcholine neurotransmission in the striatum. II. Release in the presence of vesicular transmitter stores. J Pharmacol Exp Ther 237:193-203.

Parton RG (2003) Caveolae--from ultrastructure to molecular mechanisms. Nat Rev Mol Cell Biol 4:162-167.

Patel A, Uhl G, Kuhar MJ (1993) Species differences in dopamine transporters: postmortem changes and glycosylation differences. J Neurochem 61:496-500.

Patel AP, Cerruti C, Vaughan RA, Kuhar MJ (1994) Developmentally regulated glycosylation of dopamine transporter. Brain Res Dev Brain Res 83:53-58.

Penmatsa A, Wang KH, Gouaux E (2013) X-ray structure of dopamine transporter elucidates antidepressant mechanism. Nature 503:85-90.

Pereira DB, Schmitz Y, Meszaros J, Merchant P, Hu G, Li S, Henke A, Lizardi-Ortiz JE, Karpowicz RJ, Jr., Morgenstern TJ, Sonders MS, Kanter E, Rodriguez PC, Mosharov EV, Sames D, Sulzer D (2016) Fluorescent false neurotransmitter reveals functionally silent dopamine vesicle clusters in the striatum. Nat Neurosci 19:578-586.

Pinsonneault JK, Han DD, Burdick KE, Kataki M, Bertolino A, Malhotra AK, Gu HH, Sadee W (2011) Dopamine transporter gene variant affecting expression in human brain is associated with bipolar disorder. Neuropsychopharmacology 36:1644-1655.

Pizzo AB, Karam CS, Zhang Y, Ma CL, McCabe BD, Javitch JA (2014) Amphetamine-induced behavior requires CaMKII-dependent dopamine transporter phosphorylation. Mol Psychiatry 19:279-281.

Raiteri M, Angelini F, Levi G (1974) A simple apparatus for studying the release of neurotransmitters from synaptosomes. Eur J Pharmacol 25:411-414.

Rao A, Simmons D, Sorkin A (2011) Differential subcellular distribution of endosomal compartments and the dopamine transporter in dopaminergic neurons. Mol Cell Neurosci 46:148-158.

Rao A, Richards TL, Simmons D, Zahniser NR, Sorkin A (2012) Epitope-tagged dopamine transporter knock-in mice reveal rapid endocytic trafficking and filopodia targeting of the transporter in dopaminergic axons. FASEB J 26:1921-1933.

Rayport S, Sulzer D, Shi WX, Sawasdikosol S, Monaco J, Batson D, Rajendran G (1992) Identified postnatal mesolimbic dopamine neurons in culture: morphology and electrophysiology. J Neurosci 12:4264-4280.

Renard HF, Simunovic M, Lemiere J, Boucrot E, Garcia-Castillo MD, Arumugam S, Chambon V, Lamaze C, Wunder C, Kenworthy AK, Schmidt AA, McMahon HT, Sykes C, Bassereau P, Johannes L (2015) Endophilin-A2 functions in membrane scission in clathrin-independent endocytosis. Nature 517:493-496.

Richardson BD, Saha K, Krout D, Cabrera E, Felts B, Henry LK, Swant J, Zou MF, Newman AH, Khoshbouei H (2016) Membrane potential shapes regulation of dopamine transporter trafficking at the plasma membrane. Nat Commun 7:10423.

Rickhag M, Hansen FH, Sorensen G, Strandfelt KN, Andresen B, Gotfryd K, Madsen KL, Vestergaard-Klewe I, Ammendrup-Johnsen I, Eriksen J, Newman AH, Fuchtbauer EM, Gomeza J, Woldbye DP, Wortwein G, Gether U (2013) A C-terminal PDZ domain-binding sequence is required for striatal distribution of the dopamine transporter. Nat Commun 4:1580.

Ritz MC, Lamb RJ, Goldberg SR, Kuhar MJ (1987) Cocaine receptors on dopamine transporters are related to self-administration of cocaine. Science 237:1219-1223.

Roberts DC, Koob GF, Klonoff P, Fibiger HC (1980) Extinction and recovery of cocaine self-administration following 6-hydroxydopamine lesions of the nucleus accumbens. Pharmacol Biochem Behav 12:781-787.

Robinson DL, Venton BJ, Heien ML, Wightman RM (2003) Detecting subsecond dopamine release with fast-scan cyclic voltammetry in vivo. Clin Chem 49:1763-1773.

Rocha BA, Fumagalli F, Gainetdinov RR, Jones SR, Ator R, Giros B, Miller GW, Caron MG (1998) Cocaine self-administration in dopamine-transporter knockout mice. Nat Neurosci 1:132-137.

Rogaeva E et al. (2007) The neuronal sortilin-related receptor SORL1 is genetically associated with Alzheimer disease. Nat Genet 39:168-177.

Rojas R, van Vlijmen T, Mardones GA, Prabhu Y, Rojas AL, Mohammed S, Heck AJ, Raposo G, van der Sluijs P, Bonifacino JS (2008) Regulation of retromer recruitment to endosomes by sequential action of Rab5 and Rab7. J Cell Biol 183:513-526.

Rudnick G, Kramer R, Blakely RD, Murphy DL, Verrey F (2014) The SLC6 transporters: perspectives on structure, functions, regulation, and models for transporter dysfunction. Pflugers Arch 466:25-42.

Sabharanjak S, Sharma P, Parton RG, Mayor S (2002) GPI-anchored proteins are delivered to recycling endosomes via a distinct cdc42-regulated, clathrin-independent pinocytic pathway. Dev Cell 2:411-423.

Saheki Y, De Camilli P (2012) Synaptic vesicle endocytosis. Cold Spring Harb Perspect Biol 4:a005645.

Sakrikar D, Mazei-Robison MS, Mergy MA, Richtand NW, Han Q, Hamilton PJ, Bowton E, Galli A, Veenstra-Vanderweele J, Gill M, Blakely RD (2012) Attention deficit/hyperactivity disorder-derived coding variation in the dopamine transporter disrupts microdomain targeting and trafficking regulation. J Neurosci 32:5385-5397.

Saunders C, Ferrer JV, Shi L, Chen J, Merrill G, Lamb ME, Leeb-Lundberg LM, Carvelli L, Javitch JA, Galli A (2000) Amphetamine-induced loss of human dopamine transporter activity: an internalization-dependent and cocaine-sensitive mechanism. Proc Natl Acad Sci U S A 97:6850-6855.

Sauvonnet N, Dujeancourt A, Dautry-Varsat A (2005) Cortactin and dynamin are required for the clathrin-independent endocytosis of gammac cytokine receptor. J Cell Biol 168:155-163.

Seaman MN (2012) The retromer complex - endosomal protein recycling and beyond. J Cell Sci 125:4693-4702.

Seaman MN, McCaffery JM, Emr SD (1998) A membrane coat complex essential for endosome-to-Golgi retrograde transport in yeast. J Cell Biol 142:665-681.

Seaman MN, Marcusson EG, Cereghino JL, Emr SD (1997) Endosome to Golgi retrieval of the vacuolar protein sorting receptor, Vps10p, requires the function of the VPS29, VPS30, and VPS35 gene products. J Cell Biol 137:79-92.

Seaman MN, Harbour ME, Tattersall D, Read E, Bright N (2009) Membrane recruitment of the cargo-selective retromer subcomplex is catalysed by the small GTPase Rab7 and inhibited by the Rab-GAP TBC1D5. J Cell Sci 122:2371-2382.

Shao Y, Akmentin W, Toledo-Aral JJ, Rosenbaum J, Valdez G, Cabot JB, Hilbush BS, Halegoua S (2002) Pincher, a pinocytic chaperone for nerve growth factor/TrkA signaling endosomes. J Cell Biol 157:679-691.

Sharma A, Couture J (2014) A review of the pathophysiology, etiology, and treatment of attention-deficit hyperactivity disorder (ADHD). Ann Pharmacother 48:209-225.

Shen H, Ferguson SM, Dephoure N, Park R, Yang Y, Volpicelli-Daley L, Gygi S, Schlessinger J, De Camilli P (2011) Constitutive activated Cdc42-associated kinase (Ack) phosphorylation at arrested endocytic clathrin-coated pits of cells that lack dynamin. Mol Biol Cell 22:493-502.

Shimada S, Kitayama S, Lin CL, Patel A, Nanthakumar E, Gregor P, Kuhar M, Uhl G (1991) Cloning and expression of a cocaine-sensitive dopamine transporter complementary DNA. Science 254:576-578.

Small SA, Petsko GA (2015) Retromer in Alzheimer disease, Parkinson disease and other neurological disorders. Nat Rev Neurosci 16:126-132.

Snyder SH (2002) Forty years of neurotransmitters: a personal account. Arch Gen Psychiatry 59:983-994.

Snyder SH, Coyle JT (1969) Regional differences in H3-norepinephrine and H3-dopamine uptake into rat brain homogenates. J Pharmacol Exp Ther 165:78-86.

Sonders MS, Zhu SJ, Zahniser NR, Kavanaugh MP, Amara SG (1997) Multiple ionic conductances of the human dopamine transporter: the actions of dopamine and psychostimulants. J Neurosci 17:960-974.

Sora I, Wichems C, Takahashi N, Li XF, Zeng Z, Revay R, Lesch KP, Murphy DL, Uhl GR (1998) Cocaine reward models: conditioned place preference can be established in dopamine- and in serotonin-transporter knockout mice. Proc Natl Acad Sci U S A 95:7699-7704.

Sora I, Hall FS, Andrews AM, Itokawa M, Li XF, Wei HB, Wichems C, Lesch KP, Murphy DL, Uhl GR (2001) Molecular mechanisms of cocaine reward: combined dopamine and serotonin transporter knockouts eliminate cocaine place preference. Proc Natl Acad Sci U S A 98:5300-5305.

Sorkina T, Caltagarone J, Sorkin A (2013) Flotillins regulate membrane mobility of the dopamine transporter but are not required for its protein kinase C dependent endocytosis. Traffic 14:709-724.

Sorkina T, Hoover BR, Zahniser NR, Sorkin A (2005) Constitutive and protein kinase C-induced internalization of the dopamine transporter is mediated by a clathrin-dependent mechanism. Traffic 6:157-170.

Sorkina T, Doolen S, Galperin E, Zahniser NR, Sorkin A (2003) Oligomerization of dopamine transporters visualized in living cells by fluorescence resonance energy transfer microscopy. J Biol Chem 278:28274-28283.

Sorkina T, Richards TL, Rao A, Zahniser NR, Sorkin A (2009) Negative regulation of dopamine transporter endocytosis by membrane-proximal N-terminal residues. J Neurosci 29:1361-1374.

Sorkina T, Miranda M, Dionne KR, Hoover BR, Zahniser NR, Sorkin A (2006) RNA interference screen reveals an essential role of Nedd4-2 in dopamine transporter ubiquitination and endocytosis. J Neurosci 26:8195-8205.

St Pierre CA, Leonard D, Corvera S, Kurt-Jones EA, Finberg RW (2011) Antibodies to cell surface proteins redirect intracellular trafficking pathways. Exp Mol Pathol 91:723-732.

Stamford JA, Kruk ZL, Palij P, Millar J (1988) Diffusion and uptake of dopamine in rat caudate and nucleus accumbens compared using fast cyclic voltammetry. Brain Res 448:381-385.

Steinkellner T, Yang JW, Montgomery TR, Chen WQ, Winkler MT, Sucic S, Lubec G, Freissmuth M, Elgersma Y, Sitte HH, Kudlacek O (2012) Ca(2+)/calmodulin-dependent protein kinase IIalpha (alphaCaMKII) controls the activity of the dopamine transporter: implications for Angelman syndrome. J Biol Chem 287:29627-29635.

Sucic S, El-Kasaby A, Kudlacek O, Sarker S, Sitte HH, Marin P, Freissmuth M (2011) The serotonin transporter is an exclusive client of the coat protein complex II (COPII) component SEC24C. J Biol Chem 286:16482-16490.

Sulzer D (2007) Multiple hit hypotheses for dopamine neuron loss in Parkinson's disease. Trends Neurosci 30:244-250.

Sulzer D, Chen TK, Lau YY, Kristensen H, Rayport S, Ewing A (1995) Amphetamine redistributes dopamine from synaptic vesicles to the cytosol and promotes reverse transport. J Neurosci 15:4102-4108.

Takahara J, Arimura A, Schally AV (1974) Effect of catecholamines on the TRH-stimulated release of prolactin and growth hormone from sheep pituitaries in vitro. Endocrinology 95:1490-1494.

Takahashi N, Miner LL, Sora I, Ujike H, Revay RS, Kostic V, Jackson-Lewis V, Przedborski S, Uhl GR (1997) VMAT2 knockout mice: heterozygotes display reduced amphetamine-conditioned reward, enhanced amphetamine locomotion, and enhanced MPTP toxicity. Proc Natl Acad Sci U S A 94:9938-9943.

Tamminga CA et al. (2002) Developing novel treatments for mood disorders: accelerating discovery. Biol Psychiatry 52:589-609.

Tate CG, Blakely RD (1994) The effect of N-linked glycosylation on activity of the Na(+)- and Cl(-)-dependent serotonin transporter expressed using recombinant baculovirus in insect cells. J Biol Chem 269:26303-26310.

Teo M, Tan L, Lim L, Manser E (2001) The tyrosine kinase ACK1 associates with clathrin-coated vesicles through a binding motif shared by arrestin and other adaptors. J Biol Chem 276:18392-18398.

Thomsen M, Han DD, Gu HH, Caine SB (2009) Lack of cocaine self-administration in mice expressing a cocaine-insensitive dopamine transporter. J Pharmacol Exp Ther 331:204-211.

Torres GE, Amara SG (2007) Glutamate and monoamine transporters: new visions of form and function. Curr Opin Neurobiol 17:304-312.

Torres GE, Gainetdinov RR, Caron MG (2003a) Plasma membrane monoamine transporters: structure, regulation and function. Nat Rev Neurosci 4:13-25.

Torres GE, Carneiro A, Seamans K, Fiorentini C, Sweeney A, Yao WD, Caron MG (2003b) Oligomerization and trafficking of the human dopamine transporter. Mutational analysis identifies critical domains important for the functional expression of the transporter. J Biol Chem 278:2731-2739.

Torres GE, Yao WD, Mohn AR, Quan H, Kim KM, Levey AI, Staudinger J, Caron MG (2001) Functional interaction between monoamine plasma membrane transporters and the synaptic PDZ domain-containing protein PICK1. Neuron 30:121-134.

Tsika E, Glauser L, Moser R, Fiser A, Daniel G, Sheerin UM, Lees A, Troncoso JC, Lewis PA, Bandopadhyay R, Schneider BL, Moore DJ (2014) Parkinson's disease-linked mutations in VPS35 induce dopaminergic neurodegeneration. Hum Mol Genet 23:4621-4638.

Ungerstedt U (1976) 6-hydroxydopamine-induced degeneration of the nigrostriatal dopamine pathway: the turning syndrome. Pharmacol Ther B 2:37-40.

Urena JM, La Torre A, Martinez A, Lowenstein E, Franco N, Winsky-Sommerer R, Fontana X, Casaroli-Marano R, Ibanez-Sabio MA, Pascual M, Del Rio JA, de Lecea L, Soriano E (2005) Expression, synaptic localization, and developmental regulation of Ack1/Pyk1, a cytoplasmic tyrosine kinase highly expressed in the developing and adult brain. J Comp Neurol 490:119-132.

Usdin TB, Mezey E, Chen C, Brownstein MJ, Hoffman BJ (1991) Cloning of the cocaine-sensitive bovine dopamine transporter. Proc Natl Acad Sci U S A 88:11168-11171.

Uttamapinant C, Sanchez MI, Liu DS, Yao JZ, Ting AY (2013) Site-specific protein labeling using PRIME and chelation-assisted click chemistry. Nat Protoc 8:1620-1634.

Uttamapinant C, White KA, Baruah H, Thompson S, Fernandez-Suarez M, Puthenveetil S, Ting AY (2010) A fluorophore ligase for site-specific protein labeling inside living cells. Proc Natl Acad Sci U S A 107:10914-10919.

Uttamapinant C, Tangpeerachaikul A, Grecian S, Clarke S, Singh U, Slade P, Gee KR, Ting AY (2012) Fast, cell-compatible click chemistry with copper-

chelating azides for biomolecular labeling. Angew Chem Int Ed Engl 51:5852-5856.

van Weering JR, Verkade P, Cullen PJ (2012) SNX-BAR-mediated endosome tubulation is co-ordinated with endosome maturation. Traffic 13:94-107.

Varandas KC, Irannejad R, von Zastrow M (2016) Retromer Endosome Exit Domains Serve Multiple Trafficking Destinations and Regulate Local G Protein Activation by GPCRs. Curr Biol.

Vaughan RA, Huff RA, Uhl GR, Kuhar MJ (1997) Protein kinase C-mediated phosphorylation and functional regulation of dopamine transporters in striatal synaptosomes. J Biol Chem 272:15541-15546.

Vilarino-Guell C et al. (2011) VPS35 mutations in Parkinson disease. Am J Hum Genet 89:162-167.

Vina-Vilaseca A, Sorkin A (2010) Lysine 63-linked polyubiquitination of the dopamine transporter requires WW3 and WW4 domains of Nedd4-2 and UBE2D ubiquitin-conjugating enzymes. J Biol Chem 285:7645-7656.

Volkow ND, Fowler JS, Gatley SJ, Logan J, Wang GJ, Ding YS, Dewey S (1996) PET evaluation of the dopamine system of the human brain. J Nucl Med 37:1242-1256.

Wall SC, Gu H, Rudnick G (1995) Biogenic amine flux mediated by cloned transporters stably expressed in cultured cell lines: amphetamine specificity for inhibition and efflux. Mol Pharmacol 47:544-550.

Wang KH, Penmatsa A, Gouaux E (2015) Neurotransmitter and psychostimulant recognition by the dopamine transporter. Nature 521:322-327.

Wayment HK, Schenk JO, Sorg BA (2001) Characterization of extracellular dopamine clearance in the medial prefrontal cortex: role of monoamine uptake and monoamine oxidase inhibition. J Neurosci 21:35-44.

Welz T, Wellbourne-Wood J, Kerkhoff E (2014) Orchestration of cell surface proteins by Rab11. Trends Cell Biol 24:407-415.

Wersinger C, Sidhu A (2003) Attenuation of dopamine transporter activity by alpha-synuclein. Neurosci Lett 340:189-192.

Wheeler DD, Edwards AM, Chapman BM, Ondo JG (1993) A model of the sodium dependence of dopamine uptake in rat striatal synaptosomes. Neurochem Res 18:927-936.

Wickersham IR, Lyon DC, Barnard RJ, Mori T, Finke S, Conzelmann KK, Young JA, Callaway EM (2007) Monosynaptic restriction of transsynaptic tracing from single, genetically targeted neurons. Neuron 53:639-647.

Williams JM, Owens WA, Turner GH, Saunders C, Dipace C, Blakely RD, France CP, Gore JC, Daws LC, Avison MJ, Galli A (2007) Hypoinsulinemia regulates amphetamine-induced reverse transport of dopamine. PLoS Biol 5:e274.

Wise RA, Rompre PP (1989) Brain dopamine and reward. Annu Rev Psychol 40:191-225.

Wu Q, Reith ME, Wightman RM, Kawagoe KT, Garris PA (2001) Determination of release and uptake parameters from electrically evoked dopamine

dynamics measured by real-time voltammetry. J Neurosci Methods 112:119-133.

Wu S, Bellve KD, Fogarty KE, Melikian HE (2015) Ack1 is a dopamine transporter endocytic brake that rescues a trafficking-dysregulated ADHD coding variant. Proc Natl Acad Sci U S A 112:15480-15485.

Yamamoto BK, Novotney S (1998) Regulation of extracellular dopamine by the norepinephrine transporter. J Neurochem 71:274-280.

Yamashita A, Singh SK, Kawate T, Jin Y, Gouaux E (2005) Crystal structure of a bacterial homologue of Na+/Cl--dependent neurotransmitter transporters. Nature 437:215-223.

Yang W, Lo CG, Dispenza T, Cerione RA (2001) The Cdc42 target ACK2 directly interacts with clathrin and influences clathrin assembly. J Biol Chem 276:17468-17473.

Yokoyama N, Miller WT (2003) Biochemical properties of the Cdc42-associated tyrosine kinase ACK1. Substrate specificity, authphosphorylation, and interaction with Hck. J Biol Chem 278:47713-47723.

Zhang D, Isack NR, Glodowski DR, Liu J, Chen CC, Xu XZ, Grant BD, Rongo C (2012) RAB-6.2 and the retromer regulate glutamate receptor recycling through a retrograde pathway. J Cell Biol 196:85-101.

Zhu S, Zhao C, Wu Y, Yang Q, Shao A, Wang T, Wu J, Yin Y, Li Y, Hou J, Zhang X, Zhou G, Gu X, Wang X, Bustelo XR, Zhou J (2015) Identification of a Vav2-dependent mechanism for GDNF/Ret control of mesolimbic DAT trafficking. Nat Neurosci 18:1084-1093.

Zhu SJ, Kavanaugh MP, Sonders MS, Amara SG, Zahniser NR (1997) Activation of protein kinase C inhibits uptake, currents and binding associated with the human dopamine transporter expressed in Xenopus oocytes. J Pharmacol Exp Ther 282:1358-1365.

Zimprich A et al. (2011) A mutation in VPS35, encoding a subunit of the retromer complex, causes late-onset Parkinson disease. Am J Hum Genet 89:168-175.

Zou Z, Horowitz LF, Montmayeur JP, Snapper S, Buck LB (2001) Genetic tracing reveals a stereotyped sensory map in the olfactory cortex. Nature 414:173-179.